NASA/CR-2005-213526

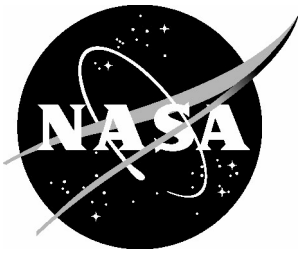

Modular Engine Noise Component Prediciton System (MCP) Technical Description and Assessment Document

William H. Herkes and David H. Reed
Boeing Commercial Airplane Company, Seattle, Washington

June 2005

The NASA STI Program Office . . . in Profile

Since its founding, NASA has been dedicated to the advancement of aeronautics and space science. The NASA Scientific and Technical Information (STI) Program Office plays a key part in helping NASA maintain this important role.

The NASA STI Program Office is operated by Langley Research Center, the lead center for NASA's scientific and technical information. The NASA STI Program Office provides access to the NASA STI Database, the largest collection of aeronautical and space science STI in the world. The Program Office is also NASA's institutional mechanism for disseminating the results of its research and development activities. These results are published by NASA in the NASA STI Report Series, which includes the following report types:

- TECHNICAL PUBLICATION. Reports of completed research or a major significant phase of research that present the results of NASA programs and include extensive data or theoretical analysis. Includes compilations of significant scientific and technical data and information deemed to be of continuing reference value. NASA counterpart of peer-reviewed formal professional papers, but having less stringent limitations on manuscript length and extent of graphic presentations.

- TECHNICAL MEMORANDUM. Scientific and technical findings that are preliminary or of specialized interest, e.g., quick release reports, working papers, and bibliographies that contain minimal annotation. Does not contain extensive analysis.

- CONTRACTOR REPORT. Scientific and technical findings by NASA-sponsored contractors and grantees.

- CONFERENCE PUBLICATION. Collected papers from scientific and technical conferences, symposia, seminars, or other meetings sponsored or co-sponsored by NASA.

- SPECIAL PUBLICATION. Scientific, technical, or historical information from NASA programs, projects, and missions, often concerned with subjects having substantial public interest.

- TECHNICAL TRANSLATION. English-language translations of foreign scientific and technical material pertinent to NASA's mission.

Specialized services that complement the STI Program Office's diverse offerings include creating custom thesauri, building customized databases, organizing and publishing research results ... even providing videos.

For more information about the NASA STI Program Office, see the following:

- Access the NASA STI Program Home Page at ***http://www.sti.nasa.gov***

- E-mail your question via the Internet to help@sti.nasa.gov

- Fax your question to the NASA STI Help Desk at (301) 621-0134

- Phone the NASA STI Help Desk at (301) 621-0390

- Write to:
  NASA STI Help Desk
  NASA Center for AeroSpace Information
  7121 Standard Drive
  Hanover, MD 21076-1320

NASA/CR-2005-213526

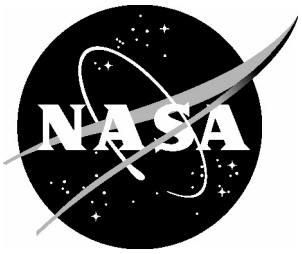

Modular Engine Noise Component Prediciton System (MCP) Technical Description and Assessment Document

William H. Herkes and David H. Reed
Boeing Commercial Airplane Company, Seattle, Washington

National Aeronautics and
Space Administration

Langley Research Center
Hampton, Virginia 23681-2199

Prepared for Langley Research Center
under Contract NAS1-97040

June 2005

Available from:

NASA Center for AeroSpace Information (CASI)
7121 Standard Drive
Hanover, MD 21076-1320
(301) 621-0390

National Technical Information Service (NTIS)
5285 Port Royal Road
Springfield, VA 22161-2171
(703) 605-6000

Table of Contents

List of Figures

1 Abstract

This report describes an empirical prediction procedure for turbofan engine noise. The procedure generates predicted noise levels for several noise components, including inlet- and aft-radiated fan noise, and jet-mixing noise. This report discusses the noise source mechanisms, the development of the prediction procedures, and the assessment of the accuracy of these predictions. Finally, some recommendations for future work are presented.

2 Introduction

This report describes the development and assessment of a prediction procedure for turbofan engine noise. This work was performed by The Boeing Company under funding from NASA contract NAS1-97040, Task 10. The noise prediction procedure is based on an empirical procedure that has evolved over many years at The Boeing Company. This prediction program is known as the Modular Engine Noise Component Prediction System (MCP). The data used to develop this program include both full-scale engine data and small-scale model data, and include data obtained from testing done by Boeing, by the engine manufacturers, and by NASA.

The specific work done under this contract included: migrating selected component modules from an existing Unix-based prediction program to a Windows/PC operating system; developing a new user interface; making updates to selected prediction modules, taking advantage of additional data; and assessing the predictions with measured data. Of particular interest in this work was the accuracy of the predictions for very high bypass ratio (greater than eight) engines.

In order to generate a noise estimate, the user specifies the appropriate engine properties (including both geometry and performance parameters), the microphone locations, the atmospheric conditions, and certain data processing options. The program is modular, meaning that the user specifies which engine noise components will be predicted. The version of the program described here allows the user to predict three components: inlet-radiated fan noise, aft-radiated fan noise, and jet noise. These components are described in Sections 4, 5, and 6, respectively.

MCP predicts one-third octave band noise levels over the frequency range of 50 to 10,000 Hertz. It also calculates overall sound pressure levels and certain subjective noise metrics (e.g., perceived noise levels).

Features of the program include the ability to:

- predict either static, steady state “test stand” noise levels, or airplane flyover noise levels
- predict either polar arc microphone levels or sideline microphone levels
- predict either free-field or 4-foot pole microphone ground-reflected levels
- add deltas to selected components (e.g., to account for acoustic lining effects, installation effects, etc.,)

A separate Program Users’ Guide has been written, and sample input and output files have been included with the software package delivered to NASA. This report addresses the development and assessment of the procedure.

3 Noise Component Modeling of Measured Data

The development of empirical component predictions depends upon the separation of the measured data into the various component noise sources. This process, and the measured data used, are briefly described in this section.

3.1 Component Modeling Process

The development of an MCP module generally uses measured data that has gone through a component modeling process. For this study the process was used to create data that are in the following form: static, 150-ft polar arc (i.e., static test stand-type data); free-field (i.e., no ground reflection effects); noise component-separated; and hardwall (i.e., no acoustic treatment).

The accuracy of these modeled measurements is very dependent on the particular way the data were originally acquired. The separation of tones is more accurate if narrowband data were taken. The separation of noise radiating out of the inlet from noise radiating out of the nozzles is more accurate if the measurements were made using acoustic barriers. And the development of a hardwall model is more accurate if actual hardwall configurations were tested (and the modeling process does not rely on lining prediction methods to determine the attenuation due to the acoustic treatment).

There are general guidelines and procedures for the component modeling process, although the process also relies on a certain amount of "engineering judgment." The process is described in Reference 1 and summarized here.

3.1.1 Jet Noise Identification

The measured aft-arc spectra are assumed to be set exclusively by jet noise in the low frequencies. The exact number of frequency bands that is attributed exclusively to jet noise is a function of radiation angle and primary jet velocity.

A predicted spectra shape is compared to the measured spectra over these jet-noise-controlled frequency bands. The difference between these two spectra is defined by a second-order curve fit. This curve fit is then added to the predicted data over the jet-noise-controlled frequencies. Beyond these frequencies the predicted spectra is adjusted by the value of the curve fit at the last exclusively jet noise frequency.

This process essentially produces jet noise spectra that are curve-fits of the measured spectra for the low (exclusively jet noise) frequencies. Beyond these frequencies the spectra shape is based on predictions, and the levels are set to be continuous with the curve-fitted lower frequencies.

3.1.2 Forward and Aft Noise Separation

Once the jet noise component has been removed from the measured spectra the remaining spectra are divided into noise radiating out of the inlet and noise radiating out of the primary and fan exhaust nozzles. This forward/aft split is determined by examining the local minima in directivity plots. The directivity roll-off rates have been derived from barrier data. If barrier data are available for the specific test data being modeled, these data are used for determining the forward/aft split.

3.1.3 Tone Identification

The component separation process uses the engine blade and vane counts, and the engine rotation speed, to identify the frequency where the various turbomachinery-related tones (including fan/compressor interaction tones and buzzsaw noise) will occur. When narrowband data are available these data are used to determine the levels of the tones. In the absence of narrowband data, a one-third octave band tone separation procedure is used to determine the tone levels.

3.1.4 Aft-fan, Turbine, and Core Broadband Noise Separation

The aft-radiated broadband noise is separated into fan, turbine, and core noise components. This process is guided by knowledge, for the particular engine geometry and operating conditions, of the frequency range over which these components occur and their general spectra shape.

3.2 Component-modeled Measurements

The component models used for the prediction assessment discussed in this report consist of ten different engine data sets, although not all components were present in all the data sets. These data sets included 127 individual power points, of which 48 were for bypass ratios greater than eight.

4 Forward-radiated Fan Noise

This section discusses the noise associated with the fan that is radiated out of the engine inlet.

4.1 Noise Source Mechanisms

The forward-radiated fan noise (inlet noise) component consists of three separate subcomponents, associated with different noise-generation mechanisms. These subcomponents are described in this section.

4.1.1 Tone Subcomponent

Fan noise is generated by unsteady aerodynamic loading on rigid surfaces such as the fan blades and the stator vanes. Unsteady aerodynamic loading associated with periodic flow fluctuations results in tone noise. This can be due to a number of sources, such as the interaction of an inlet wake with the rotating fan blades. The steady (when viewed from rotating reference frame) lift and drag forces on rotating fan blades result in harmonic fluctuations in the non-rotating reference frame. These fluctuations appear at the blade passing frequency and its harmonics.

4.1.2 Broadband Subcomponent

When the unsteady aerodynamic loading is associated with random flow fluctuations (such as turbulence) broadband noise is generated. This can be due to a number of sources, such as: inflow turbulence impinging on rotor blades and stator vanes; rotor wake turbulence impinging on downstream stators; and interaction of the blade tip flow with the turbulent wall boundary layer. In addition, there are a number of possible sources of rotor or stator broadband self-noise; turbulent boundary layers; turbulent wakes; and incoherent trailing edge vortex shedding.

4.1.3 Buzzsaw Subcomponent

When the blades rotate at supersonic tip speeds, bow shocks form at their leading edges. These react non-linearly with each other as they propagate upstream through the inlet. Slight variations in shock strengths result in a pressure spectrum with discrete tones at the shaft rotational frequency and its harmonics. This noise is referred to as multiple pure tone noise, buzzsaw noise, or combination tone noise.

4.2 Procedure Development

The forward-radiated fan noise prediction module is known as INLET3. The development of the procedure is described in this section.

4.2.1 Broadband Subcomponent

The development of the INLET3 broadband subcomponent module is described in Reference 1 and summarized here.

The module was developed using five sets of component-modeled measurements, each data set including a range of power points for a particular engine. These five engine data sets covered a wide range of fan diameters, included narrow and wide chord fans, and contained some power points with bypass ratios greater than eight.

The general approach was to develop three empirical correlations. The first one correlated the overall sound power level (normalized to a reference fan diameter) to an appropriate parameter relating to the engine operating condition; the second correlated a normalized spectra shape to normalized frequency bands; and the third correlated a normalized directivity shape to emission angle. The primary functional dependencies of these correlations are as follow:

$$\text{spl}(M_{tip}, f, \theta) = \text{oapwl}(M_{tip}) + \text{spectral correlation}(f) + \text{directivity correlation}(\theta)$$

where

spl = sound pressure level
M_{tip} = fan tip Mach number
f = frequency
θ = emission angle
oapwl = overall sound power level (over all relevant frequencies and angles)

In terms of the metrics used this equation is:

$$\text{spl} = [\text{oapwl}] + [\text{pwl} - \text{oapwl}] + [\text{spl} - \text{pwl}]$$

where

pwl = sound power level (over all relevant angles at a particular frequency)

These correlations are discussed in the following sections.

4.2.1.1 Overall Sound Power Level

The inlet-radiated fan broadband noise was modeled as two sources. The first source is located at the trailing edge of the rotor, or at the fan exit guide vanes, and is affected by the propagation in the rotor as well as in the inlet. The second source is located near the leading edge of the rotor and is only affected by the propagation in the inlet. The first source dominates at subsonic fan tip speeds, and the second dominates at high fan tip speeds. The overall sound power (normalized to a reference fan diameter) is equal to the sum of these two source terms, and is represented as a function of relative tip Mach number and the number of fan exit guide vanes. This correlation collapses data to within about +/- 3 db over the full range of tip speeds, with the largest deviations occurring at the supersonic tip speeds.

4.2.1.2 Spectra Shape

The normalized spectra shape was derived by plotting and curve-fitting normalized power levels versus normalized frequency. The normalized power level was defined as the sound power level minus the overall sound power level. The frequency was normalized by the blade passing frequency and a Reynolds number, as described in Reference 1. There were actually two different normalized spectra shapes derived, one for subsonic fan tip speeds and one for supersonic fan tip speeds.

4.2.1.3 Directivity Shape

The normalized directivity shape was derived by plotting and curve-fitting normalized sound pressure levels versus emission angle. The normalized sound pressure level was defined as the sound pressure level minus the sound power level. Similar to the normalized spectra shapes, there were two normalized directivity shapes derived, one for subsonic fan tip speeds and one for supersonic fan tip speeds.

4.2.2 Tone Subcomponent

The inlet-radiated fan tone noise prediction is based on an empirical correlation as shown in Figure 1 and Figure 2. The predicted tone level is the sum of the appropriate sound pressure level (as a function of harmonic number and fan tip Mach number) and directivity adjustment (as a function of harmonic number and emission angle), corrected to the appropriate fan diameter by 20 log (fan diameter / 1 foot).

4.2.3 Buzzsaw Subcomponent

The inlet-radiated fan buzzsaw noise prediction is based on an empirical correlation as shown in Figure 3 and Figure 4. The predicted buzzsaw levels are the sum of the appropriate sound pressure levels (as functions of harmonic number and fan tip Mach number) and directivity adjustments (as a function emission angle), corrected to the appropriate fan diameter by 20 log (fan diameter / 1 foot).

4.3 Assessment

The data used for assessment of the INLET3 module consisted of ten different engine data sets. These data sets included 127 individual power points, of which 48 were for bypass ratios greater than eight.

4.3.1 Broadband and Buzzsaw Subcomponents

The accuracy of the INLET3 broadband and buzzsaw noise predictions was examined both on the basis of individual spectra comparisons and on the basis of averaged, normalized spectra comparisons.

Comparisons of individual predicted spectra and modeled-data spectra, for selected power points, are shown in Figure 5 through Figure 16. From each of the ten engine data sets, power points were chosen that represented: a relatively low subsonic fan tip speed; a relatively high subsonic fan tip speed; a relatively low supersonic fan tip speed (if available); and a relatively high supersonic fan tip speed (if available).

In addition, spectra from all the 127 power points were incorporated into smoothed, averaged, normalized spectra in order to present an overall measure of the accuracy of the procedure (Figure 17 through Figure 22). These spectra were normalized by referencing the third-octave frequency band to the blade passing frequency (i.e., 10log[1/3-octave freq. band / bpf]). Once normalized, the spectra were grouped (as either subsonic or supersonic fan tip speed) and fitted with a third order curve. In addition to considering all the power points in one grouping, comparisons were made using only data for bypass ratios greater than eight.

For both the individual and the averaged spectra comparisons, results are shown for static, 150-foot polar arc, free-field data for three emission angles: 30, 60, and 90 degrees relative to the inlet axis. In the case of the supersonic fan tip speeds the figures show spectra for the summed fan broadband plus buzzsaw noise subcomponents. The reason for this is that, although these subcomponents are predicted separately, it is sometimes difficult to accurately separate them during the component modeling process.

The following observations regarding the inlet broadband and buzzsaw predictions are made based on the averaged spectra comparisons:

- The prediction trends for the higher bypass ratios (greater than eight) are similar to those for the lower bypass ratios.
- The peak sound pressure level tends to be overpredicted. For the subsonic fan tip speeds the overprediction is less (averaging less than 4 db) than for the supersonic cases, i.e., including buzzsaw noise (averaging over 10 db in some cases).
- The peak frequency band is, on the average, fairly well predicted. The exception to this is the 90-degree, subsonic tip speed case, where the predicted peak frequency band is several bands higher than the modeled measurements.
- The predicted low frequency rolloff is much less than shown in the modeled measurements.
- Except for the above-mentioned rolloff rate, the spectra shape is fairly well predicted for the subsonic fan tip speeds. For the supersonic fan tip speeds the predicted spectra tend to be flatter and smoother than the modeled measurements.
- The lower angles (e.g., 30 degrees) are better predicted than the higher ones (e.g., 90 degrees).
- The buzzsaw noise (judging from the smoothed averaged spectra comparisons and from the low frequency sub-harmonic tones in the individual spectra comparisons) is overpredicted.

4.3.2 Tone Subcomponent

The accuracy of the INLET3 tone noise predictions was examined on the basis of individual spectra comparisons. Comparisons of predicted spectra and modeled-data spectra, for selected power points, are shown in Figure 23 through Figure 31. From each of eight engine data sets, power points were chosen that represented: a relatively low power point; a medium power point; and a relatively high power point. The comparisons are shown for static, 150-foot polar arc, free-field data for three emission angles: 30, 60, and 90 degrees relative to the inlet axis.

The following observations regarding the inlet tone predictions can be made from these comparisons:

- The fundamental and first harmonic are overpredicted in most cases (about two-thirds of the time).
- In about half the cases the fundamental and first harmonic are predicted to within approximately 3 db of the modeled measurements.
- There is no evident correlation of inlet tone prediction accuracy with either angle or power level.

5 Aft-radiated Fan Noise

This section discusses the noise associated with the fan that is radiated out of the fan exhaust duct.

5.1 Noise Source Mechanisms

The aft-radiated fan noise (aft fan noise) component consists of two separate subcomponents, associated with different noise-generation mechanisms. These subcomponents are described in this section.

5.1.1 Tone Subcomponent

The source mechanisms for the aft-radiated tone noise are similar to those for the inlet-radiated tone noise (Section 4.1.1).

5.1.2 Broadband Subcomponent

The source mechanisms for the inlet-radiated broadband noise are similar to those for the inlet-radiated broadband noise (Section 4.1.2).

5.2 Procedure Development

The aft-radiated fan noise prediction module is known as AFTFN7. The development of the procedure is described in this section.

5.2.1 Broadband Subcomponent

The aft fan noise module was developed using nine sets of component-modeled measurements. These nine engine data sets included 108 individual power points, of which 48 were for bypass ratios greater than eight.

The general approach was to develop three empirical correlations. The first one correlated the normalized overall sound power level to an appropriate parameter relating to the engine operating condition; the second correlated a normalized spectra shape to normalized frequency bands; and the third correlated a normalized directivity shape to emission angle. The primary functional dependencies of these correlations are as follow:

$$spl(fpr, f, \theta) = oapwl(fpr) + \text{spectral correlation}(f) + \text{directivity correlation}(\theta)$$

where

spl = sound pressure level
fpr = fan pressure ratio
f = frequency
θ = emission angle
oapwl = overall sound power level (over all relevant frequencies and angles)

In terms of the metrics used this equation is:

$$spl = [oapwl] + [spl - oaspl] + [oaspl - oapwl]$$

where

oaspl = overall sound pressure level (over all relevant frequencies at a particular angle)

These correlations are discussed in the following sections.

5.2.1.1 Overall Sound Power Level

Numerous correlations were examined in an attempt to best collapse the overall sound power levels for the various sets of modeled measurements. Ultimately the best correlation (based on the smallest range of the 95 percent prediction confidence bands) was achieved by plotting a normalized overall sound power level versus fan pressure ratio as shown in Figure 32. As shown in this figure the overall sound power level was normalized by four additional terms: a 20 log (fan diameter) term; a 50 log (fan tip Mach number) term; a 15 log (fan solidity) term (solidity being defined as the ratio of fan tip chord divided by fan tip spacing); and a "delta fan pressure ratio" term. The inclusion of other terms was examined, but none resulted in an improved correlation. These other terms included: a rotor/stator spacing term; a stator-to-vane ratio term, various terms involving the number, span, and wetted area of the fan exit guide vanes; and a term involving the bypass ratio.

The derivation of the "delta fan pressure ratio" term deserves further explanation. The relationship between fan pressure ratio and fan tip Mach number was fairly similar for all the engines used in the correlation, as shown in Figure 33. However, those differences that did exist were examined for their possible effect on noise. This was done by plotting normalized overall power level as a function of the difference in the fan pressure from the mean fan pressure ratio as shown in Figure 34. A linear curve fit through this relationship was then applied to the normalized overall sound pressure level as shown in Figure 32.

5.2.1.2 Spectra Shape

The normalized spectra shape was derived by plotting, and curve-fitting, normalized sound pressure levels versus normalized frequency, as shown in Figure 35. For each power point from each of the different engine data sets used in the correlation process, the spectrum at the peak overall sound pressure level emission angle was chosen. The normalized sound pressure level was defined as the sound pressure level minus the overall sound pressure level (for that particular emission angle). The normalized frequency was

defined as the third-octave frequency band relative to the blade passing frequency (i.e., 10log[1/3-octave freq. band / bpf]).

The effect of bypass ratio on spectra shape was examined as shown in Figure 36. While the spectra shapes showed some differences for the different bypass ratio groupings, there did not appear to be a quantifiable trend.

The effect of fan tip Mach number on spectra shape was examined as shown in Figure 37. There was some difference in the higher frequency rolloff rate for subsonic and supersonic tip speeds, but this difference was not incorporated into the correlation

The spectra shape characteristics of the various engines in the correlation were compared by curve fitting all of the power points for each particular engine, as shown in Figure 38. Engine to engine differences were seen, but there was no obvious, simple geometry or performance parameter the seemed to control these differences.

5.2.1.3 Directivity Shape

The normalized directivity shape was derived by plotting normalized overall sound pressure levels versus emission angle, as shown in Figure 39. The normalized overall sound pressure level was defined as the overall sound pressure level (at the particular angle) minus the overall sound power level. Two directivity shapes were derived; one for subsonic fan tip speeds and one for supersonic fan tip speeds.

For this correlation it was felt that a "cluster-to-cluster" connecting of points was a better representation of the correlation than a least squares curve fit.

5.2.2 Tone Subcomponent

The aft-radiated fan tone noise prediction is based on an empirical correlation as shown in Figure 40 and Figure 41. The predicted tone level is the sum of the appropriate sound pressure level (as a function of harmonic number and fan tip Mach number) and directivity adjustment (as a function of harmonic number, fan tip Mach number, and emission angle), corrected to the appropriate fan diameter by 20 log (fan diameter / 1 foot).

5.3 Assessment

The data used for assessment of the AFTFN7 module consisted of nine different engine data sets. These data sets included 108 individual power points, of which 48 were for bypass ratios greater than eight.

5.3.1 Broadband Subcomponent

The accuracy of the AFTFN7 broadband noise predictions was examined both on the basis of individual spectra comparisons and on the basis of averaged, normalized spectra comparison.

Comparisons of individual predicted spectra and modeled-data spectra, for selected power points, are shown in Figure 42 through Figure 50. From each of the nine engine data sets, power points were chosen that represented: a relatively low power point; a medium power point; and a relatively high power point.

In addition, spectra from all the 108 power points were incorporated into smoothed, averaged, normalized spectra in order to present an overall measure of the accuracy of the procedure (Figure 51 through Figure 53). These spectra were normalized by referencing the third-octave frequency band to the blade passing frequency (i.e., 10log[1/3-octave freq. band / bpf]). Once normalized, the spectra were grouped and fitted with a third order curve. In addition to considering all the power points in one grouping, comparisons were made using only data for bypass ratios greater than eight.

For both the individual and the averaged spectra comparisons, results are shown for static, 150-foot polar arc, free-field data for three emission angles: 90, 120, and 150 degrees relative to the inlet axis.

The following observations regarding the aft fan broadband predictions are made based on the averaged spectra comparisons:

- The prediction trends for the higher bypass ratios (greater than eight) are similar to those for the lower bypass ratios.
- The peak sound pressure level is well predicted, generally to within 1 db.

- The peak frequency band is well predicted.
- The spectra shape is fairly well predicted. These averaged spectra show a maximum difference between predicted and modeled levels of 5 db, and generally within 3 db, over the frequency range of interest.
- The prediction accuracy is reasonably consistent for the various power points and angles examined.

5.3.2 Tone Subcomponent

The accuracy of the AFTFN7 tone noise predictions was examined on the basis of individual spectra comparisons. Comparisons of predicted spectra and modeled-data spectra, for selected power points, are shown in Figure 54 through Figure 62. From each of seven engine data sets, power points were chosen that represented: a relatively low power point; a medium power point; and a relatively high power point. The comparisons are shown for static, 150-foot polar arc, free-field data for three emission angles: 90, 120, and 150 degrees relative to the inlet axis.

The following observations regarding the aft fan tone predictions can be made from these comparisons:

- The fundamental and first harmonic are overpredicted in most cases (about two-thirds of the time).
- In about half the cases the fundamental and first harmonic are predicted to within approximately 6 db of the modeled measurements.
- There is no evident correlation of inlet tone prediction accuracy with either angle or power level.

6 Jet Noise

This section discusses the noise generated by the jet exhaust flow.

6.1 Noise Source Mechanisms

Jet exhaust noise is comprised of turbulent mixing noise, shock-associated noise, and noise due to the installation effects of the engine on the airframe. These subcomponents are described in this section.

6.1.1 Turbulent Mixing Noise Subcomponents

The jet mixing noise is generated from the mixing associated with three flow streams; the primary (core or inner) flow stream; the secondary (fan or outer) flow stream, and the mixed (or merged) flow stream.

The noise in the primary jet region is generated by the turbulent mixing of the primary and secondary flows. Similarly, the noise in the secondary jet region is generated by the turbulent mixing of the secondary and the ambient flows.

The mixed jet flow stream refers to the merged primary and secondary flow streams, although there is no clear boundary defining the transition of these separate flows into a mixed flow. The noise in this region is generated by the turbulent mixing of the merged and the ambient flows.

6.1.2 Shock-associated Subcomponent

Shock-associated noise is believed to be generated by the large-scale turbulent structures in the mixing layer interacting with the quasi-periodic shock cells of an improperly expanded jet. This localized deformation of the shock wave results in the emission of sound. Unlike screech tones, this noise is broadband, although strongly peaked.

6.1.3 Jet Installation Effects

The installation of an engine on an airframe affects the jet noise component. These effects include the acoustic effect of the jet exhaust flow interacting with airplane wing surfaces and the effect of noise reflecting off the wing surfaces.

6.2 Procedure Development

The jet noise prediction module is known as JEN6E. The development of the procedure is described in this section.

6.2.1 Turbulent Mixing Noise Subcomponents

The JEN6E turbulent mixing subcomponent modules are based on Reference 2, and also discussed in Reference 3, and are summarized here. JEN6E is a standard method in SAE ARP 876, appendix C, for the calculation of subsonic coaxial jet noise.

While the prediction method was empirically derived, consideration was given to the physics of the jet noise generation and propagation processes in selecting the correlation parameters for the data. The values of the empirical parameters were based primarily on model jet noise and source location data. Full-scale static engine data and flight test data were also used to assess the formulation and to modify some of the parameters as appropriate.

The coaxial jet is conceptually divided into the three source regions described in Section 6.1.1. The empirical expressions for each of the subcomponents of the jet are comprised of three parts:

1. the basic one-third octave band sound pressure level associated with the shear layer velocity differences, the turbulent eddy convection velocities, and the ambient flow effects;
2. normalization factors associated with ambient pressure, density (or temperature), spherical divergence, geometric and acoustic near-field effects, atmospheric attenuation, and external plug effects;
3. the effects of internal acoustic excitation.

The basic formula for the calculation of the sound pressure level for each of these subcomponents can be expressed as:

$$spl = [Z1 \log (FV + Z2] * [\log (S) - Z3 \log (FV) - Z4]^2 + Z5 \log (FV) + Z6$$

The source strength function, FV, is a function of non-dimensional (referenced to the ambient speed of sound) shear layer velocity difference, eddy convection velocity, and the ambient flow effects. It also includes the scaling of sound pressure level with the jet and ambient flow acoustic Mach numbers (i.e., flight effects). The various coefficients (Z1 through Z6) and the source strength for each subcomponent is calculated by using the appropriate values for the velocity (primary, secondary, or mixed), jet diameter (primary or mixed), and Strouhal number. The Strouhal number for each subcomponent is defined using the shear velocity layer velocity difference, the subcomponent jet diameter and source frequency. All the coefficients (Z1 through Z6) are more directivity dependent than Strouhal number dependent. The expression for Z6 includes a normalization factor and an acoustic excitation adjustment. Each of the subcomponent sources has its own source location distribution associated with it.

6.2.2 Shock-associated Subcomponent

The JEN6E shock-associated noise subcomponent module is based Reference 4, and the coding logic is taken from Reference 5.

6.2.3 Jet Installation Effects

When a jet noise prediction is made for an installed engine, an additional term is included to account for the interaction of the jet exhaust flow with the wing surfaces.

6.3 Assessment

The data used for assessment of the JEN6E module consisted of seven different engine data sets. These data sets included 104 individual power points, of which 19 were for bypass ratios greater than eight.

As discussed in Section 3.1.1, the aft-arc spectra are assumed to be set exclusively by jet noise in the low frequencies, and the exact number of frequency bands that is attributed exclusively to jet noise is a function of radiation angle and primary jet velocity. Thus the assessment of the accuracy of the jet noise prediction is based on the examination of the low-frequency portion of the aft-arc spectra.

Comparisons of predicted spectra and modeled-data spectra, for selected power points, are shown in Figure 63 through Figure 71. From each of seven engine data sets, power points were chosen that represented: a relatively low power point; a medium power point; and a relatively high power point. The comparisons are shown for static, 150-foot polar arc, free-field data for three emission angles: 90, 120, and 150 degrees relative to the inlet axis.

The following observations regarding the jet noise predictions can be made from these comparisons:

- The jet noise levels are generally well predicted (within one or two db) for the medium- and high-power points, with only a couple exceptions.
- The low power points tend to be underpredicted, typically on the order of five db.
- The prediction accuracy is consistent over the angular range of interest.

7 Concluding Remarks

The Windows/PC version of the Modular Engine Noise Component Prediction System (MCP) provides a good tool for the estimation of turbofan engine noise. The program runs on a readily-available computer platform and has an easy-to-use interface. The predictions can be made from a relatively simple set of geometry and performance input parameters. The modular structure of the program allows for future modification and expansion.

The aft fan broadband noise and the jet noise were shown to be well predicted by the program. The inlet broadband noise and the tone levels tend to be overpredicted.

Several recommendations for future development result from the present study:

- As more measured data become available, they should be incorporated into the existing prediction modules. Of particular interest is including a wider range of configurations into the empirical database. This would include such features as compound swept fan blades and jet nozzles with mixing enhancers.
- Additional and alternative correlating parameters should be examined for the empirical prediction formulations. This is particularly important if a wider range of configurations are incorporated as mentioned above.
- Additional prediction modules should be added. This could include compressor, turbine, core, and airframe modules.
- To aid in the development of the component-modeled measurements that are necessary for developing the prediction modules, a set of static test guidelines should be adopted. This would include such things as taking narrowband noise data; measuring a hardwall (no acoustic treatment) configuration, and making measurements with forward/aft acoustic barriers in place.
- An assessment should be done on the accuracy of the predictions for flight-over noise levels. If necessary, modifications should be made for improved flight effects calculations.

8 Acknowledgments

Recognition is due to numerous people who contributed to this study. Guidance on the development of the prediction procedures came from Eric Nesbitt, Ulrich Ganz, Belur Shivashankara, Jerry Bielak, Srini Bhat, and Jim Reed, all of the Boeing acoustics group. Migration of the existing program from the Unix environment to the PC/Windows environment, development of the graphical user interface, and coding of the modifications to the prediction modules were done Dan McGregor, Ken Fowler, and Mike Reed, all of the Boeing computing group. The manager of the project for Boeing was Dave Reed.

General Electric and Pratt and Whitney generously allowed the use of their data for this study. Support and guidance were provided by Doug Matthews of Pratt and Whitney and Phil Gliebe of General Electric.

Finally, task management guidance was provided Bob Golub and John Rawls of the NASA-Langley Research Center.

9 References

1 Nesbitt, E. H., Ganz, U. W., Diamond, J. A., and Kosanchick III, M., "An Empirical Prediction of Inlet Radiated Broadband Noise From Full Scale Engines," AIAA 98-0470, 36th Aerospace Sciences Meeting & Exhibit, January 1998.

2 Lu, H. Y., "An Empirical Model for Prediction of Coaxial Jet Noise in Ambient Flow," AIAA 86-1912, 10th Aeroacoustics Conference, July 1986.

3 Bhat, Thonse R. S., "Co-Annular Jet Noise Model Development," NASA Contractor Final Report, Contract NAS1-20267, Task 17, Subtask 1, 1998.

4 Harper-Bourne, M., and Fisher, M. J., "The Noise from Shock Waves in Supersonic Jets," *Proceedings of the AGARD Conference on Noise Mechanisms, AGARD CP-131*, 1973.

5 Tanna, H. K., "Prediction Method for Shock-Associated Noise from Convergent Nozzles at Supercritical Conditions," proposal to SAE A21 Jet Exhaust Noise Subcommittee, July 19, 1977.

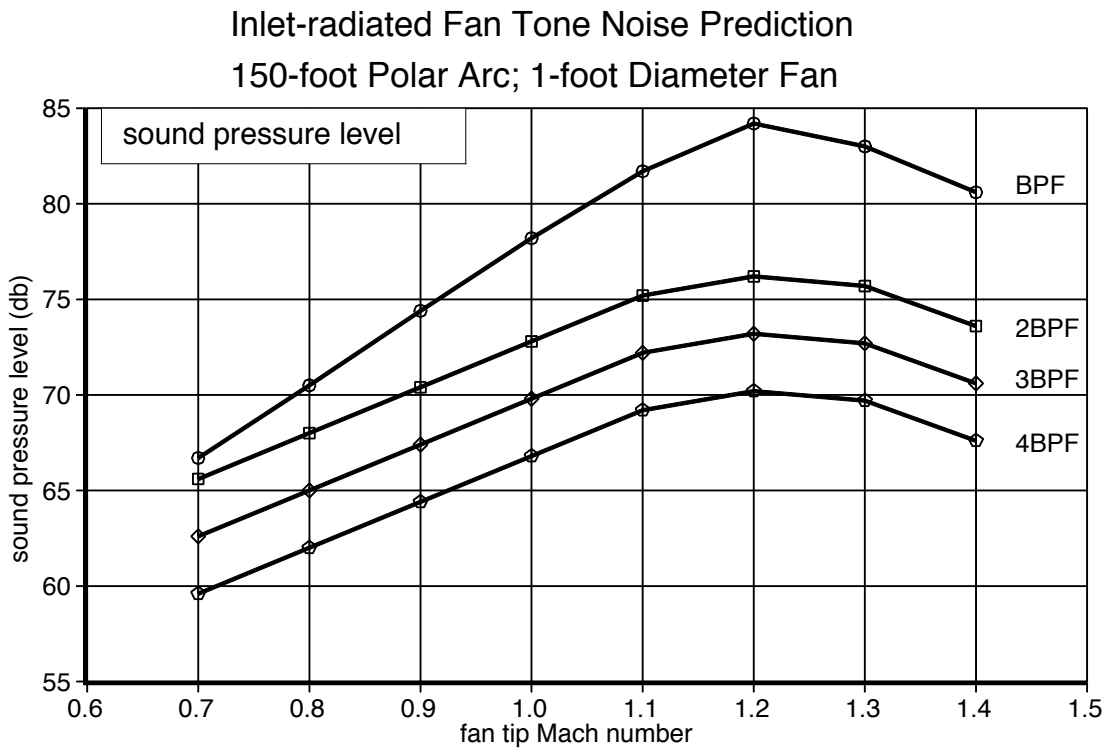

fan tip Mach number	sound pressure level (db)			
	BPF	2BPF	3BPF	4BPF
0.7	66.7	65.6	62.6	59.6
0.8	70.5	68.0	65.0	62.0
0.9	74.4	70.4	67.4	64.4
1.0	78.2	72.8	69.8	66.8
1.1	81.7	75.2	72.2	69.2
1.2	84.2	76.2	73.2	70.2
1.3	83.0	75.7	72.7	69.7
1.4	80.6	73.6	70.6	67.6

Figure 1 Inlet-radiated Fan Tone Noise Prediction – Sound Pressure Levels

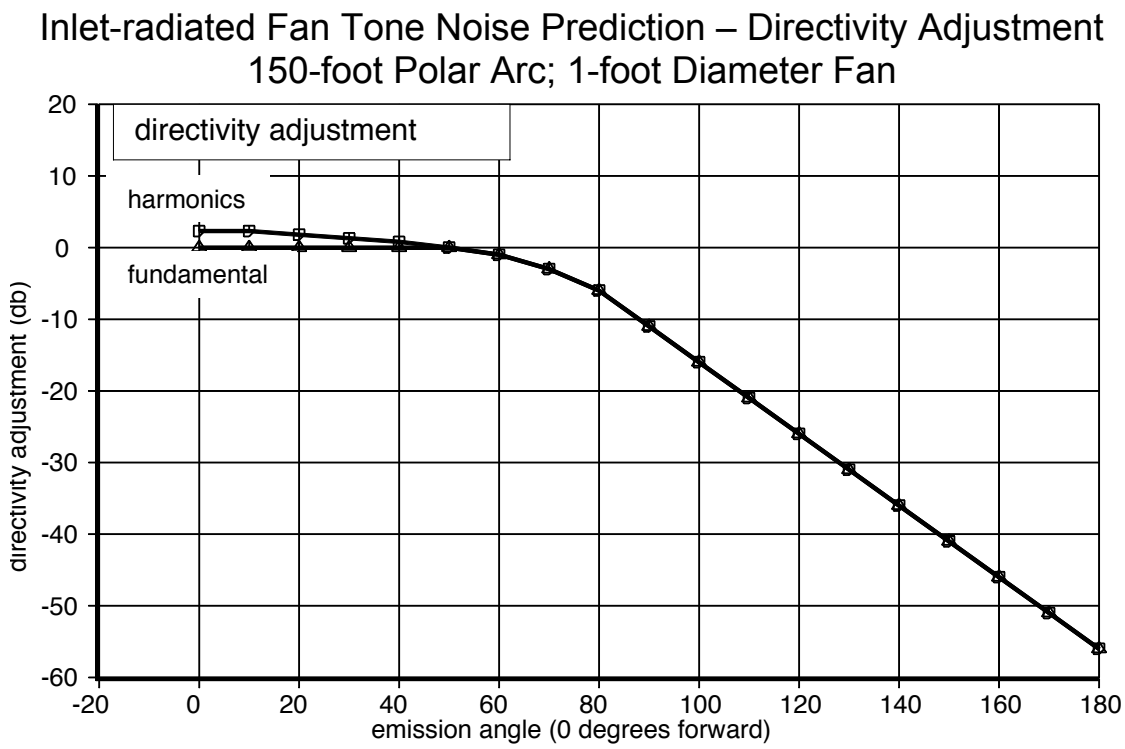

emission angle (0 degrees forward)	directivity adjustment (db)	
	fundamental	harmonics
0	0	2.3
10	0	2.3
20	0	1.8
30	0	1.3
40	0	0.8
50	0	0
60	-1	-1
70	-3	-3
80	-6	-6
90	-11	-11
100	-16	-16
110	-21	-21
120	-26	-26
130	-31	-31
140	-36	-36
150	-41	-41
160	-46	-46
170	-51	-51
180	-56	-56

Figure 2 Inlet-radiated Fan Tone Noise Prediction – Directivity Adjustments

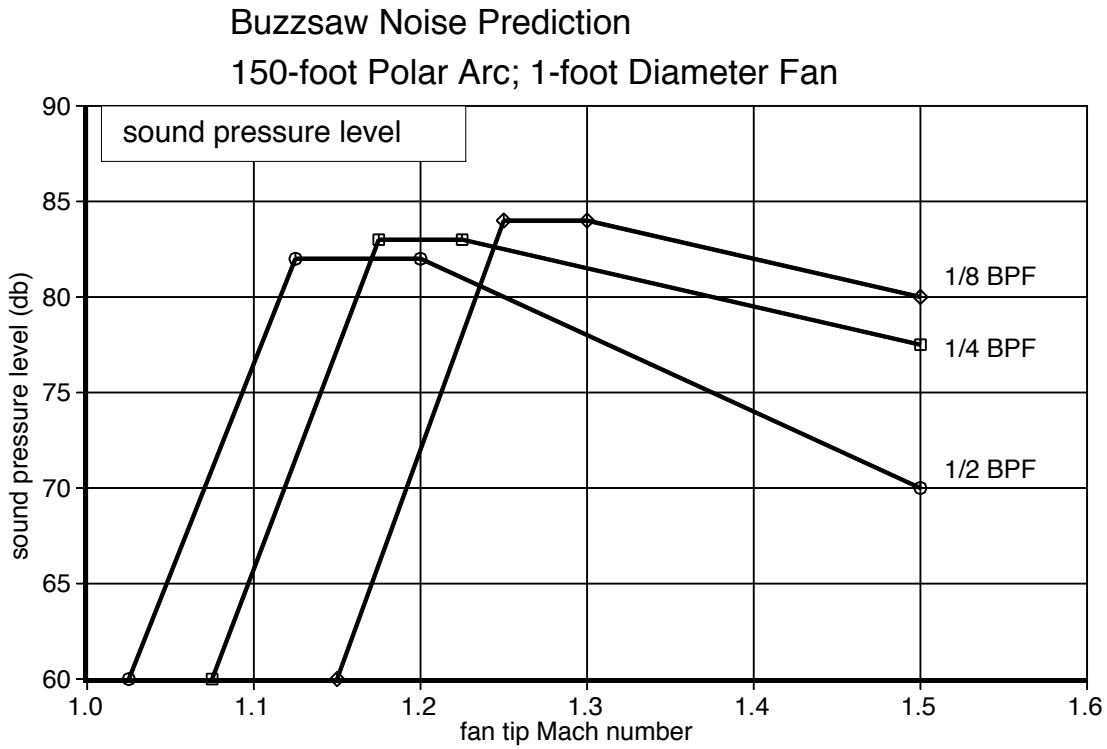

fan tip Mach number	sound pressure level (db)		
	1/2 BPF	1/4 BPF	1/8 BPF
1.025	60		
1.075		60	
1.125	82		
1.150			60
1.175		83	
1.200	82		
1.225		83	
1.250			84
1.300			84
1.500	70	77.5	80

Figure 3 Buzzsaw Noise Prediction – Sound Pressure Levels

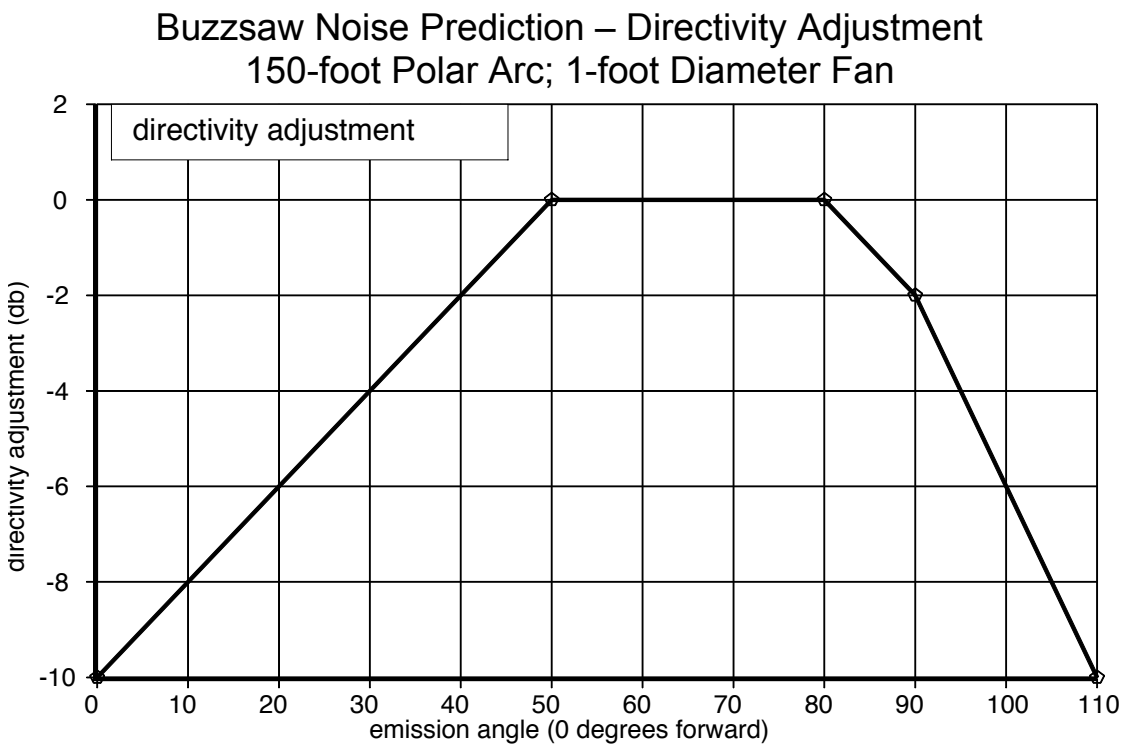

emission angle (0 degrees forward)	directivity adjustment (db)
0	-10
50	0
80	0
90	-2
110	-10

Figure 4 Buzzsaw Noise Prediction – Directivity Adjustments

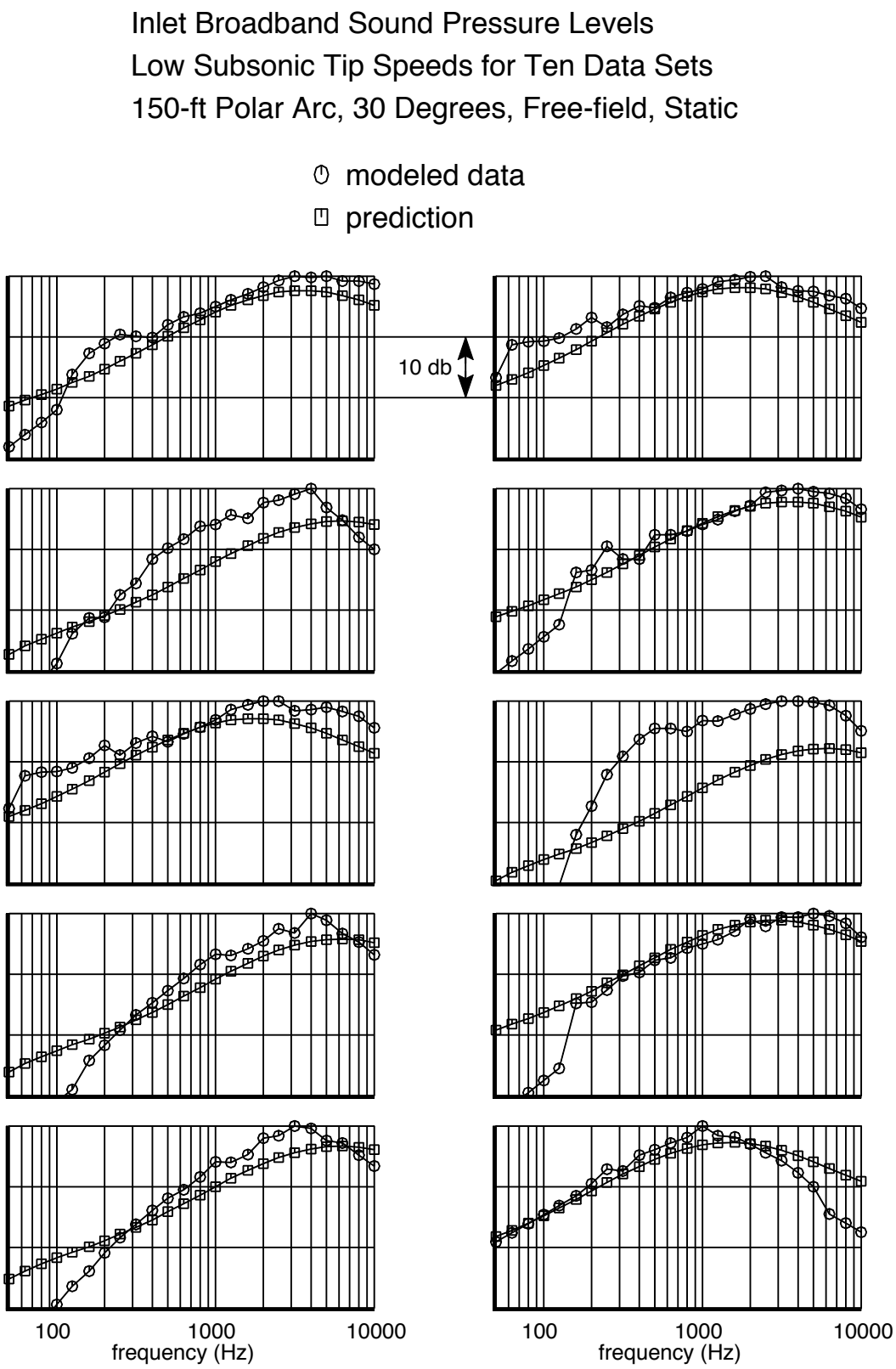

Figure 5 Inlet Broadband Comparison at Low Subsonic Tip Speed and 30 Degrees

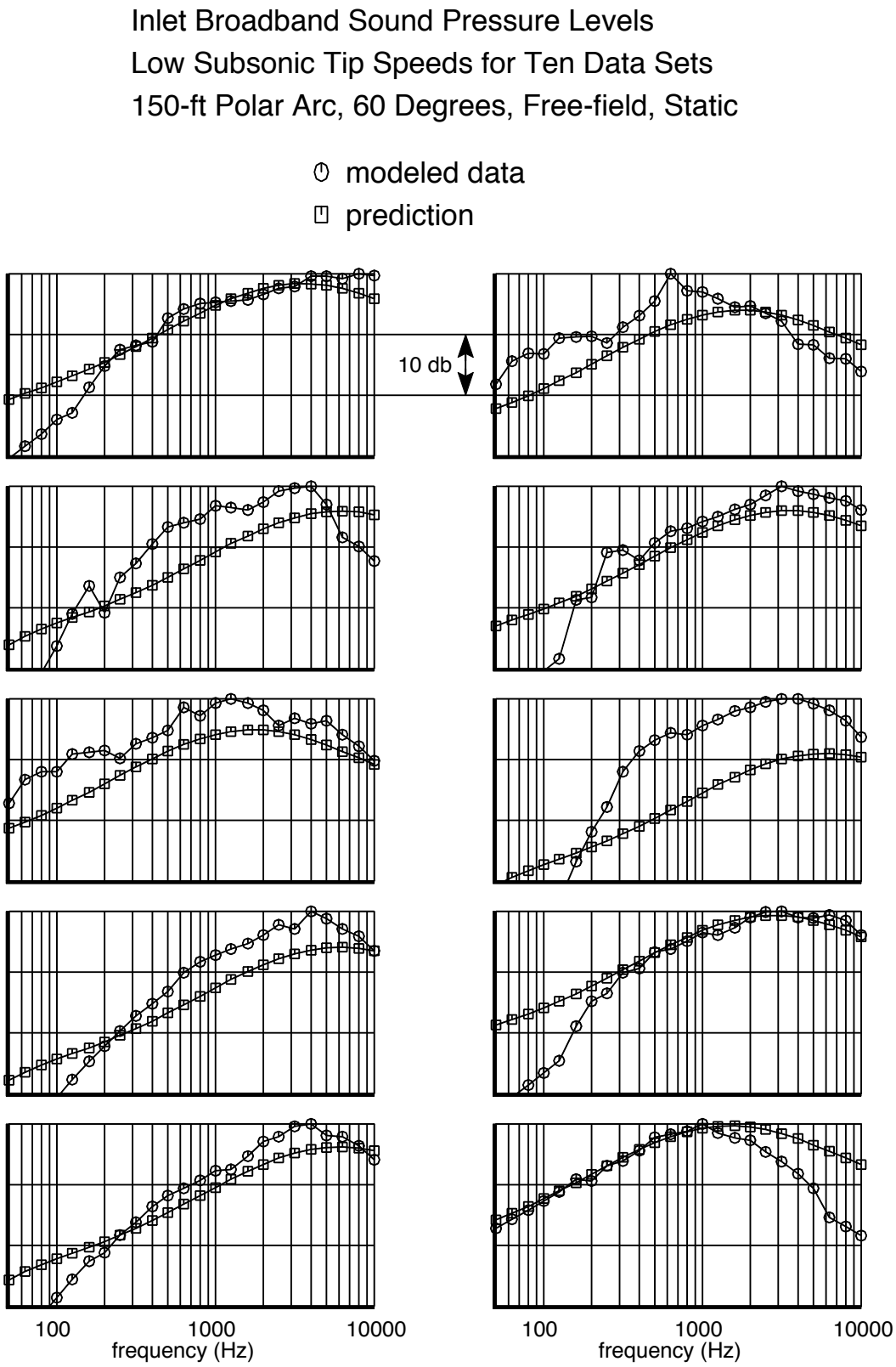

Figure 6 Inlet Broadband Comparison at Low Subsonic Tip Speed and 60 Degrees

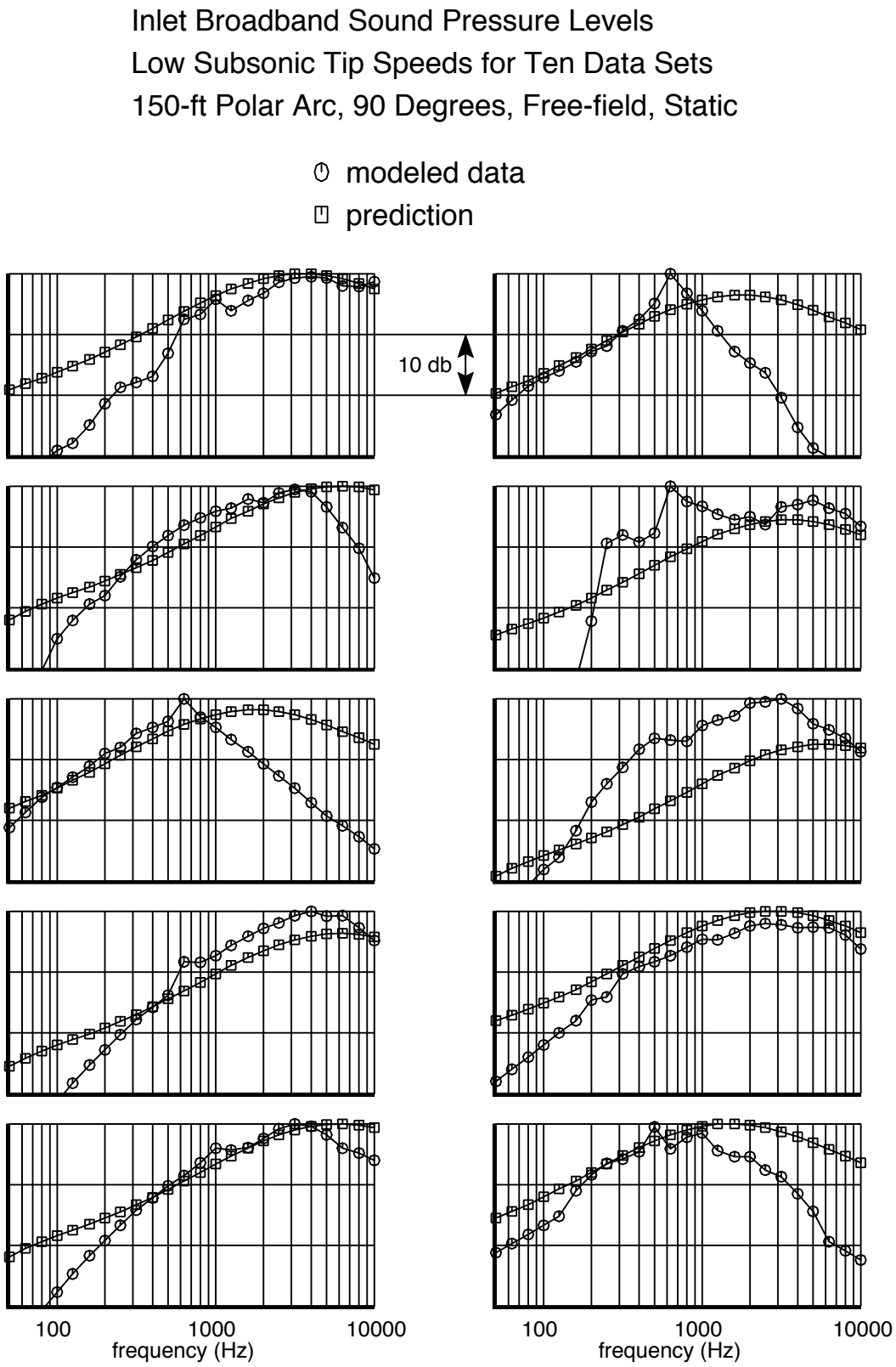

Figure 7 Inlet Broadband Comparison at Low Subsonic Tip Speed and 90 Degrees

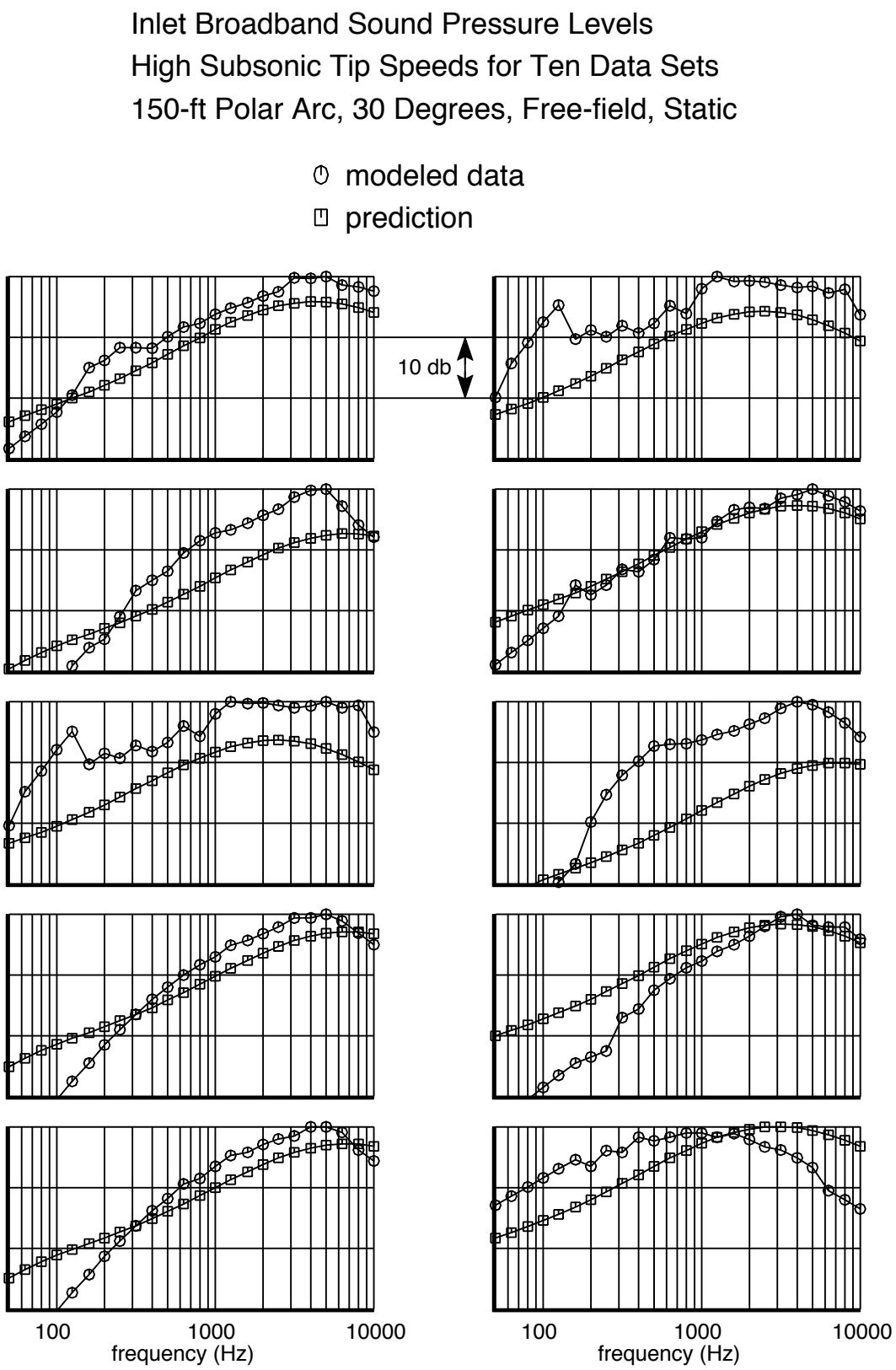

Figure 8 Inlet Broadband Comparison at High Subsonic Tip Speed and 30 Degrees

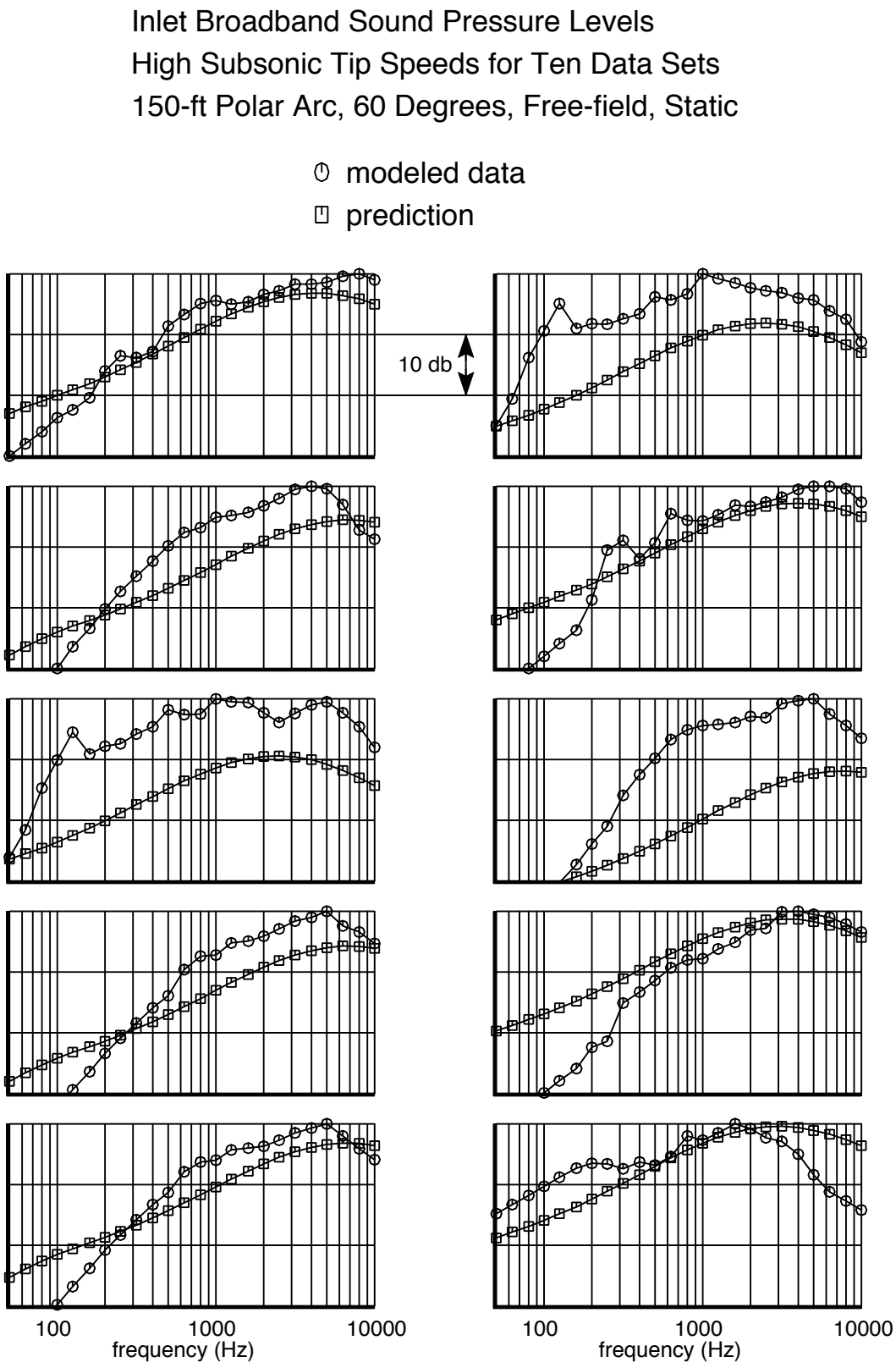

Figure 9 Inlet Broadband Comparison at High Subsonic Tip Speed and 60 Degrees

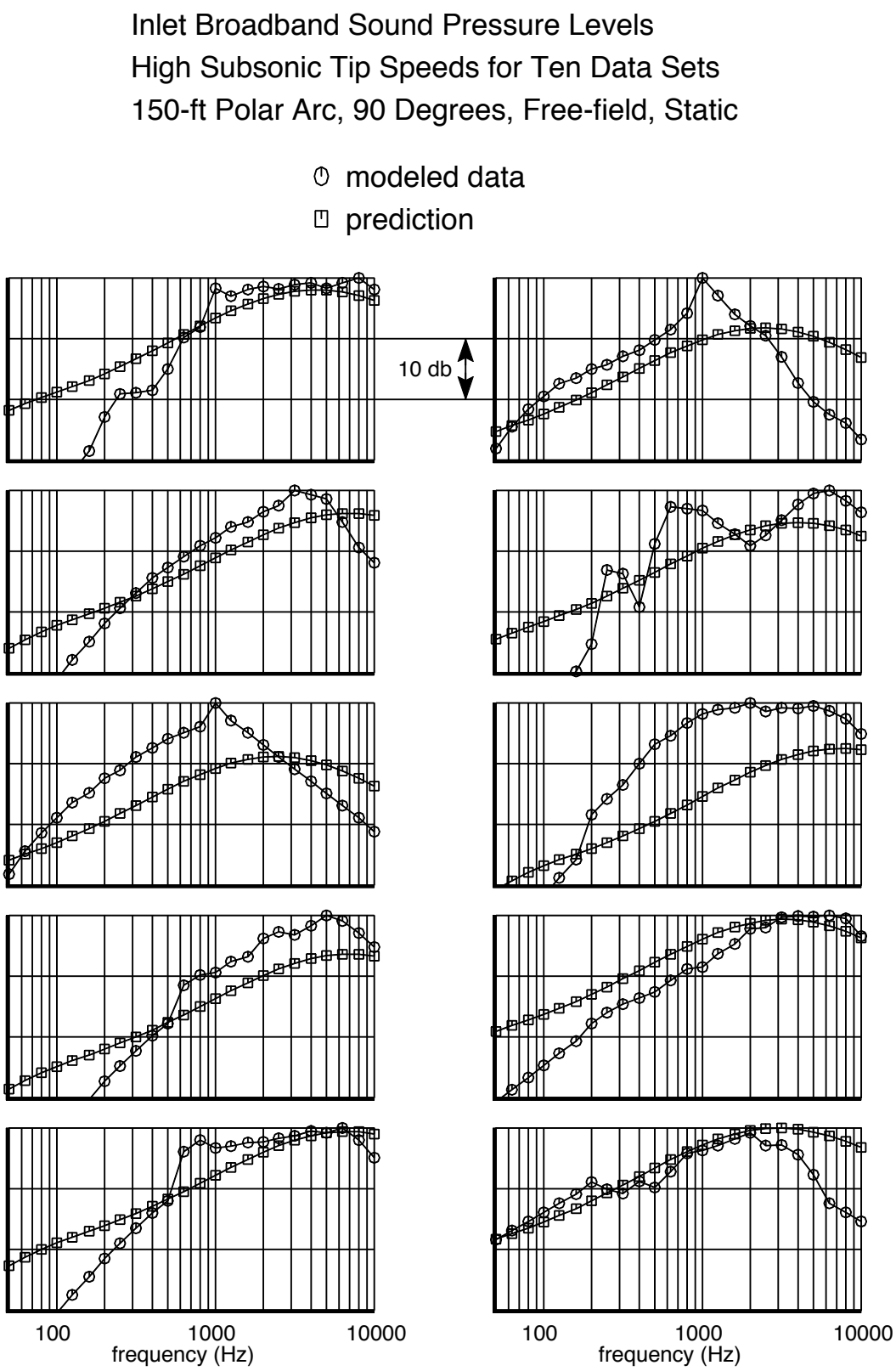

Figure 10 Inlet Broadband Comparison at High Subsonic Tip Speed and 90 Degrees

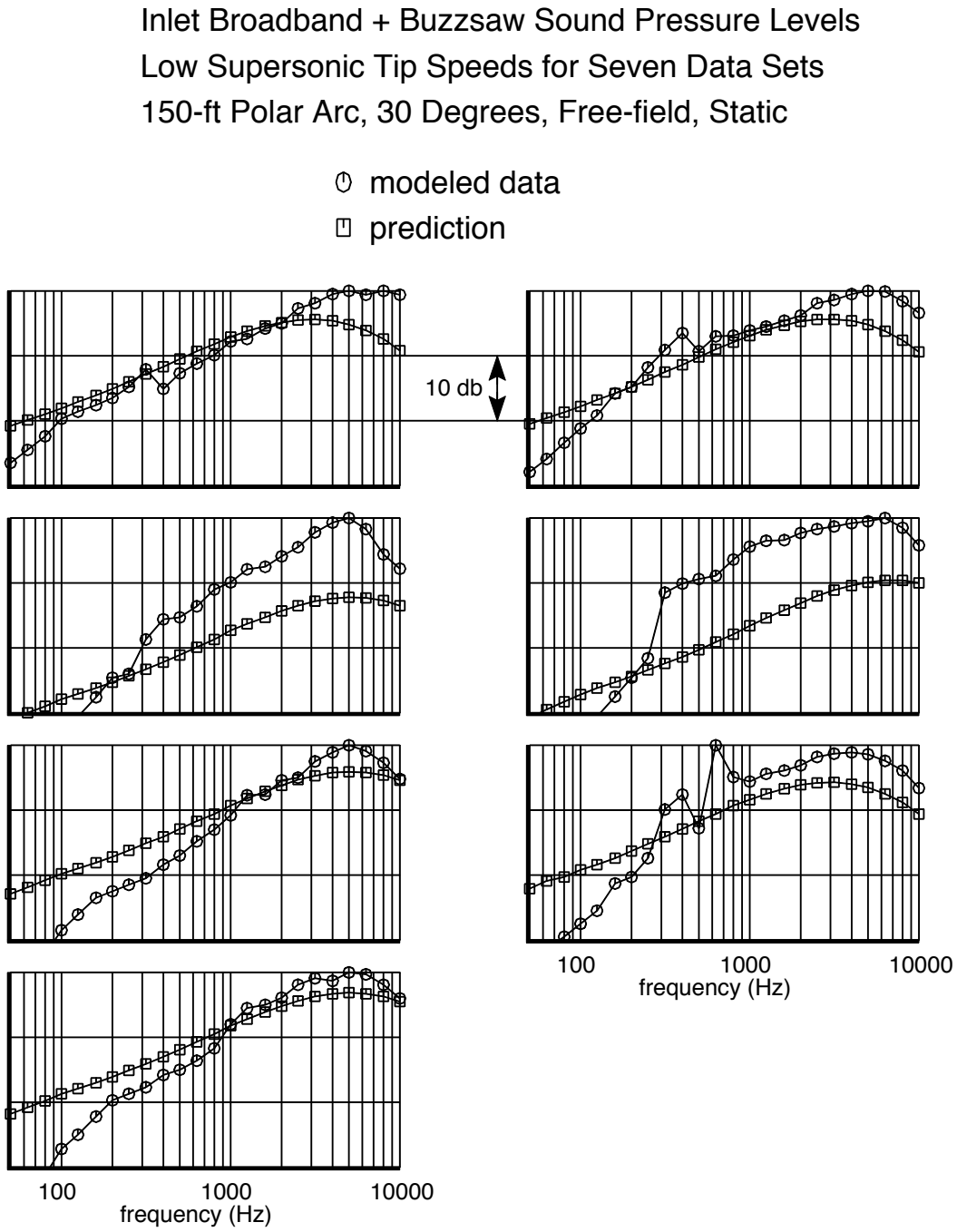

Figure 11 Inlet Broadband + Buzzsaw Comparison at Low Supersonic Tip Speed and 30 Degrees

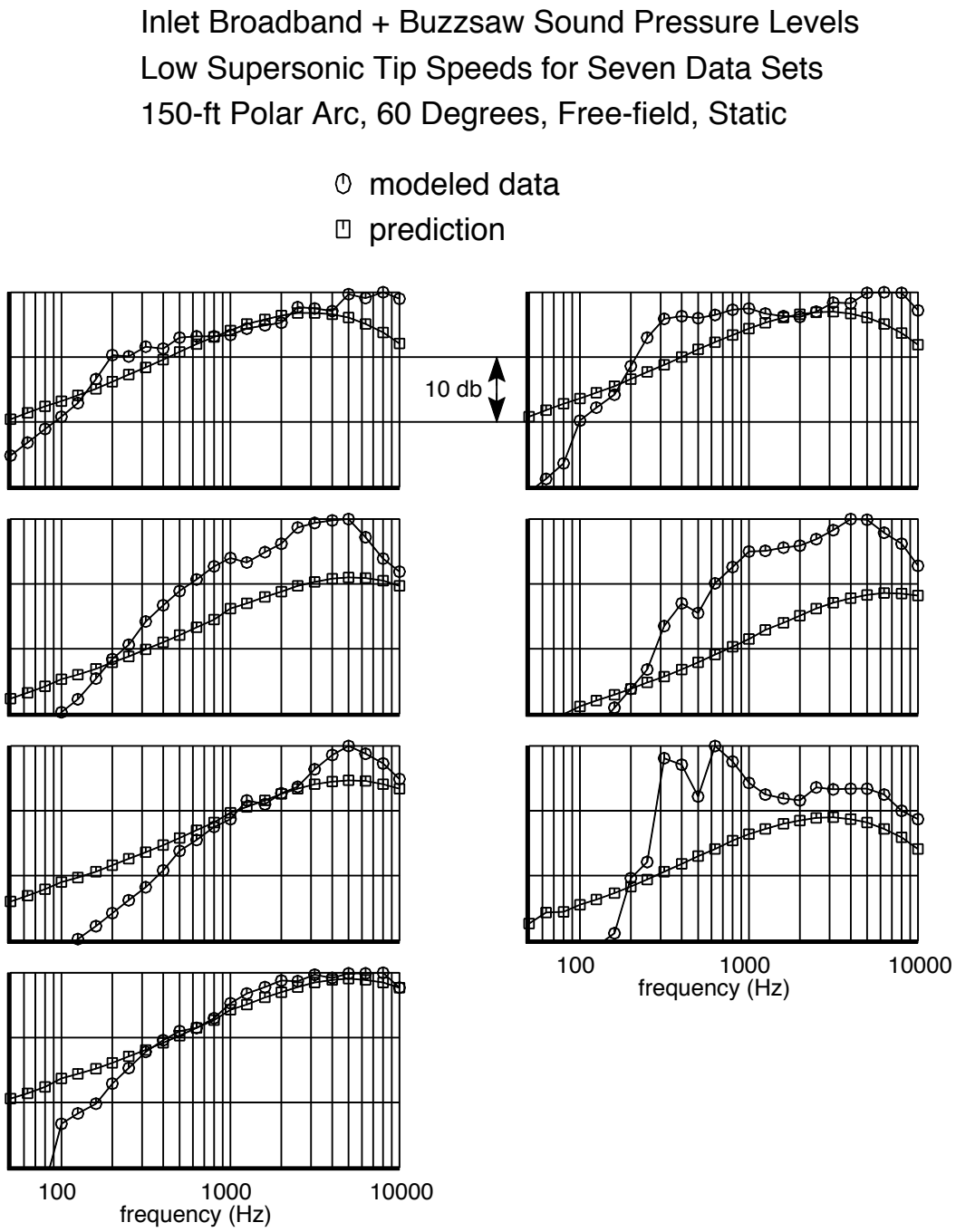

Figure 12 Inlet Broadband + Buzzsaw Comparison at Low Supersonic Tip Speed and 60 Degrees

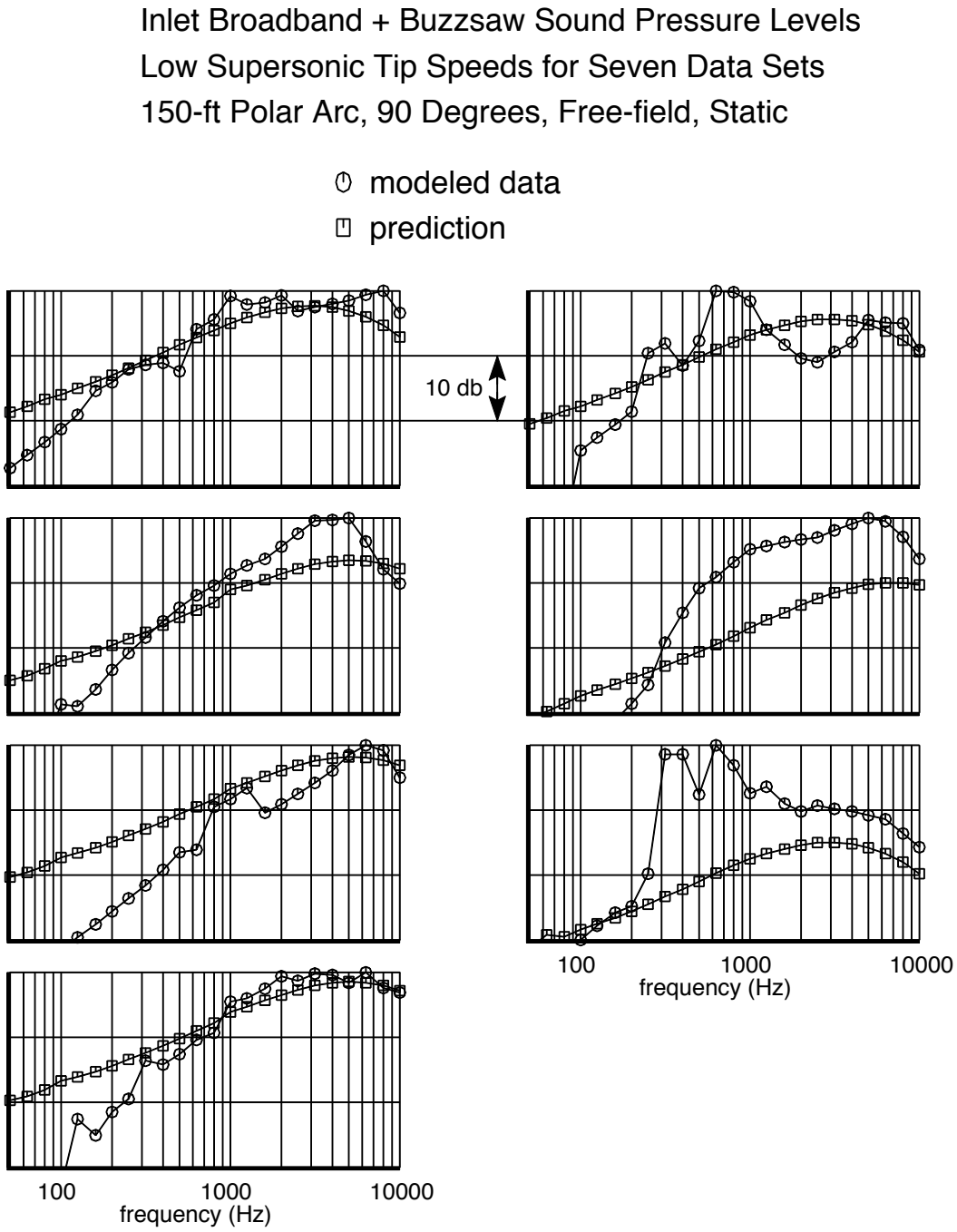

Figure 13 Inlet Broadband + Buzzsaw Comparison at Low Supersonic Tip Speed and 90 Degrees

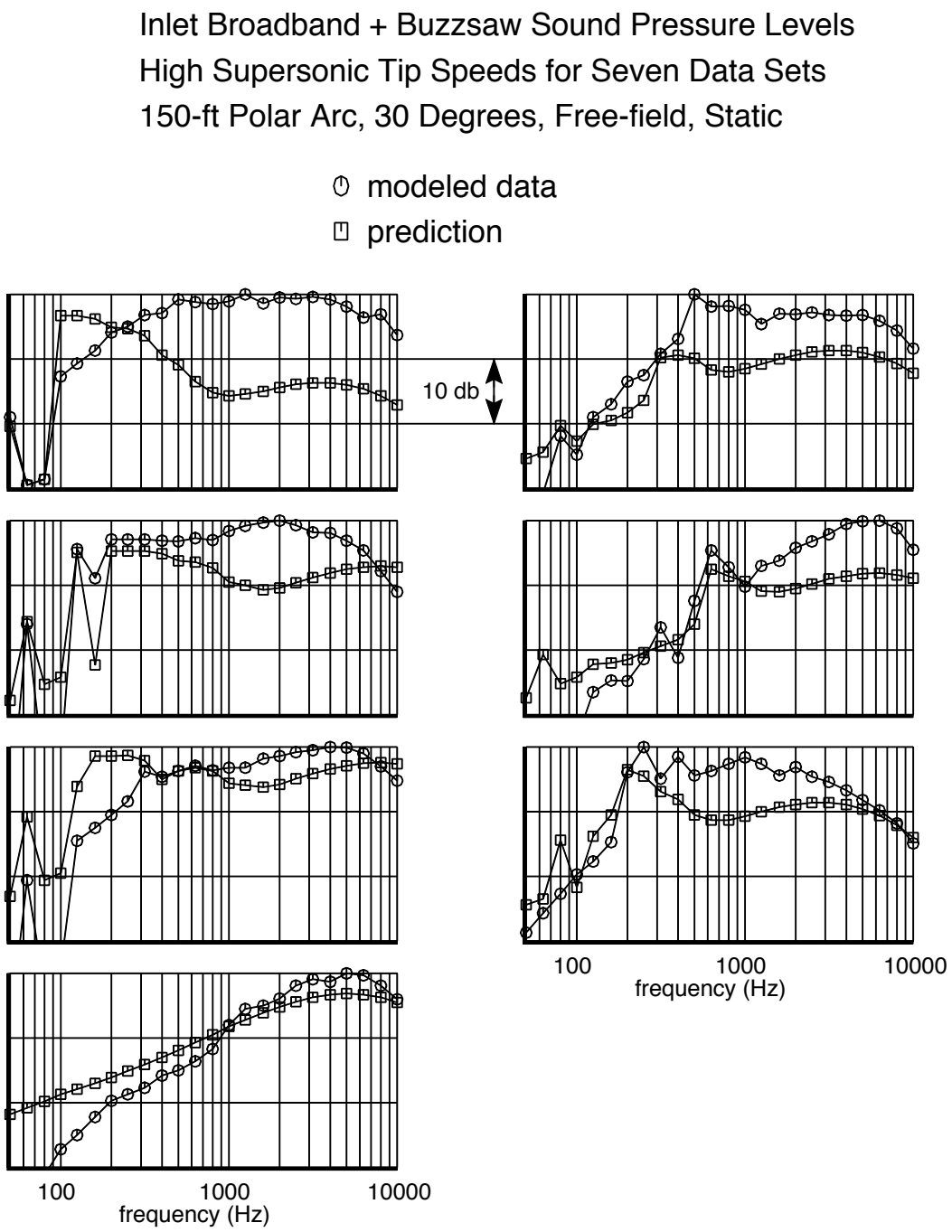

Figure 14 Inlet Broadband + Buzzsaw Comparison at High Supersonic Tip Speed and 30 Degrees

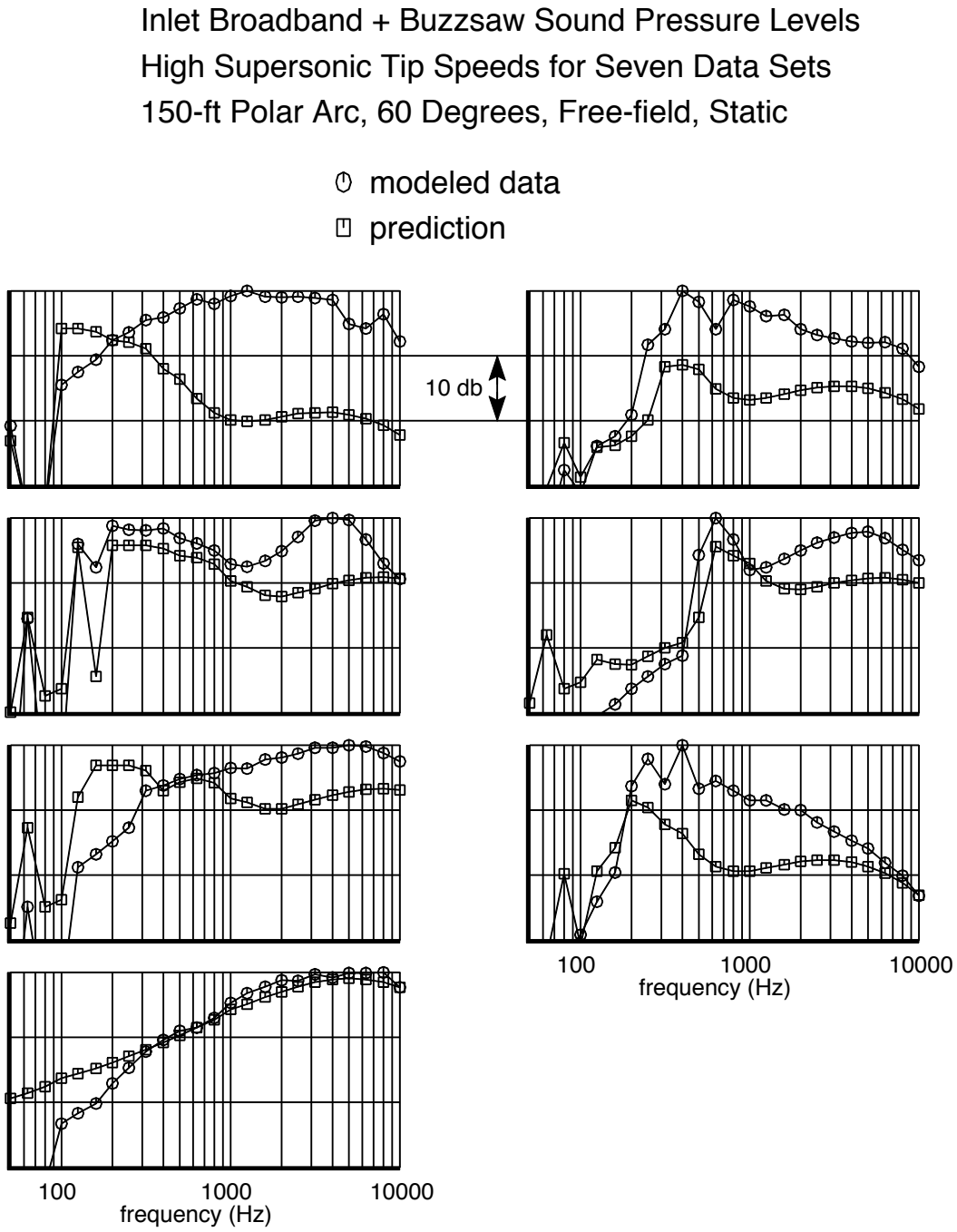

Figure 15 Inlet Broadband + Buzzsaw Comparison at High Supersonic Tip Speed and 60 Degrees

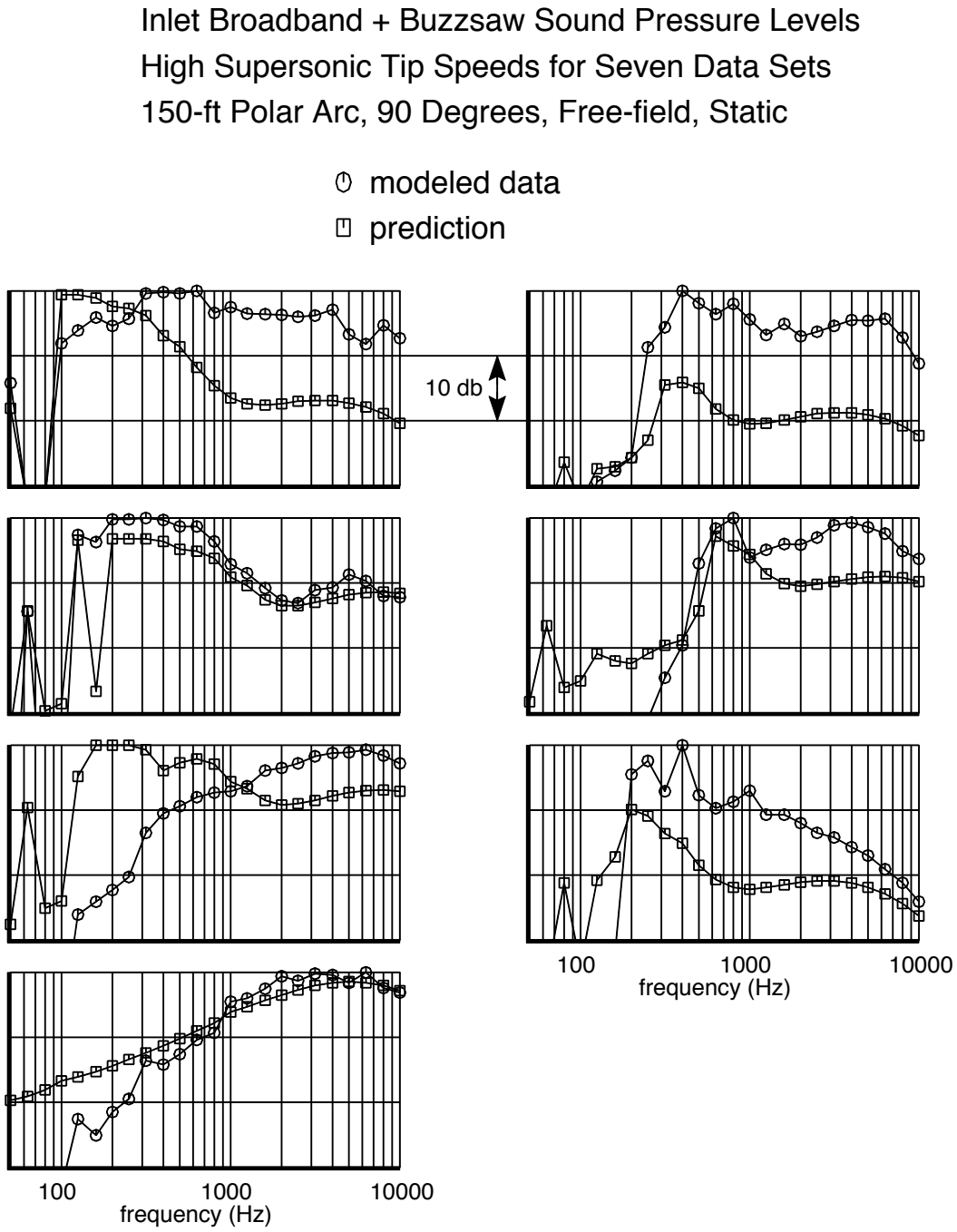

Figure 16 Inlet Broadband + Buzzsaw Comparison at High Supersonic Tip Speed and 90 Degrees

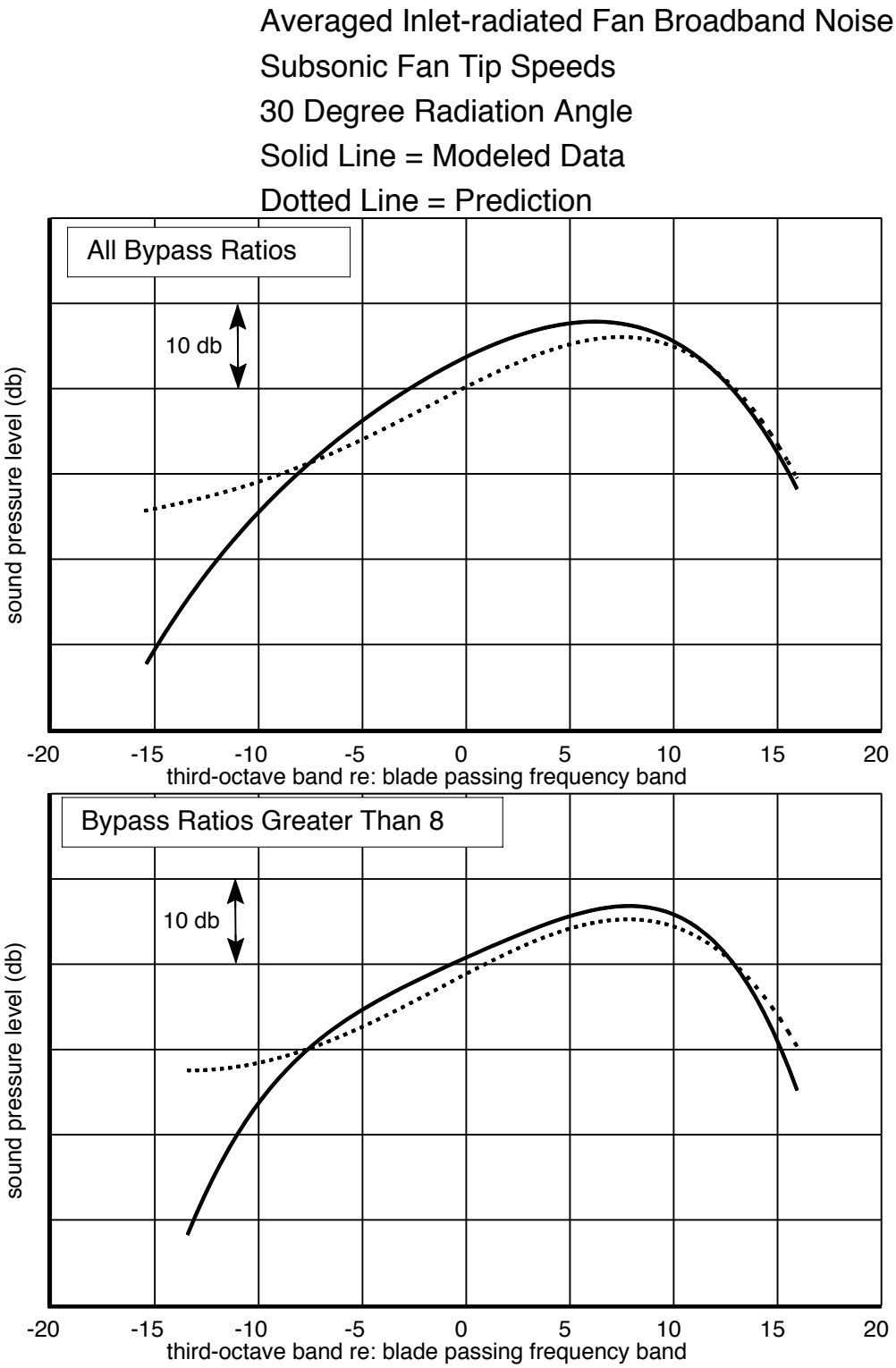

Figure 17 Averaged Inlet Broadband at Subsonic Tip Speeds and 30 Degrees

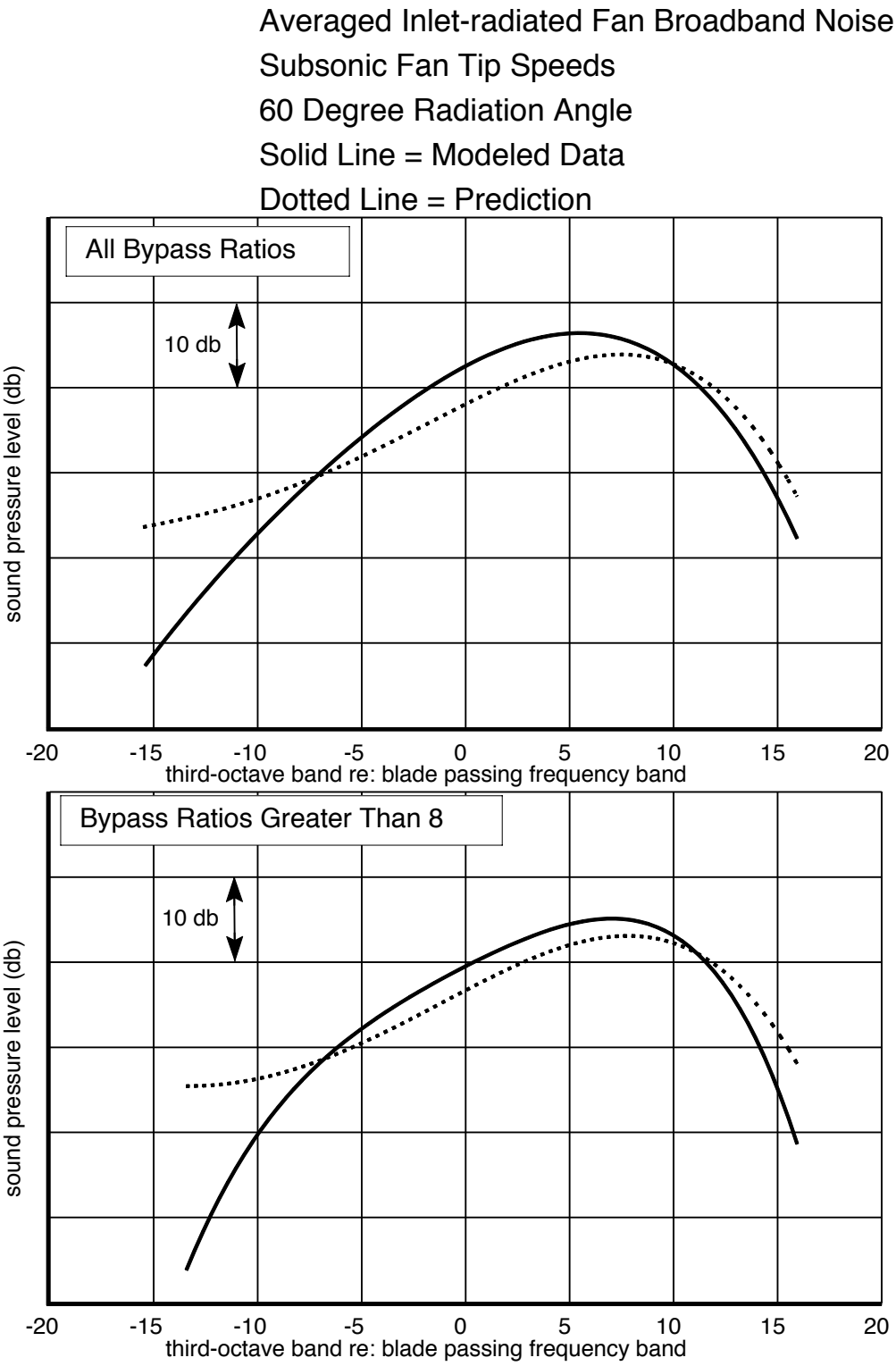

Figure 18 Averaged Inlet Broadband at Subsonic Tip Speeds and 60 Degrees

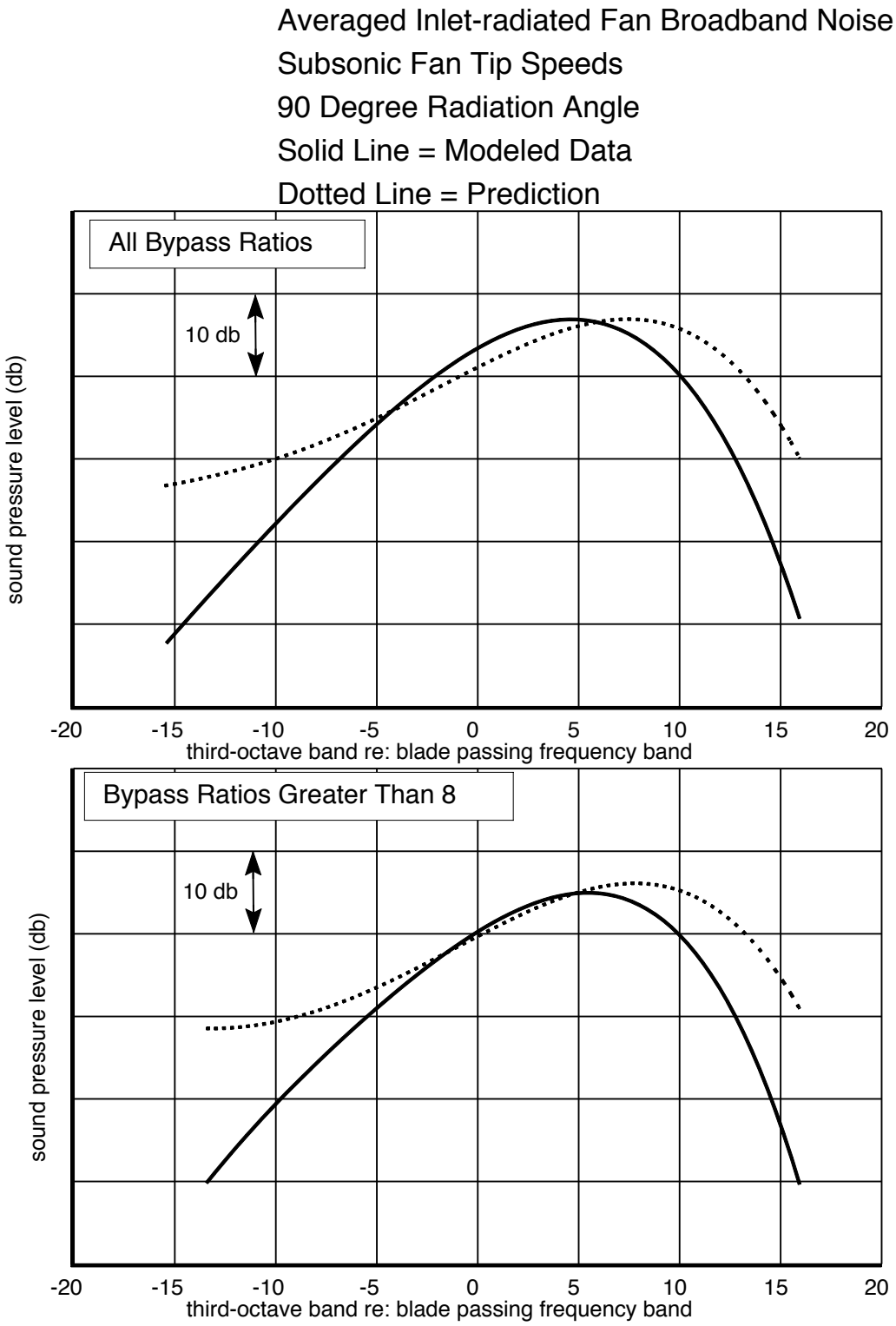

Figure 19 Averaged Inlet Broadband at Subsonic Tip Speeds and 90 Degrees

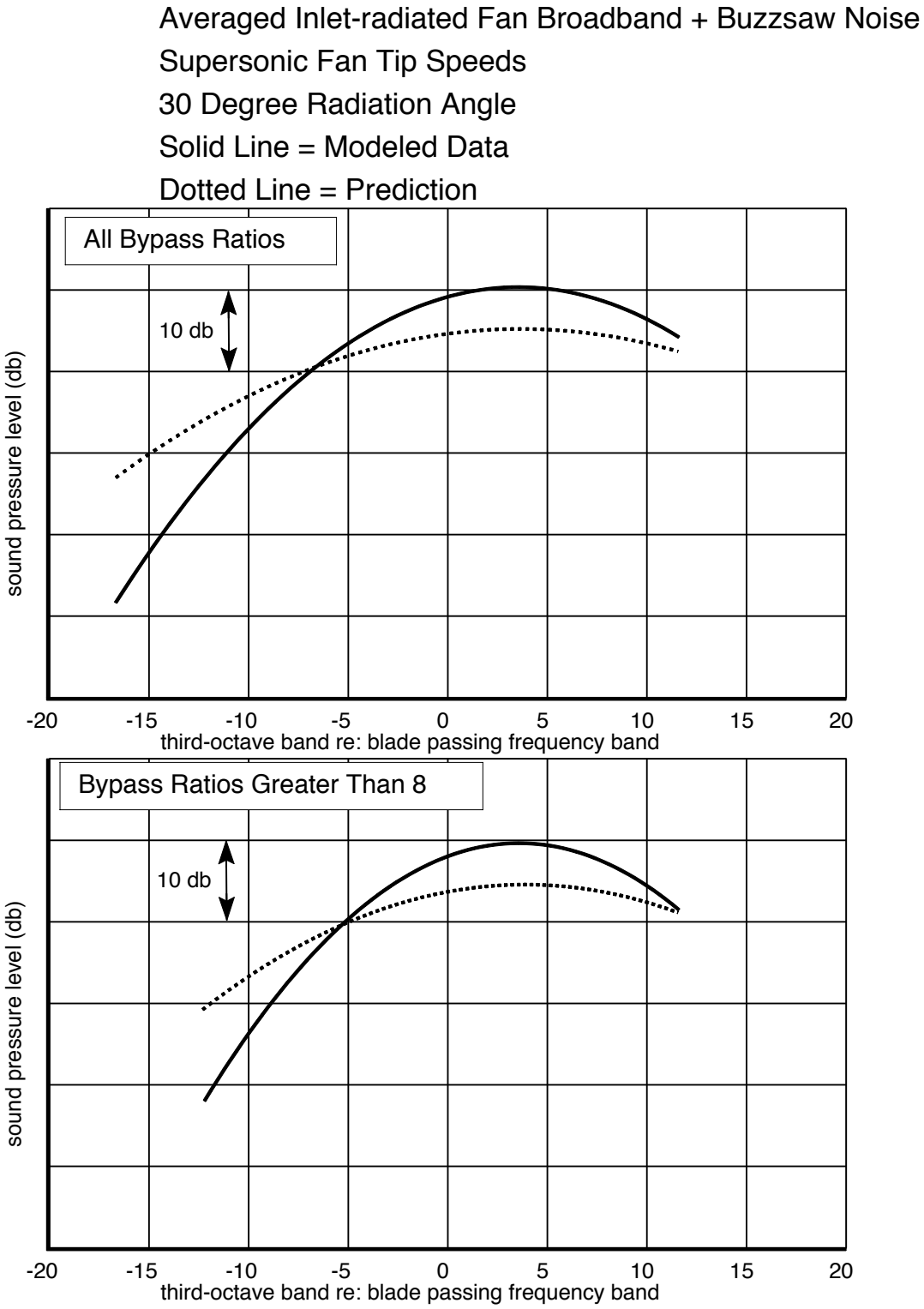

Figure 20 Averaged Inlet Broadband + Buzzsaw at Supersonic Tip Speeds and 30 Degrees

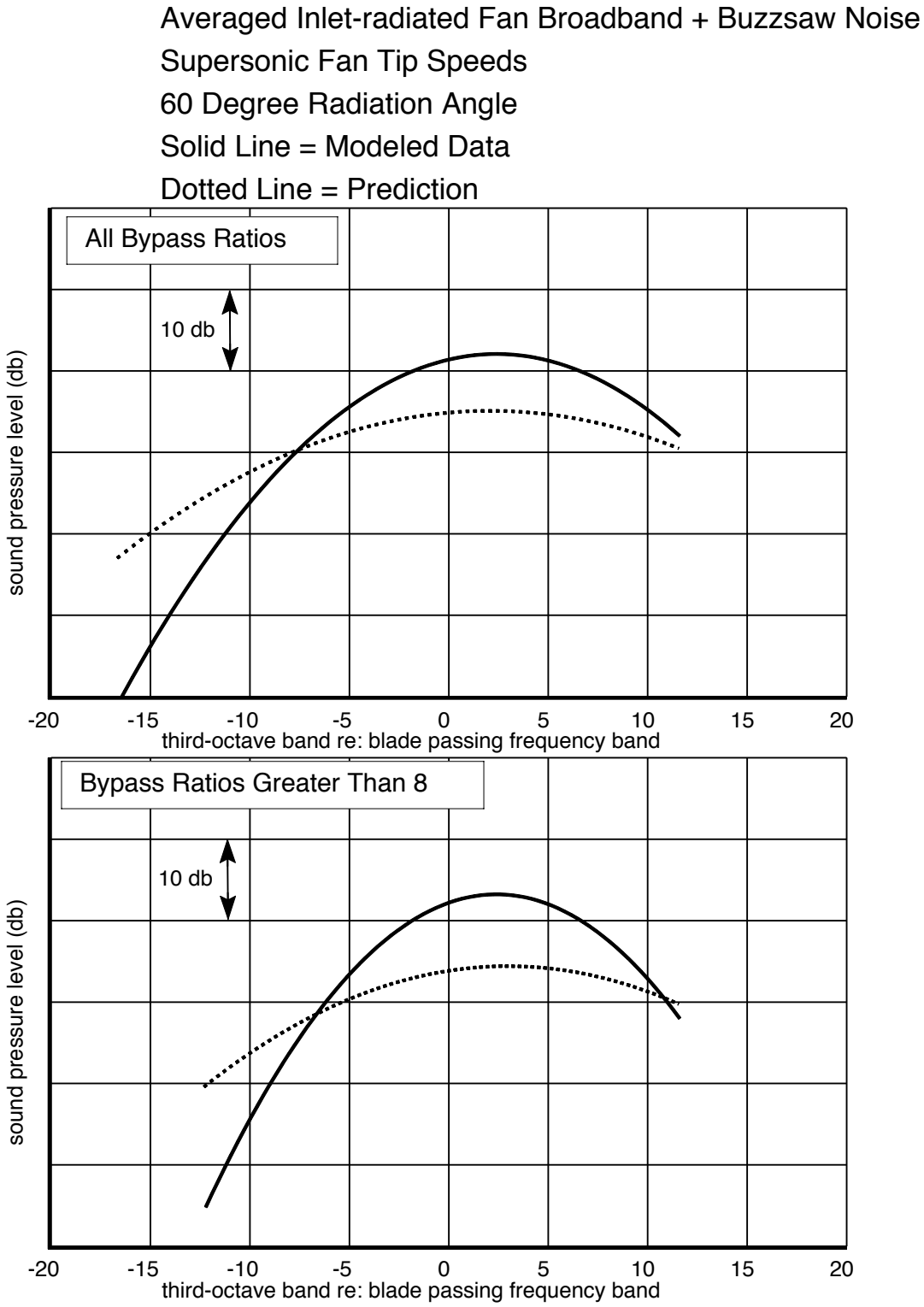

Figure 21 Averaged Inlet Broadband + Buzzsaw at Supersonic Tip Speeds and 60 Degrees

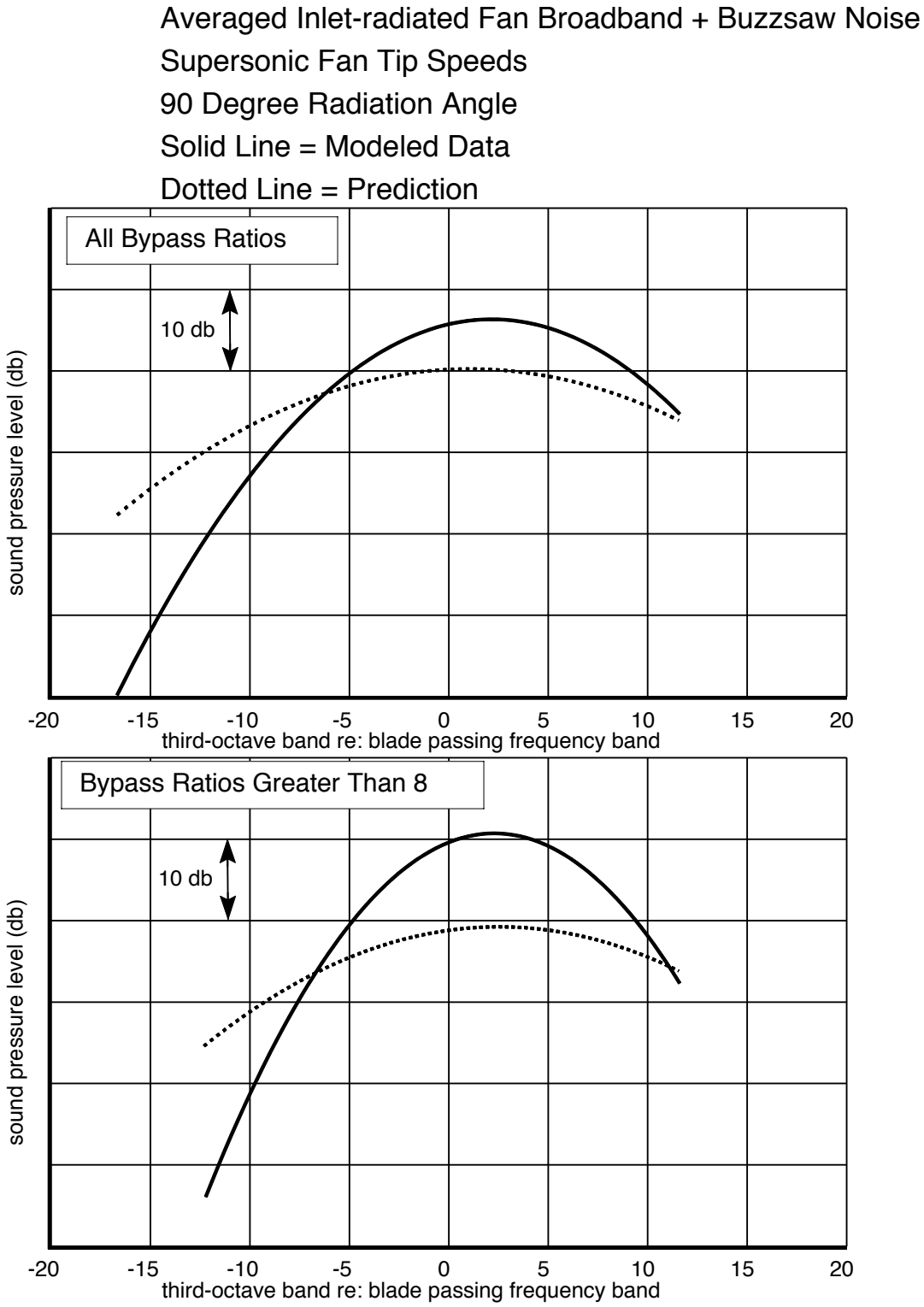

Figure 22 Averaged Inlet Broadband + Buzzsaw at Supersonic Tip Speeds and 90 Degrees

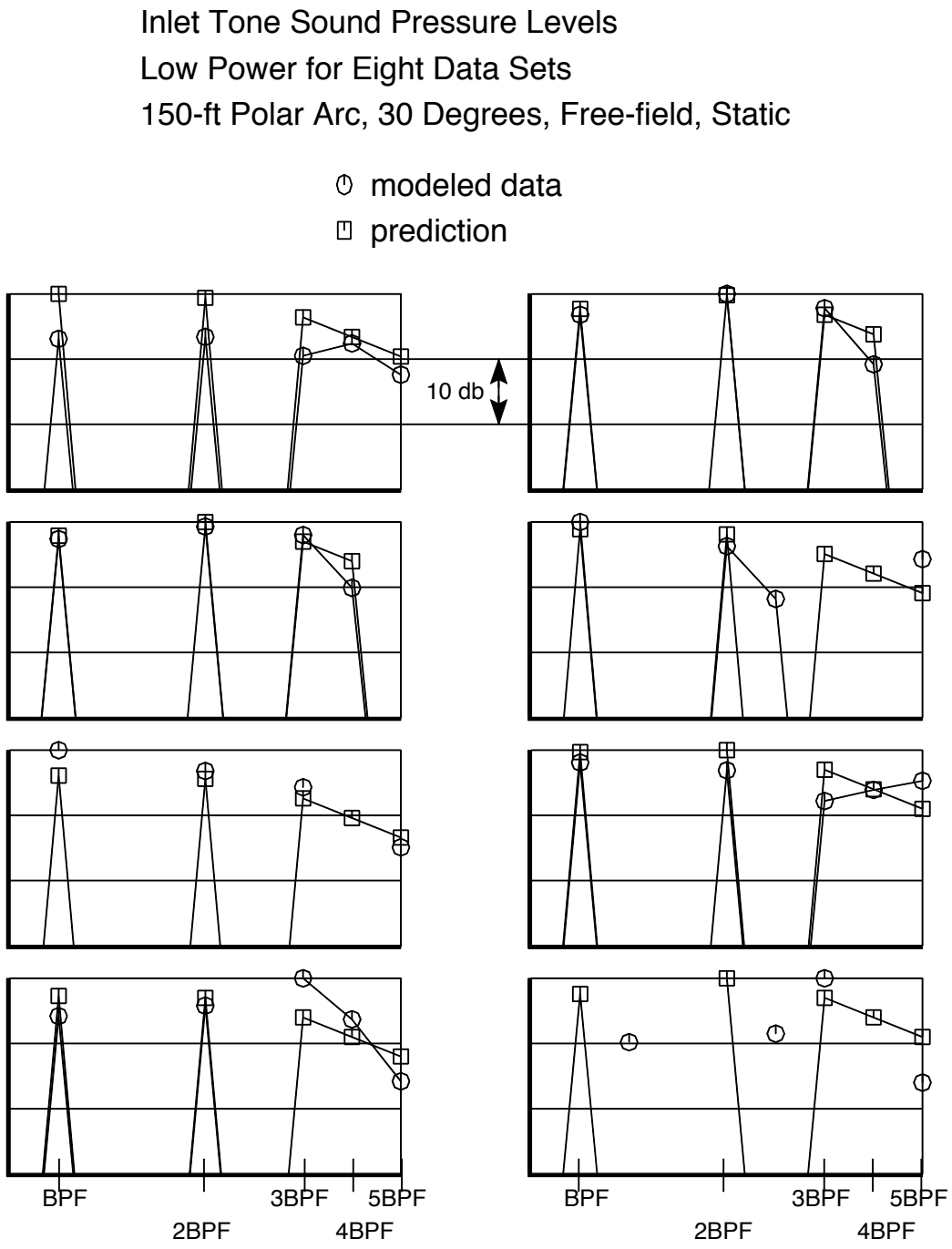

Figure 23 Inlet Tone Comparison at Low Power and 30 Degrees

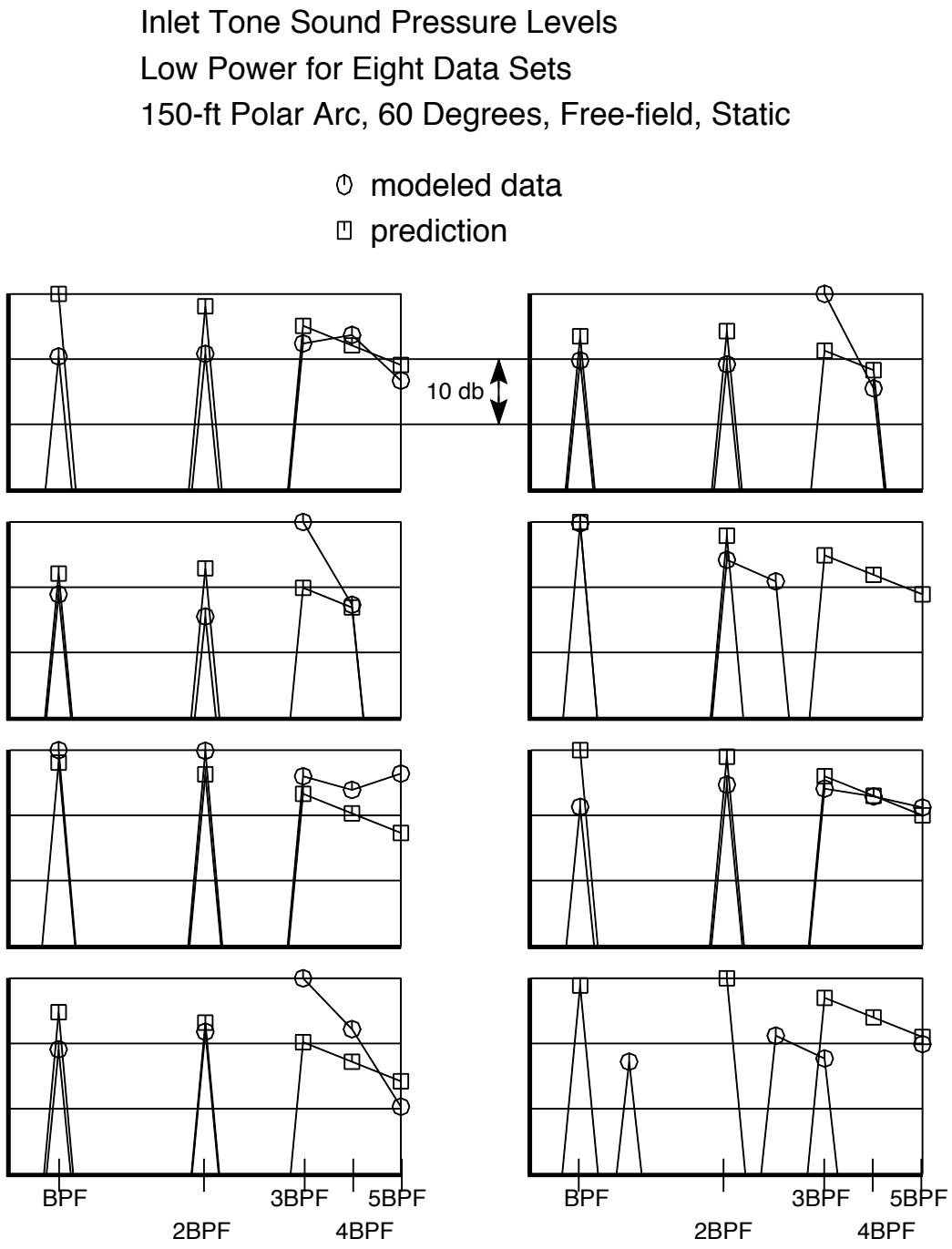

Figure 24 Inlet Tone Comparison at Low Power and 60 Degrees

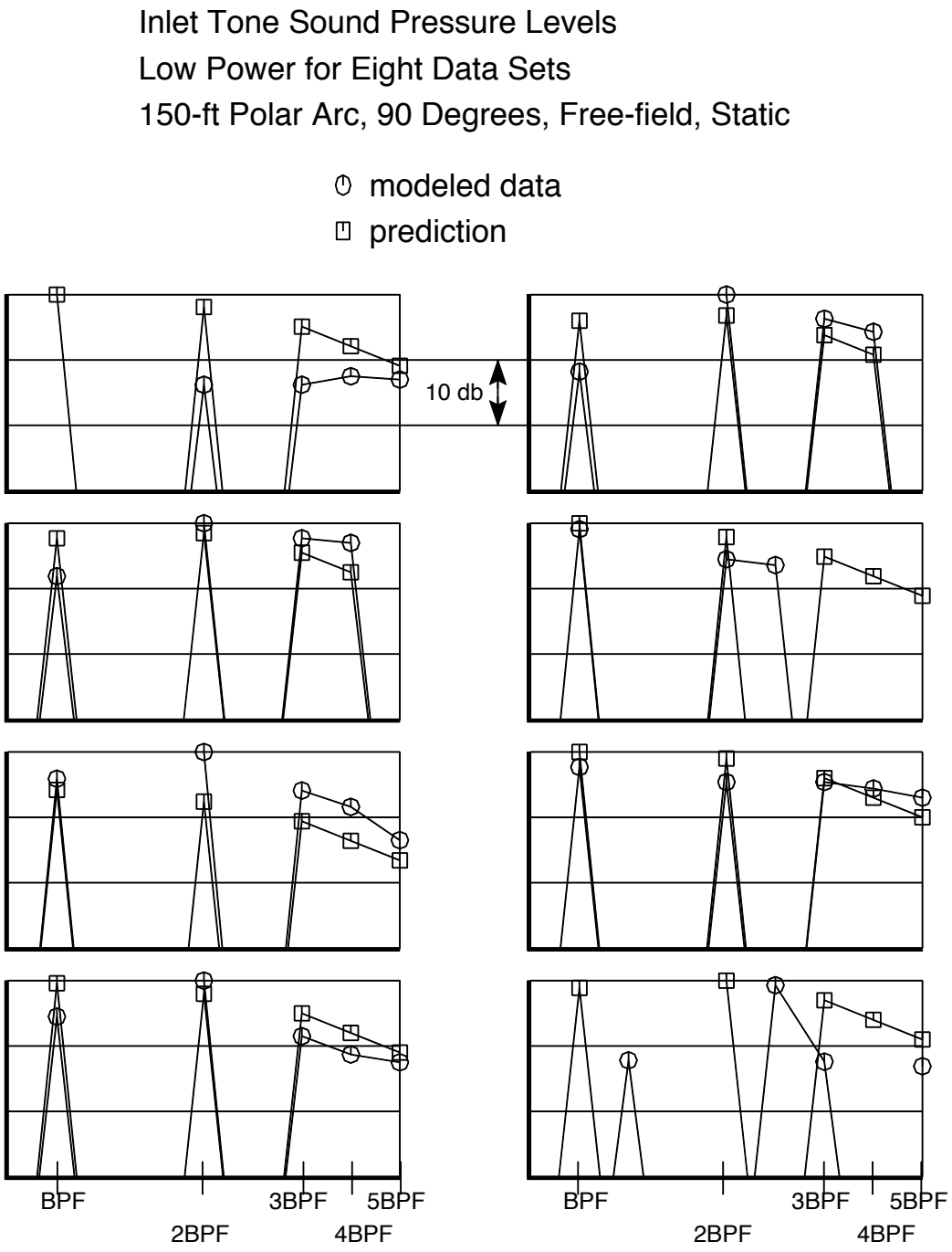

Figure 25 Inlet Tone Comparison at Low Power and 90 Degrees

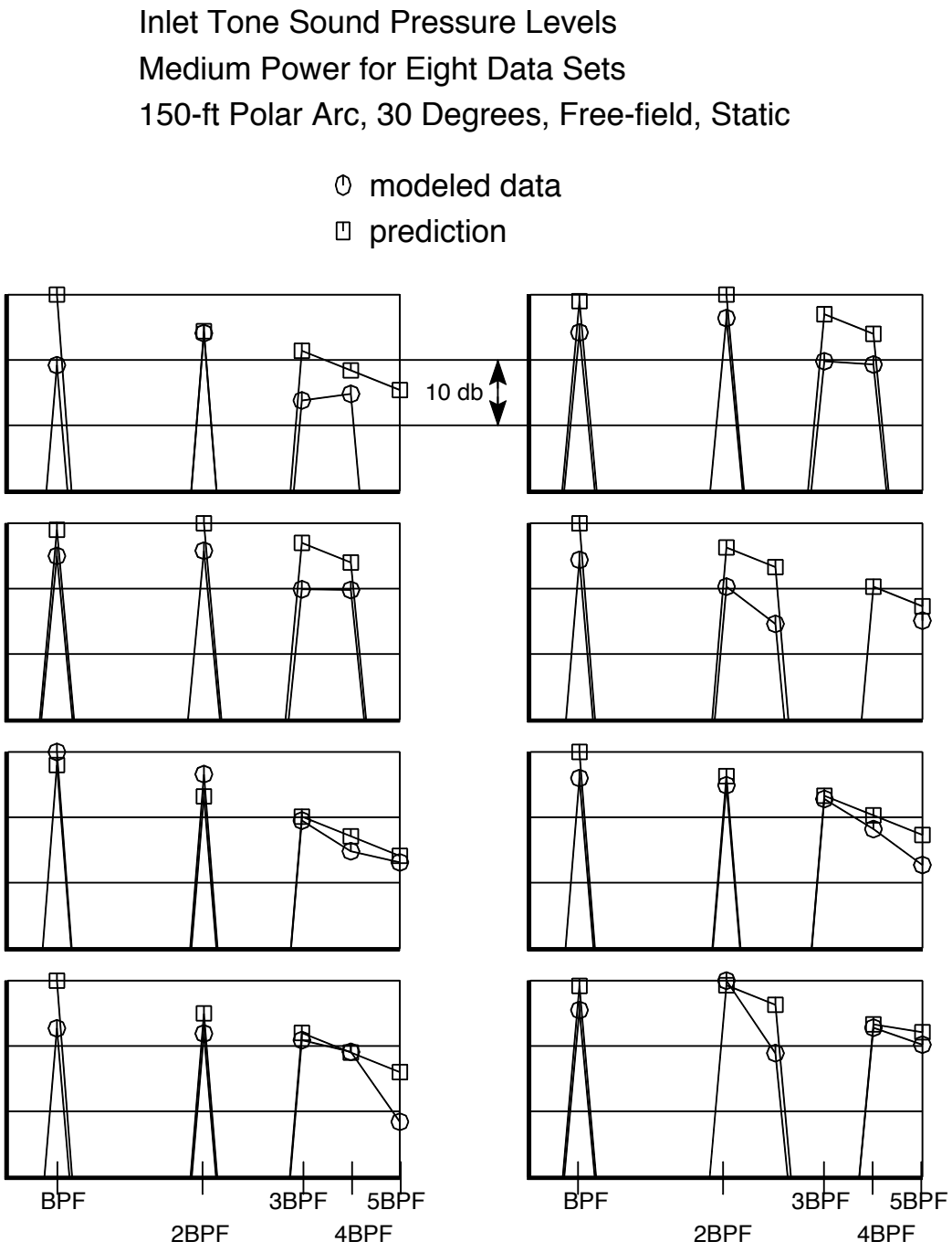

Figure 26 Inlet Tone Comparison at Medium Power and 30 Degrees

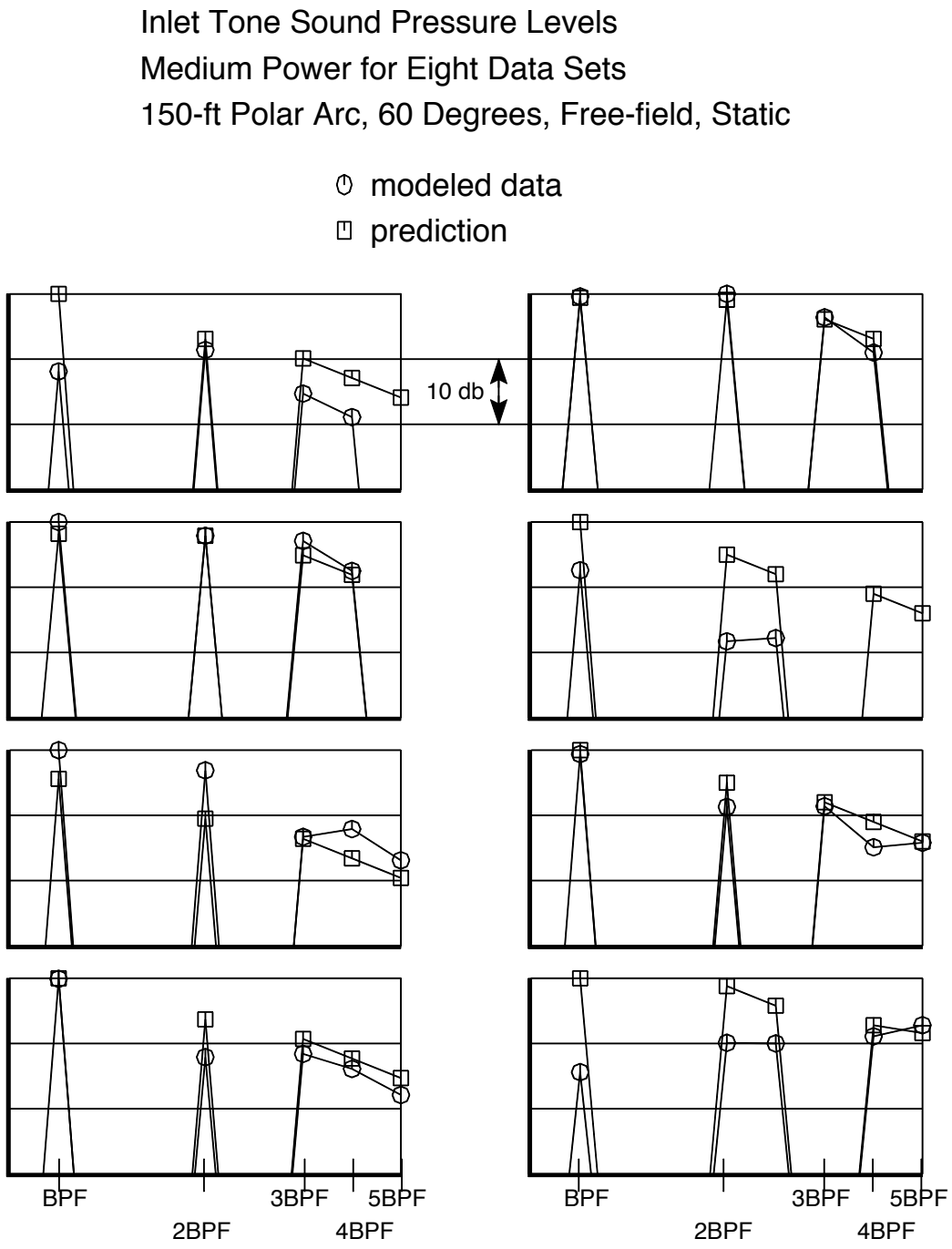

Figure 27 Inlet Tone Comparison at Medium Power and 60 Degrees

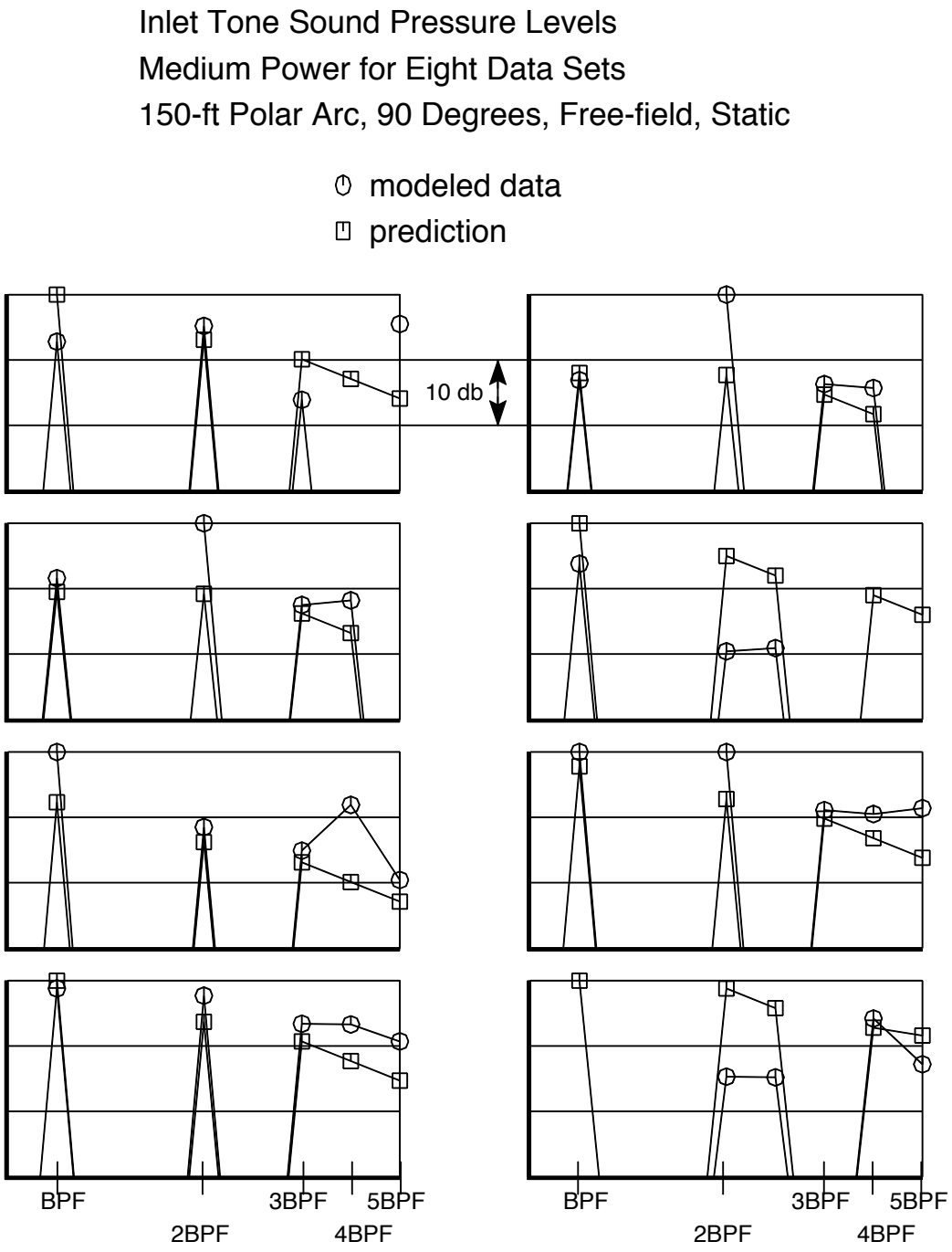

Figure 28 Inlet Tone Comparison at Medium Power and 90 Degrees

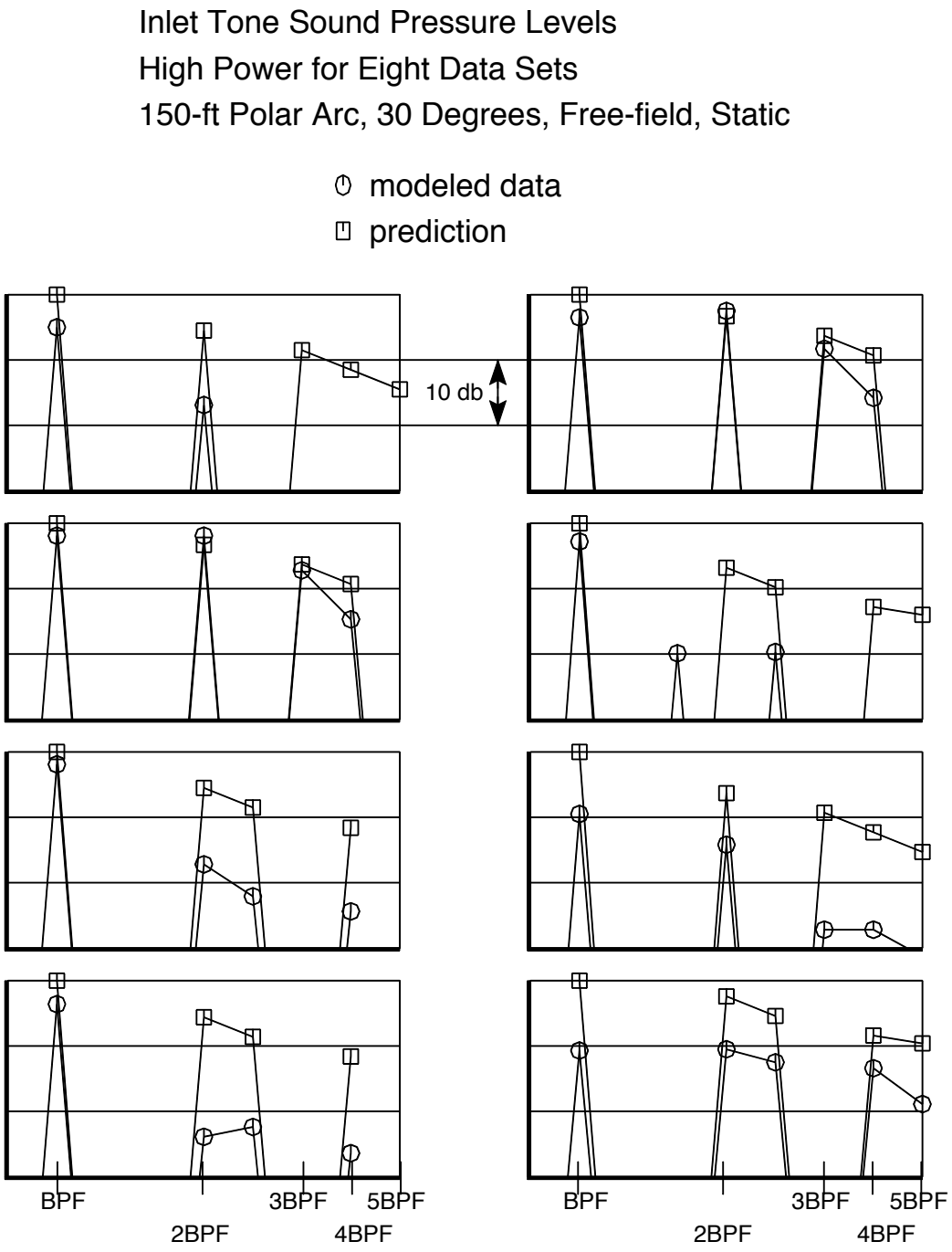

Figure 29 Inlet Tone Comparison at High Power and 30 Degrees

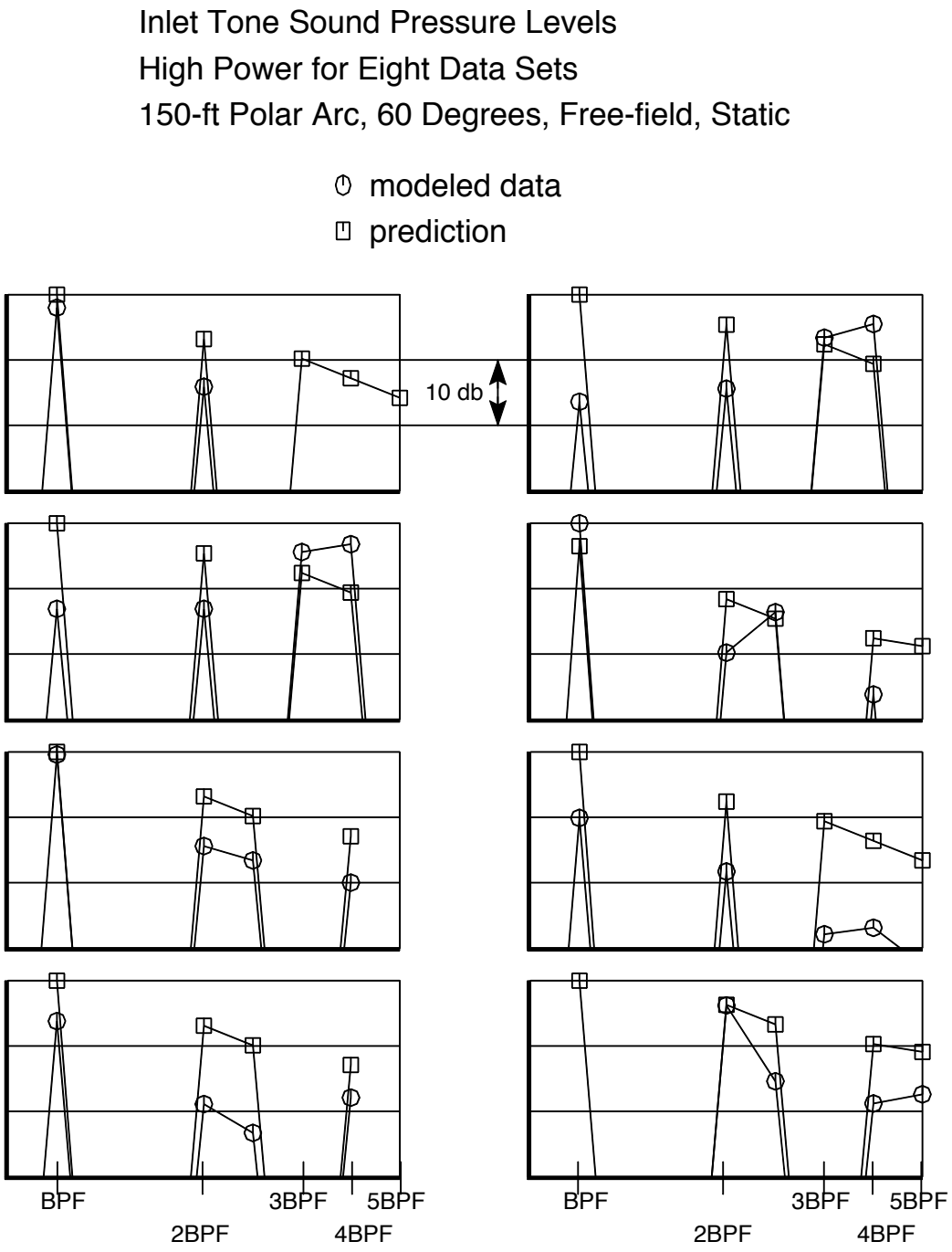

Figure 30 Inlet Tone Comparison at High Power and 60 Degrees

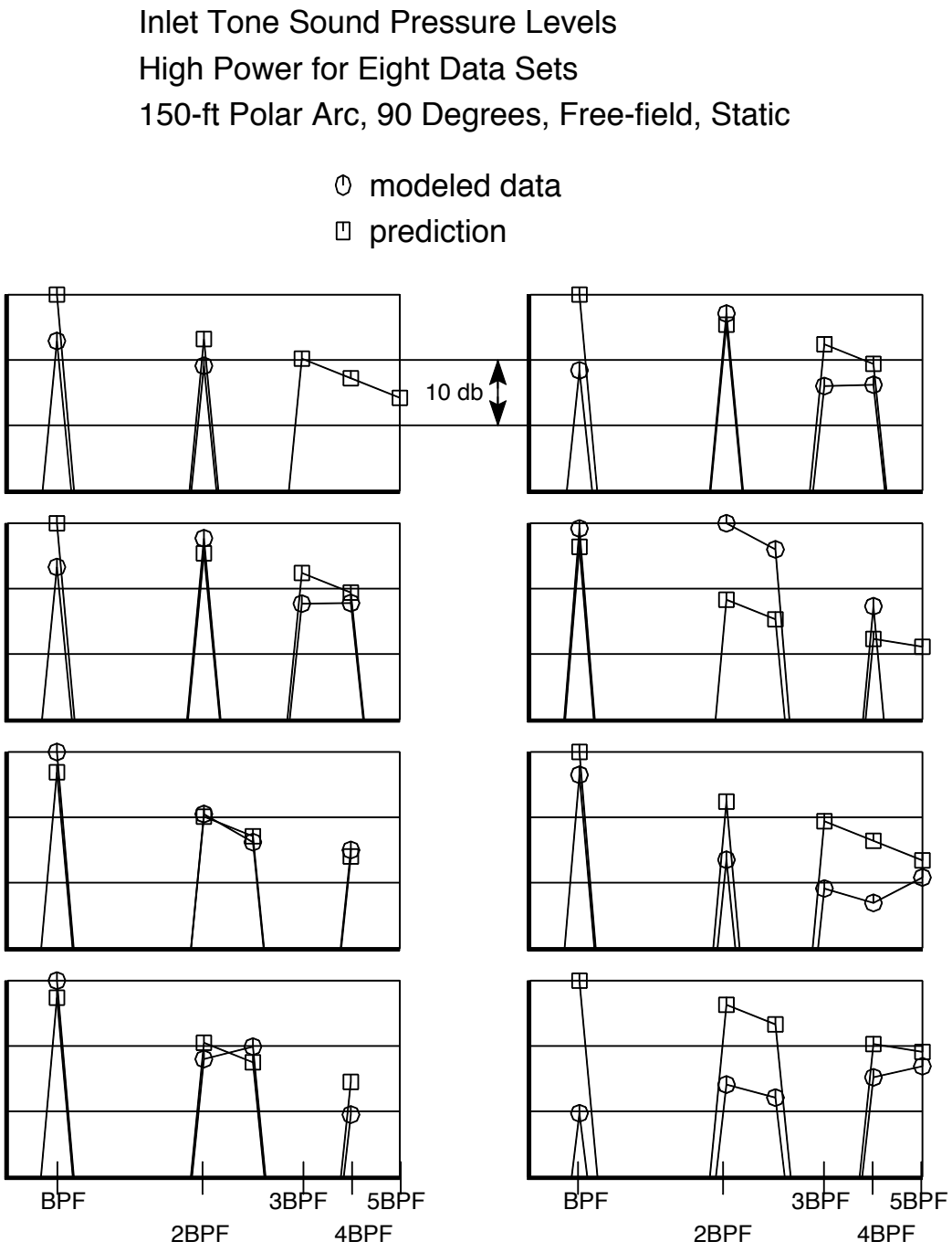

Figure 31 Inlet Tone Comparison at High Power and 90 Degrees

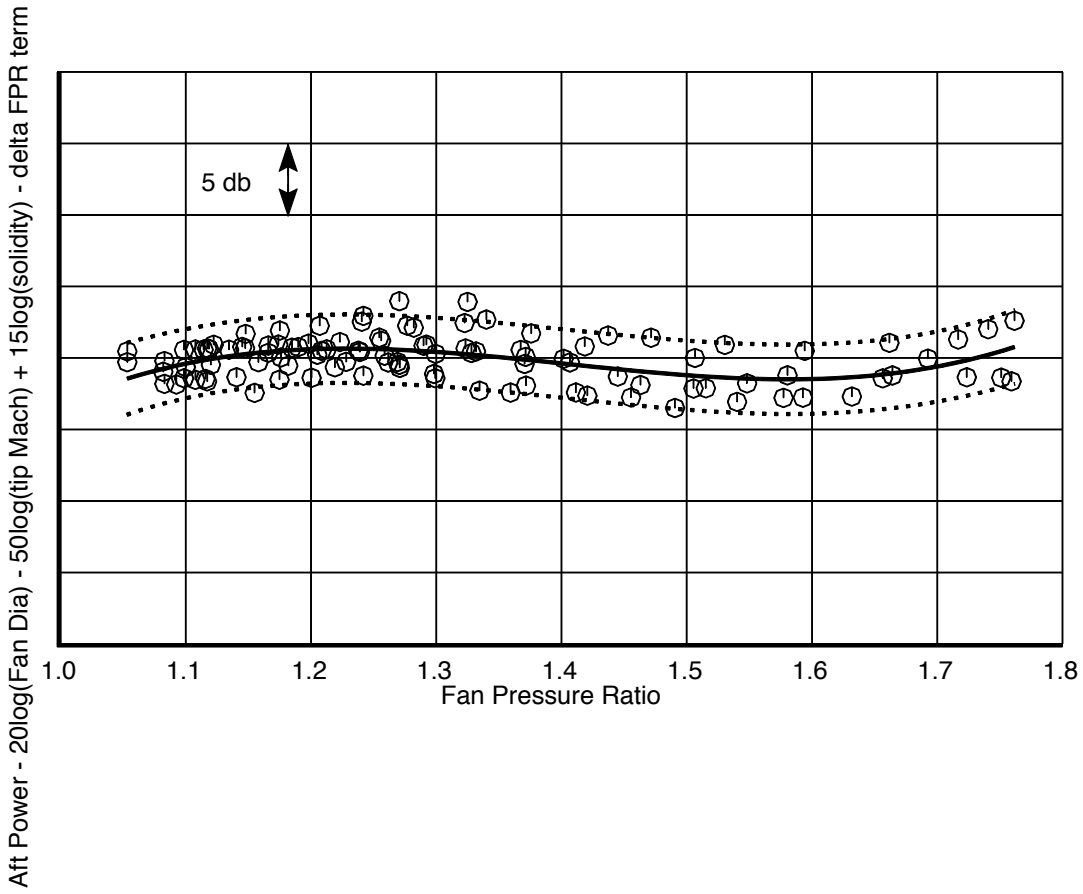

aft-radiated power = 20 log ($diam_{fan}$ / 1 inch) + 3.07 M_{tip}^3 – 19.92 M_{tip}^2 +11.76 M_{tip} + 50 log (M_{tip}) – 15 log (solidity) + 97.39 FPR^3 – 410.33 FPR^2 + 593.88 FPR – 182.39

Figure 32 Power Correlation for Aft-radiated Fan Broadband Noise

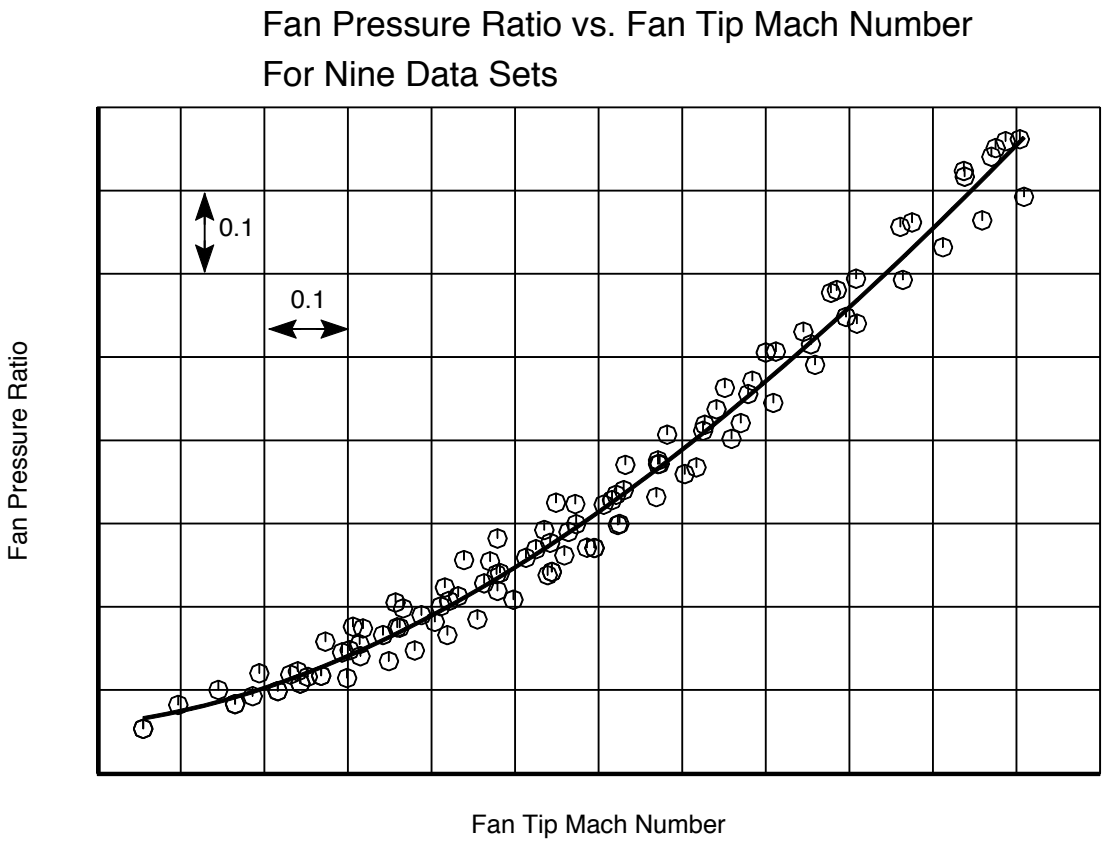

Figure 33 Fan Pressure Ratio vs. Fan Tip Mach Number

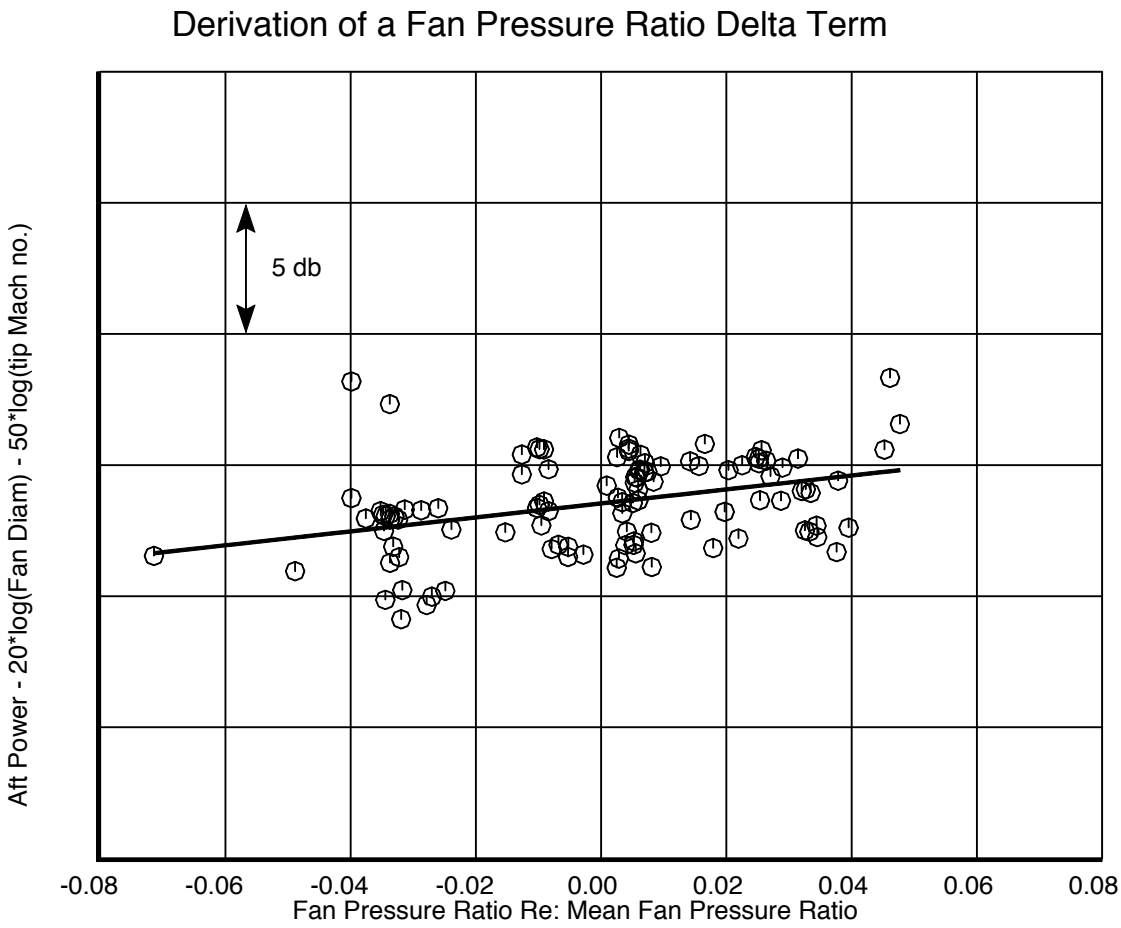

Figure 34 Derivation of a Fan Pressure Ratio Delta Term

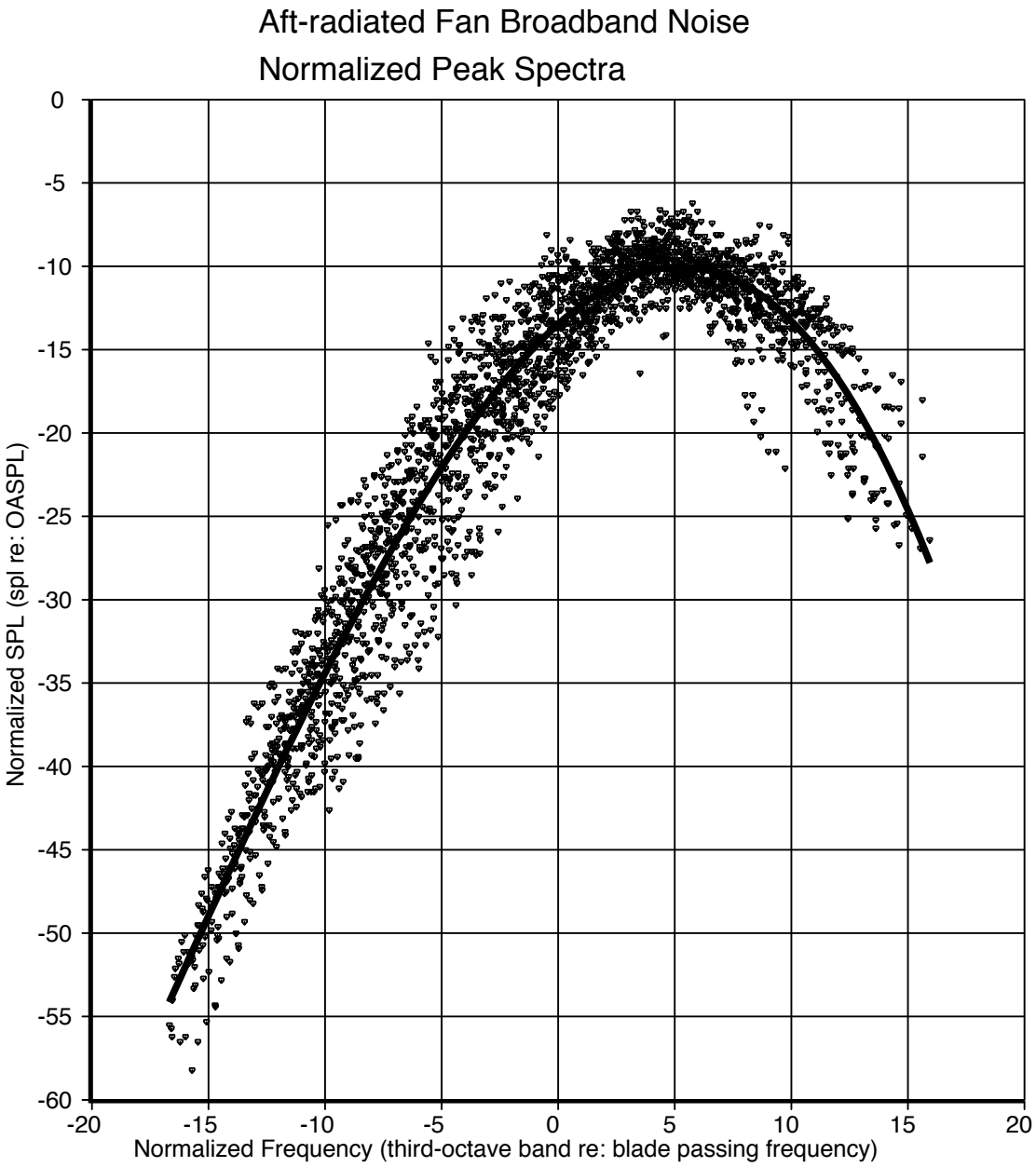

for a normalized frequency less than –15:

$spl_{norm} = 3 * freq_{norm} - 3.96$

for a normalized frequency between –15 and 15:

$spl_{norm} = -0.00195 * freq_{norm}^{3} - 0.1036 * freq_{norm}^{2} - 1.25 * freq_{norm} - 13.5$

for a normalized frequency greater than 15:

$spl_{norm} = -3.5 * freq_{norm} + 27.89$

Figure 35 Spectral Correlation for Aft-radiated Fan Broadband Noise

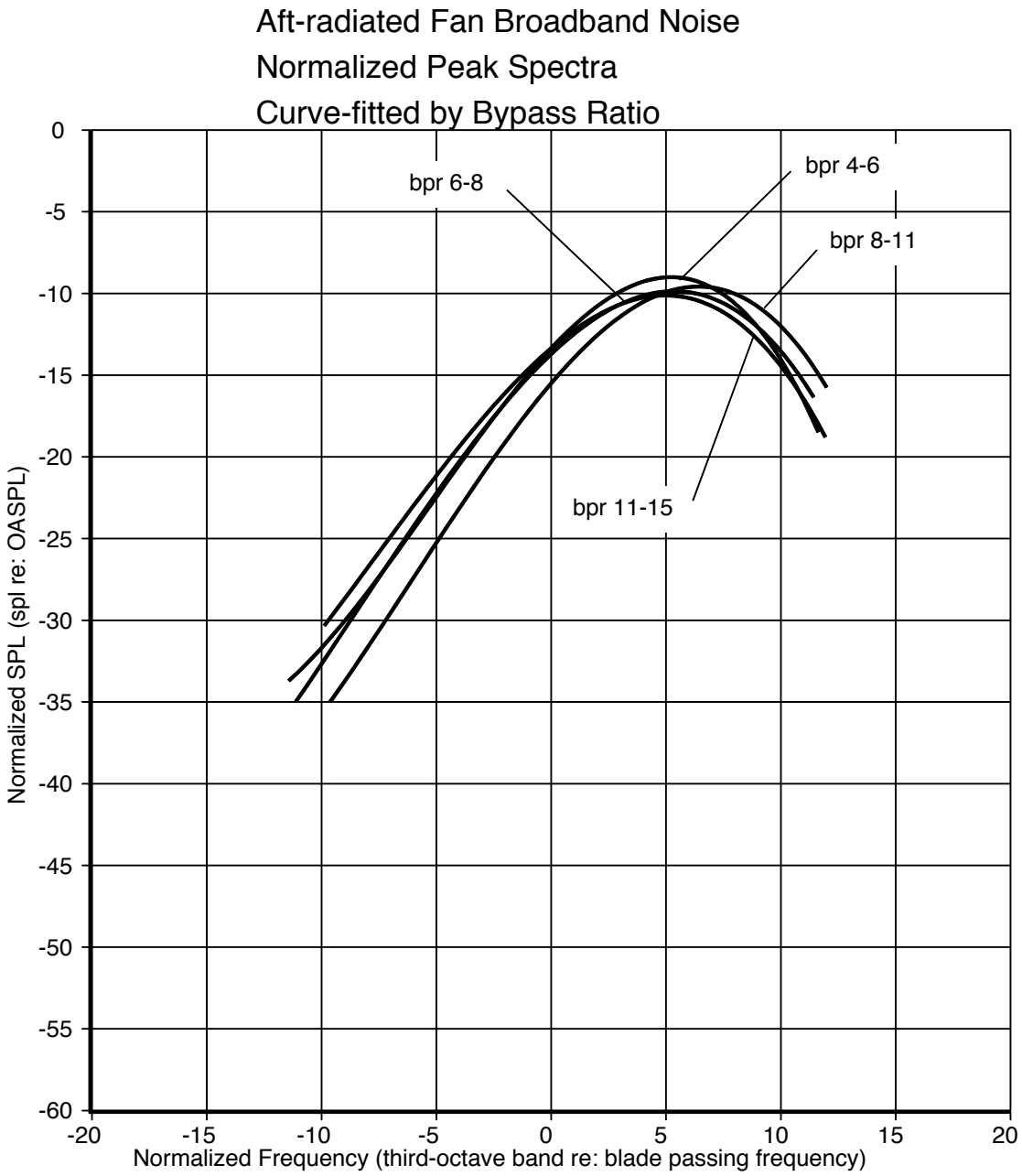

Figure 36 Spectral Correlation for Aft-radiated Fan Broadband Noise by Bypass Ratio

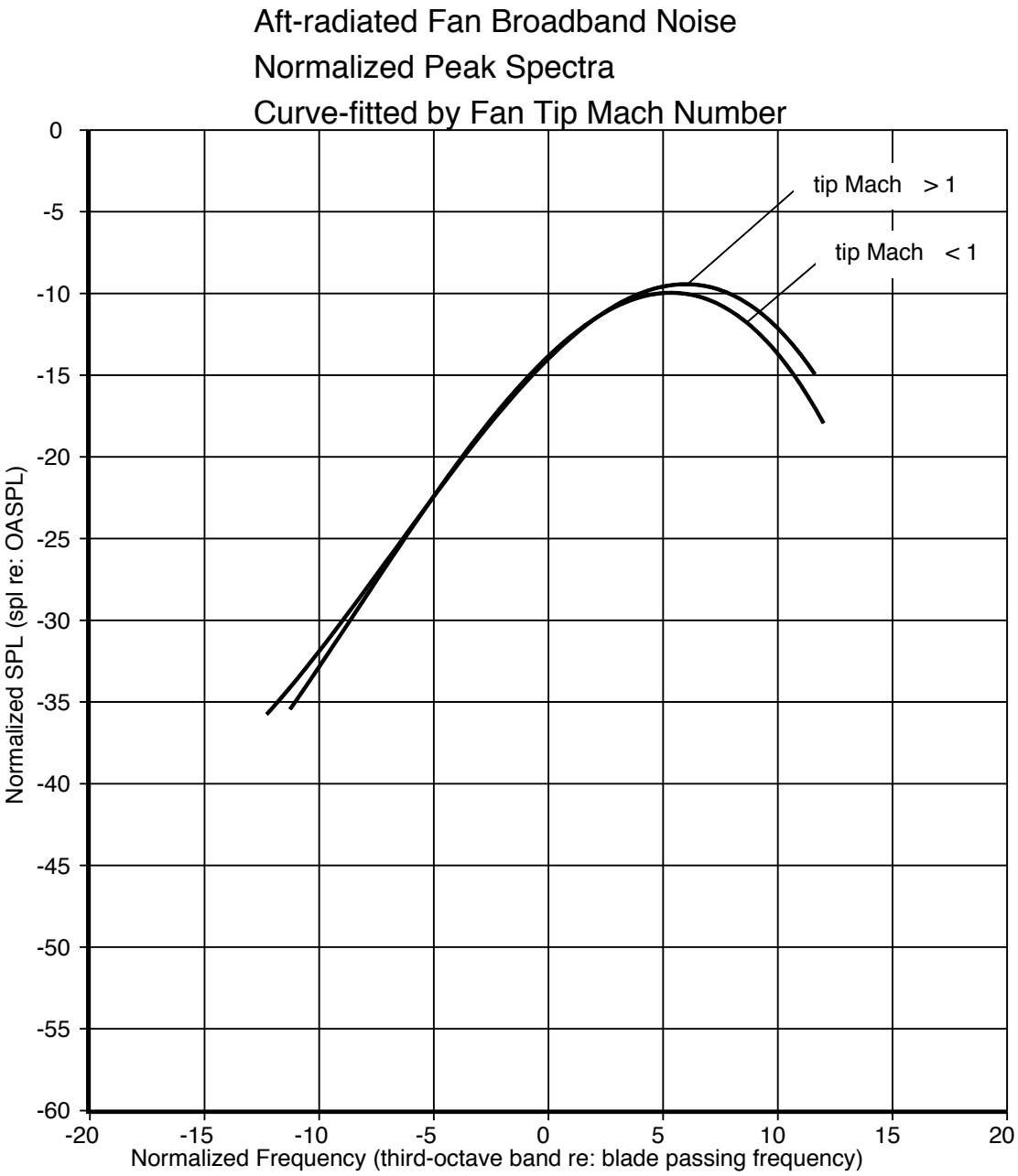

Figure 37 Spectral Correlation for Aft-radiated Fan Broadband Noise by Fan Tip Speed

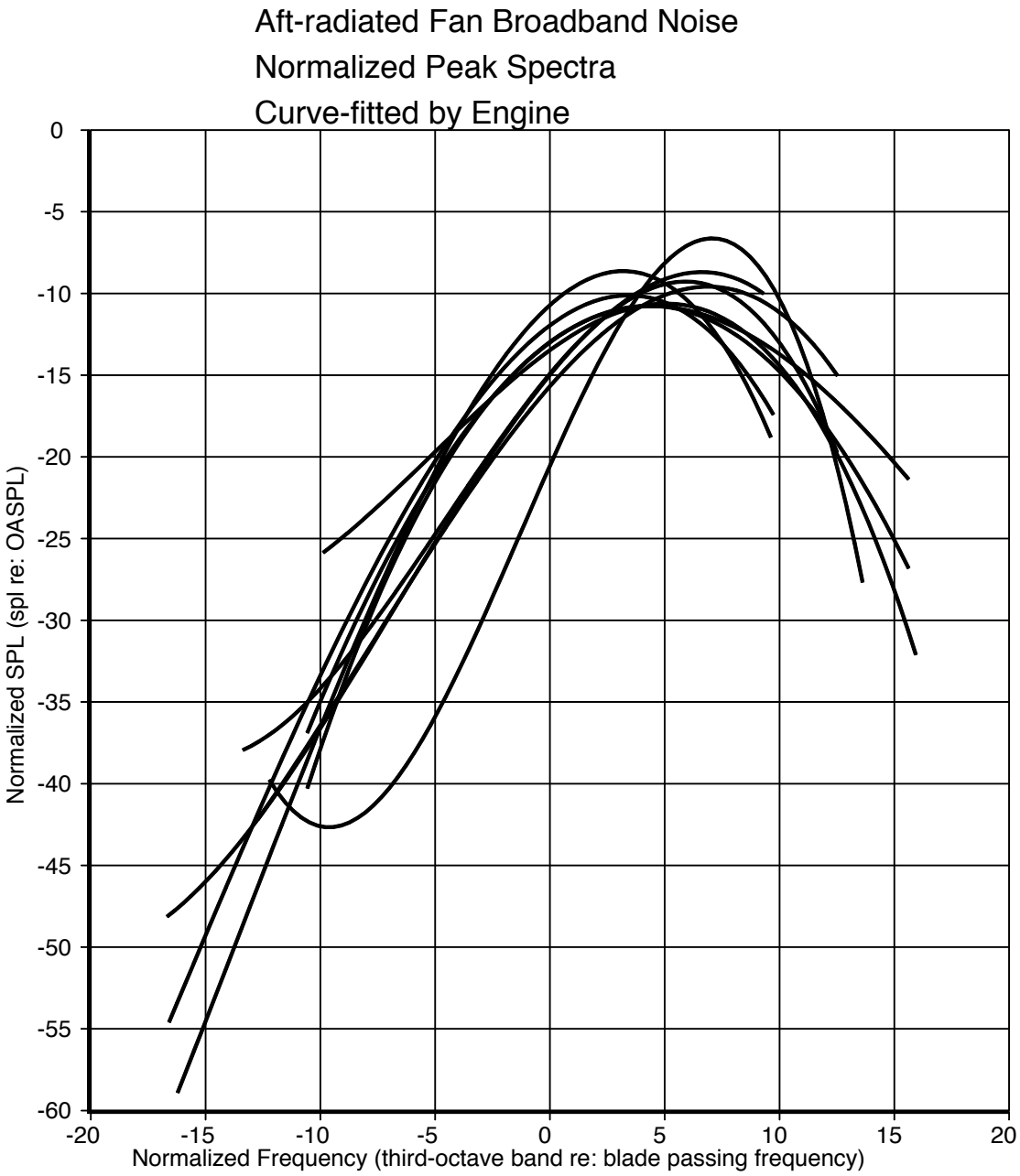

Figure 38 Spectral Correlation for Aft-radiated Fan Broadband Noise by Engine

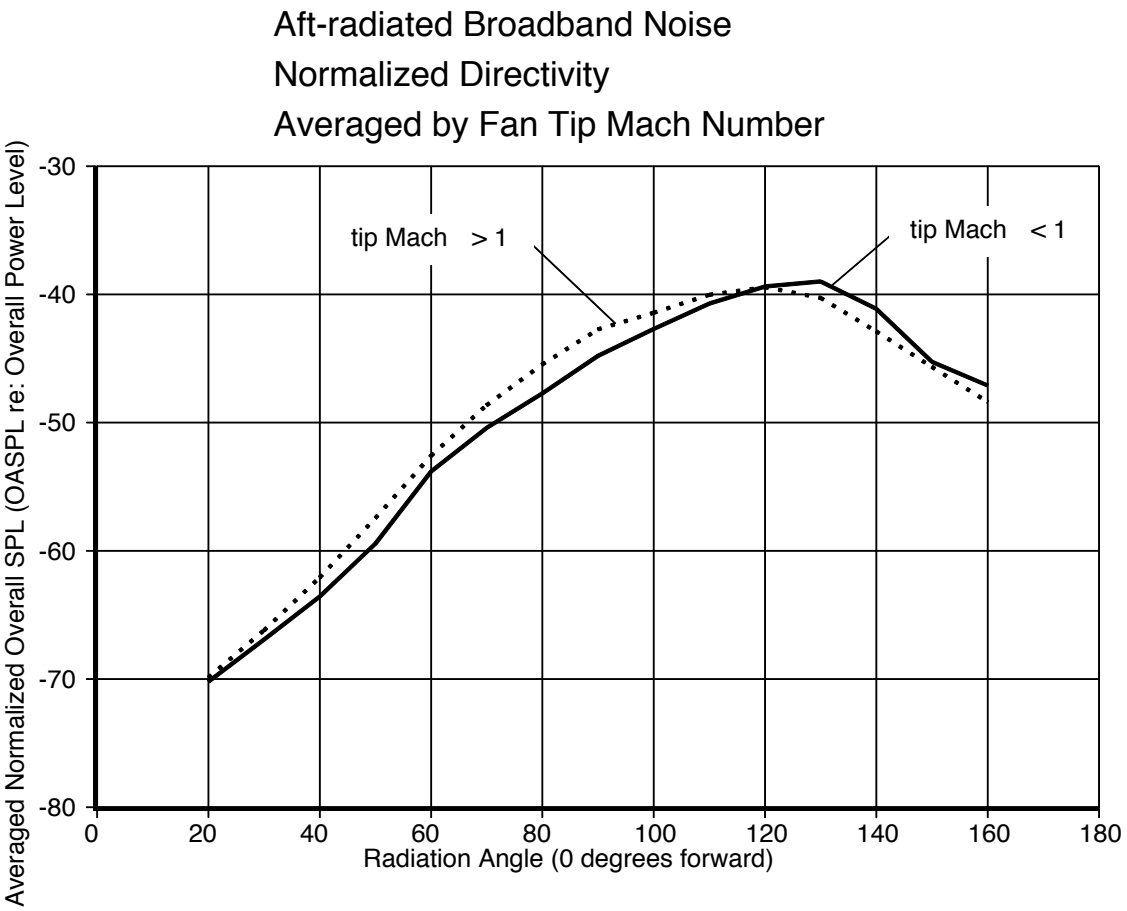

Radiation Angle (0 degrees forward)	Normalized OASPL	
	$M_{tip} < 1$	$M_{tip} > 1$
10	-75.5	-75.4
20	-70.2	-69.9
30	-66.9	-66.2
40	-63.6	-62.1
50	-59.4	-57.4
60	-53.8	-52.6
70	-50.4	-48.6
80	-47.7	-45.5
90	-44.8	-42.7

Radiation Angle (0 degrees forward)	Normalized OASPL	
	$M_{tip} < 1$	$M_{tip} > 1$
100	-42.7	-41.1
110	-40.7	-40.0
120	-39.4	-39.4
130	-39.0	-40.3
140	-41.1	-42.7
150	-45.3	-45.7
160	-47.1	-48.4
170	-52.4	-53.4

Figure 39 Directivity Correlation for Aft-radiated Fan Broadband Noise by Fan Tip Speed

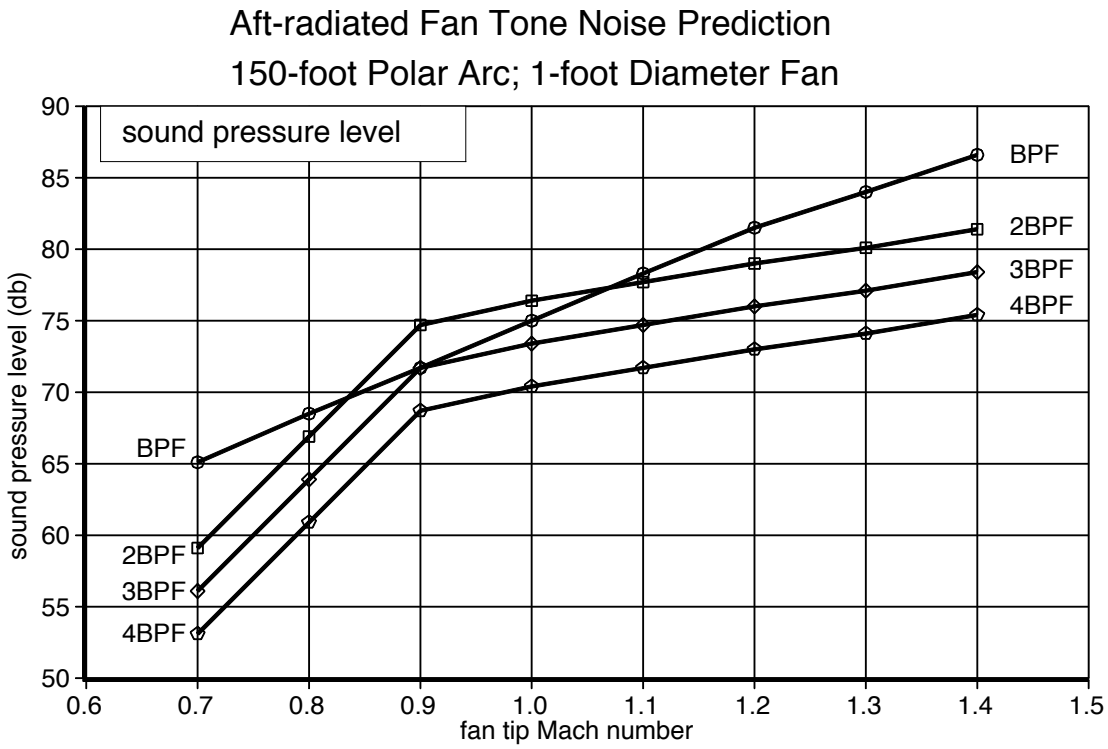

fan tip Mach number	sound pressure level (db)			
	BPF	2BPF	3BPF	4BPF
0.7	65.1	59.1	56.1	53.1
0.8	68.5	66.9	63.9	60.9
0.9	71.1	74.7	71.7	68.7
1.0	75.0	76.4	73.4	70.4
1.1	78.3	77.7	74.7	71.7
1.2	81.5	79.0	76.0	73.0
1.3	84.0	80.1	77.1	74.1
1.4	86.6	81.4	78.4	75.4

Figure 40 Aft-radiated Fan Tone Noise Prediction – Sound Pressure Levels

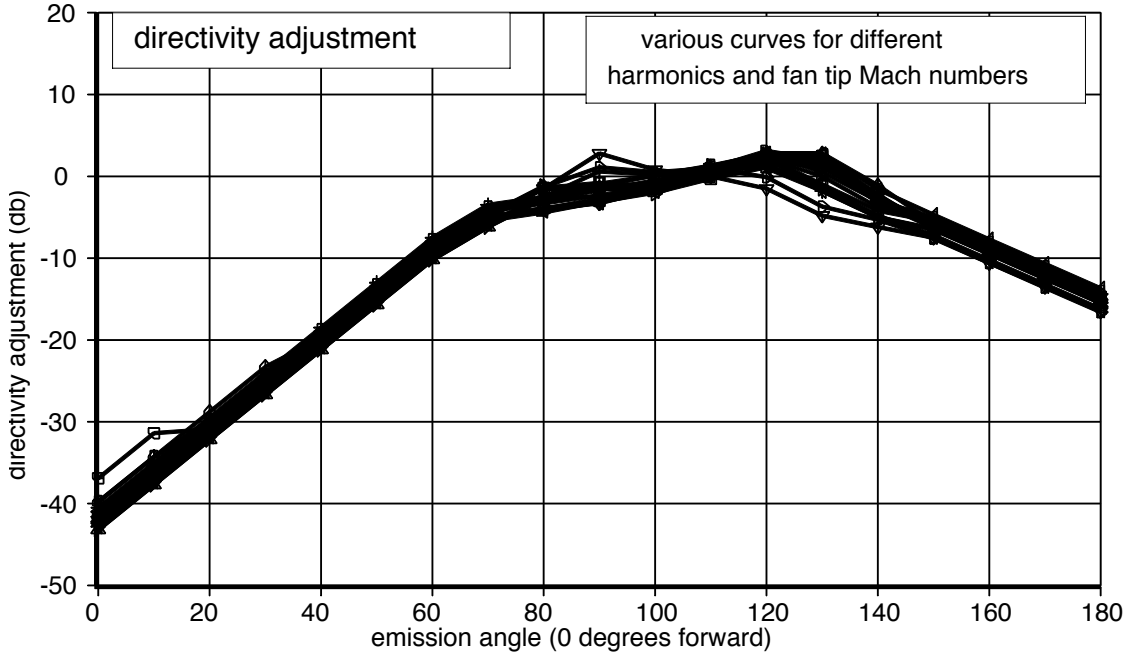

emission angle	directivity adjustment (db)								
	M_{tip} 0.78	M_{tip} 0.85	M_{tip} 0.94	M_{tip} 1.03	M_{tip} 1.12	M_{tip} 1.20	M_{tip} 1.26	M_{tip} 1.35	M_{tip} 1.40
0	-43.2	-42.0	-43.2	-39.8	-41.7	-36.9	-42.8	-41.8	-42.0
10	-37.7	-36.5	-37.7	-34.3	-36.2	-31.4	-37.3	-36.3	-36.5
20	-32.2	-31.0	-32.2	-28.8	-30.7	-30.9	-31.8	-30.8	-31.0
30	-26.7	-25.5	-26.7	-23.3	-25.2	-25.4	-26.3	-25.3	-25.5
40	-21.2	-20.0	-21.2	-19.8	-19.7	-19.9	-20.8	-19.8	-20.0
50	-15.7	-14.5	-15.7	-14.3	-14.2	-14.4	-15.3	-14.3	-14.5
60	-10.2	-9.0	-10.2	-8.8	-8.7	-8.9	-9.8	-8.8	-9.0
70	-6.2	-5.0	-6.2	-4.8	-4.7	-4.9	-5.8	-4.8	-5.0
80	-2.7	-1.5	-2.7	-1.3	-1.2	-1.4	-2.3	-1.3	-1.5
90	-2.5	-1.5	-1.5	-1.4	-1.5	-0.8	-1.2	1.1	2.8
100	-1.2	-1.4	-0.7	-1.4	-2.1	-1.2	0.1	0.5	0.8
110	0.1	0.2	0.8	0.6	0.2	0.7	1.1	1.0	0.0
120	2.8	2.4	2.0	2.2	2.0	1.3	1.0	-0.1	-1.5
130	2.8	2.5	1.0	0.0	-1.5	-1.2	-1.8	-3.7	-4.8
140	-1.1	-2.3	-2.5	-3.8	-5.0	-4.8	-5.0	-5.3	-6.2
150	-5.7	-6.2	-5.8	-5.4	-6.4	-7.2	-7.4	-7.6	-7.5
160	-8.7	-9.2	-8.8	-8.4	-9.4	-10.2	-10.4	-10.6	-10.6
170	-11.7	-12.2	-11.8	-11.4	-12.4	-13.2	-13.4	-13.6	-13.5
180	-14.7	-15.2	-14.8	-14.4	-15.4	-16.2	-16.6	-16.6	-16.5

Figure 41 Aft-radiated Fan Tone Noise Prediction – Directivity Adjustments

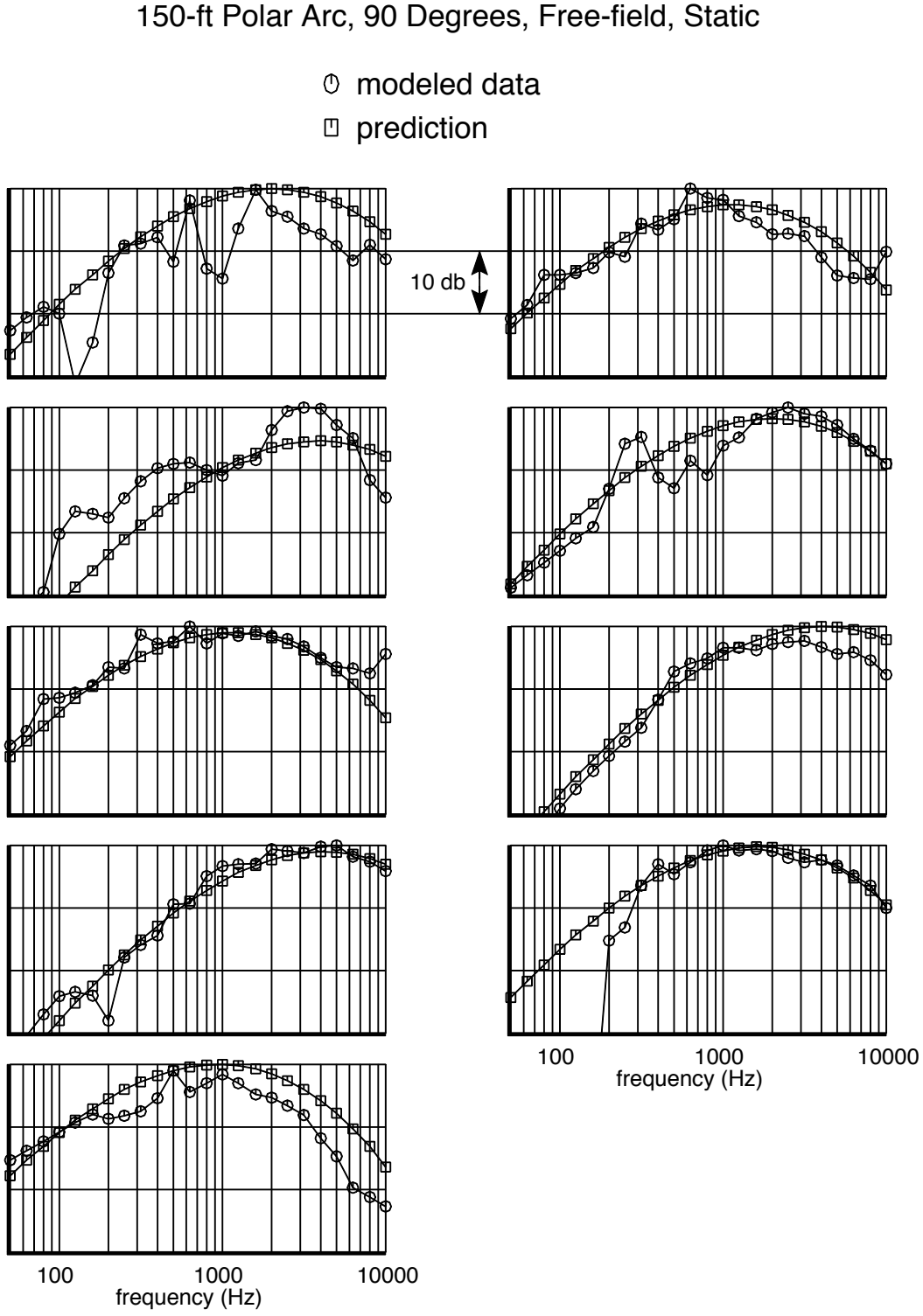

Figure 42 Aft Fan Broadband Comparison at Low Power and 90 Degrees

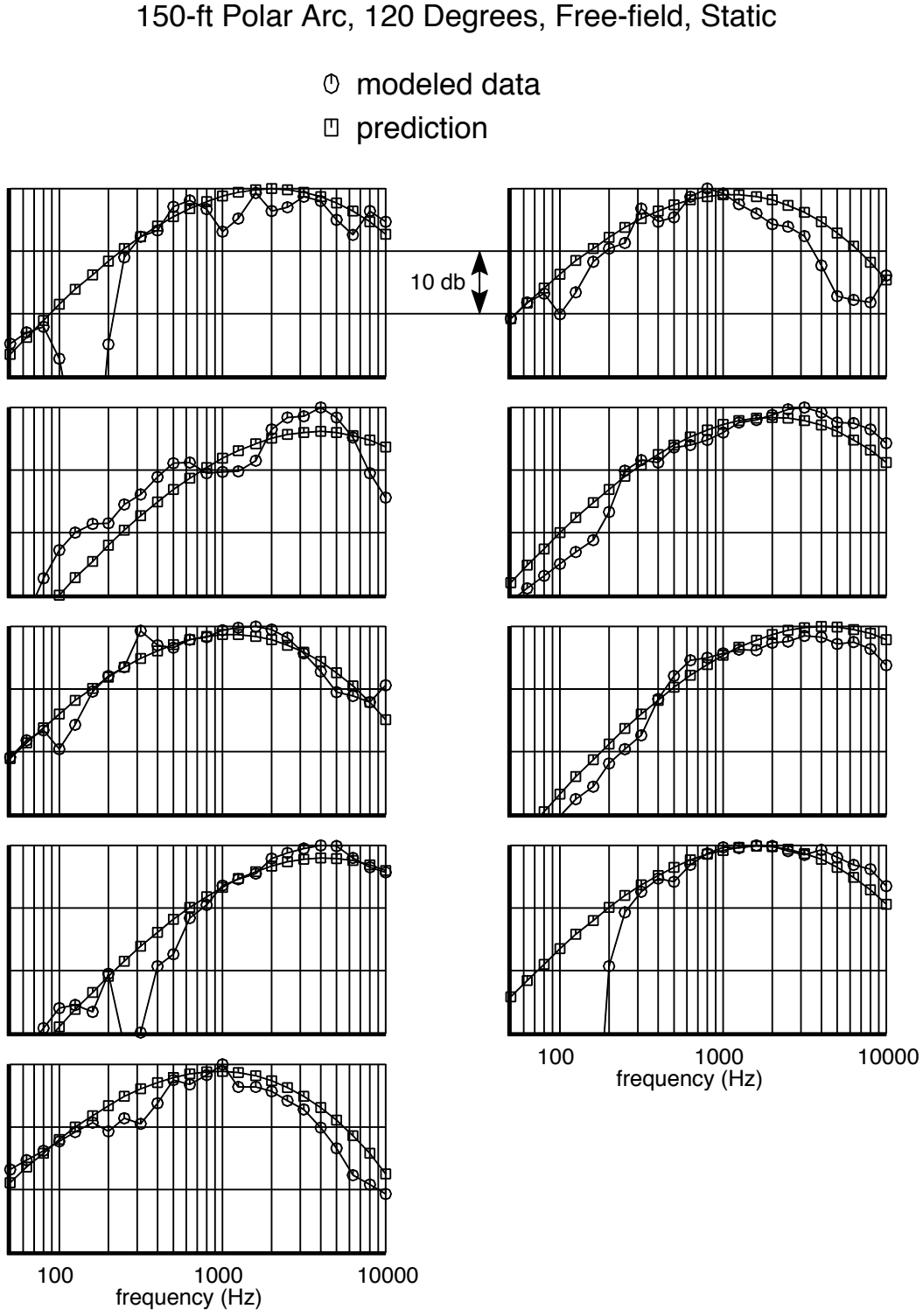

Figure 43 Aft Fan Broadband Comparison at Low Power and 120 Degrees

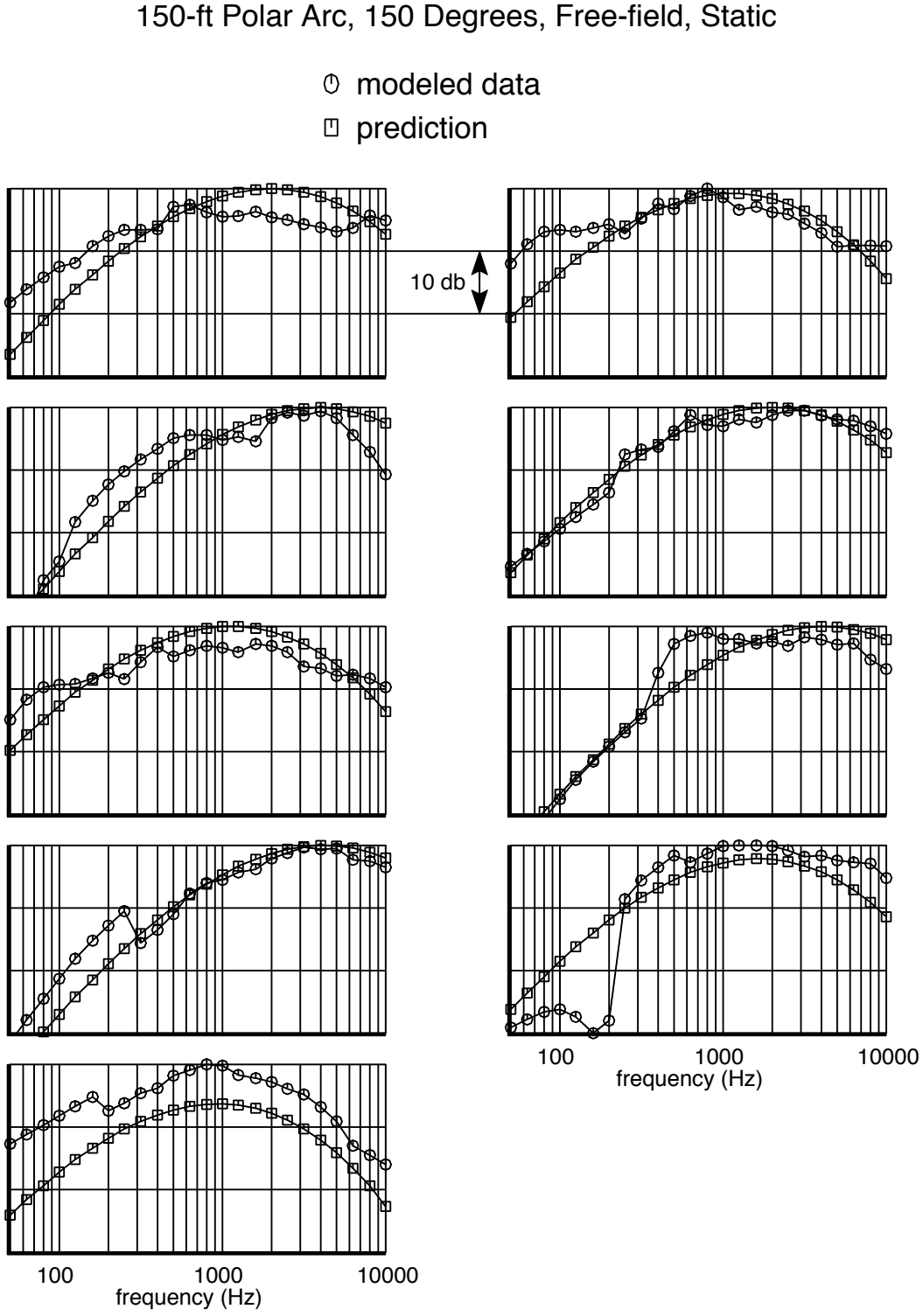

Figure 44 Aft Fan Broadband Comparison at Low Power and 150 Degrees

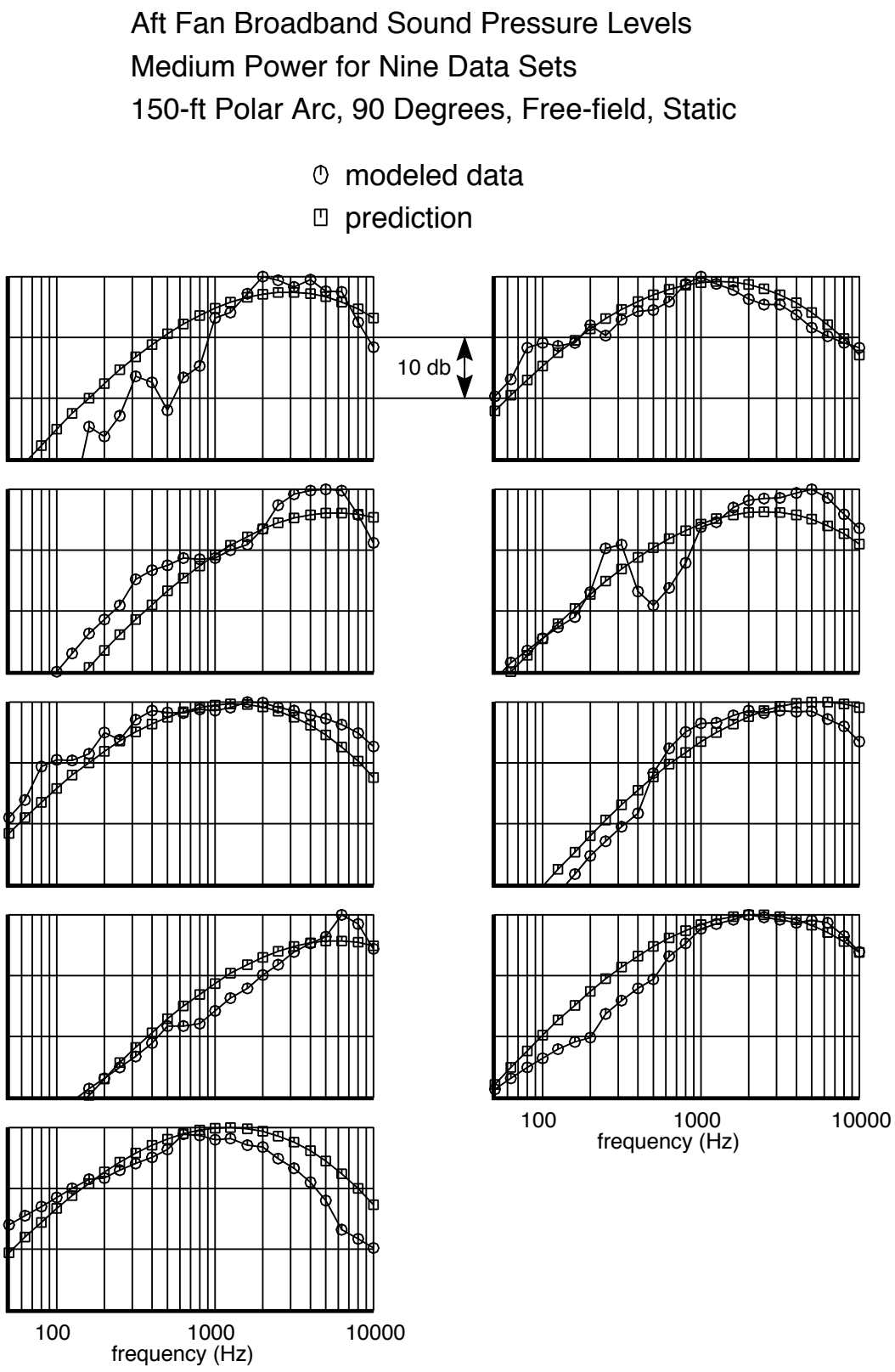

Figure 45 Aft Fan Broadband Comparison at Medium Power and 90 Degrees

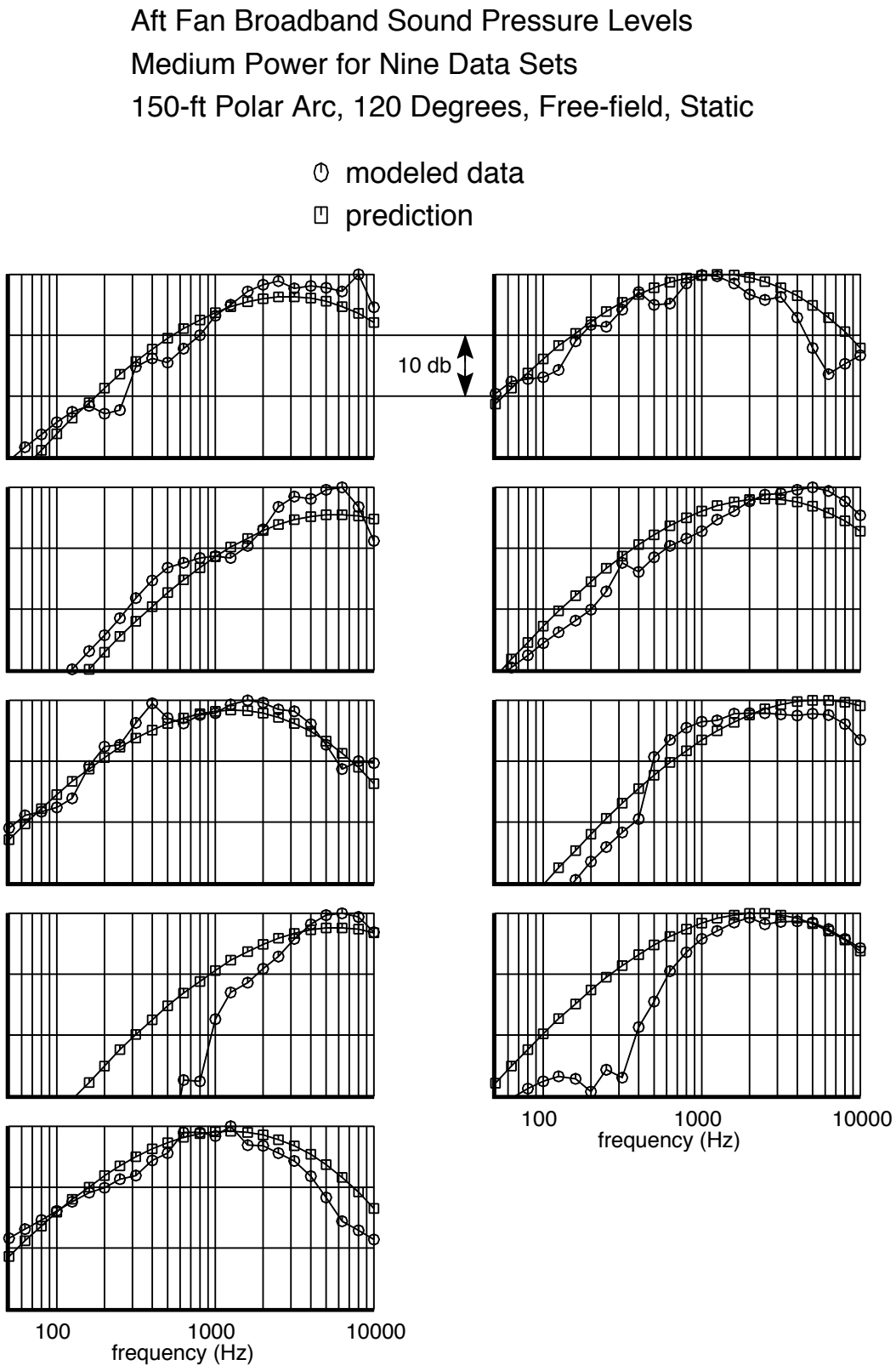

Figure 46 Aft Fan Broadband Comparison at Medium Power and 120 Degrees

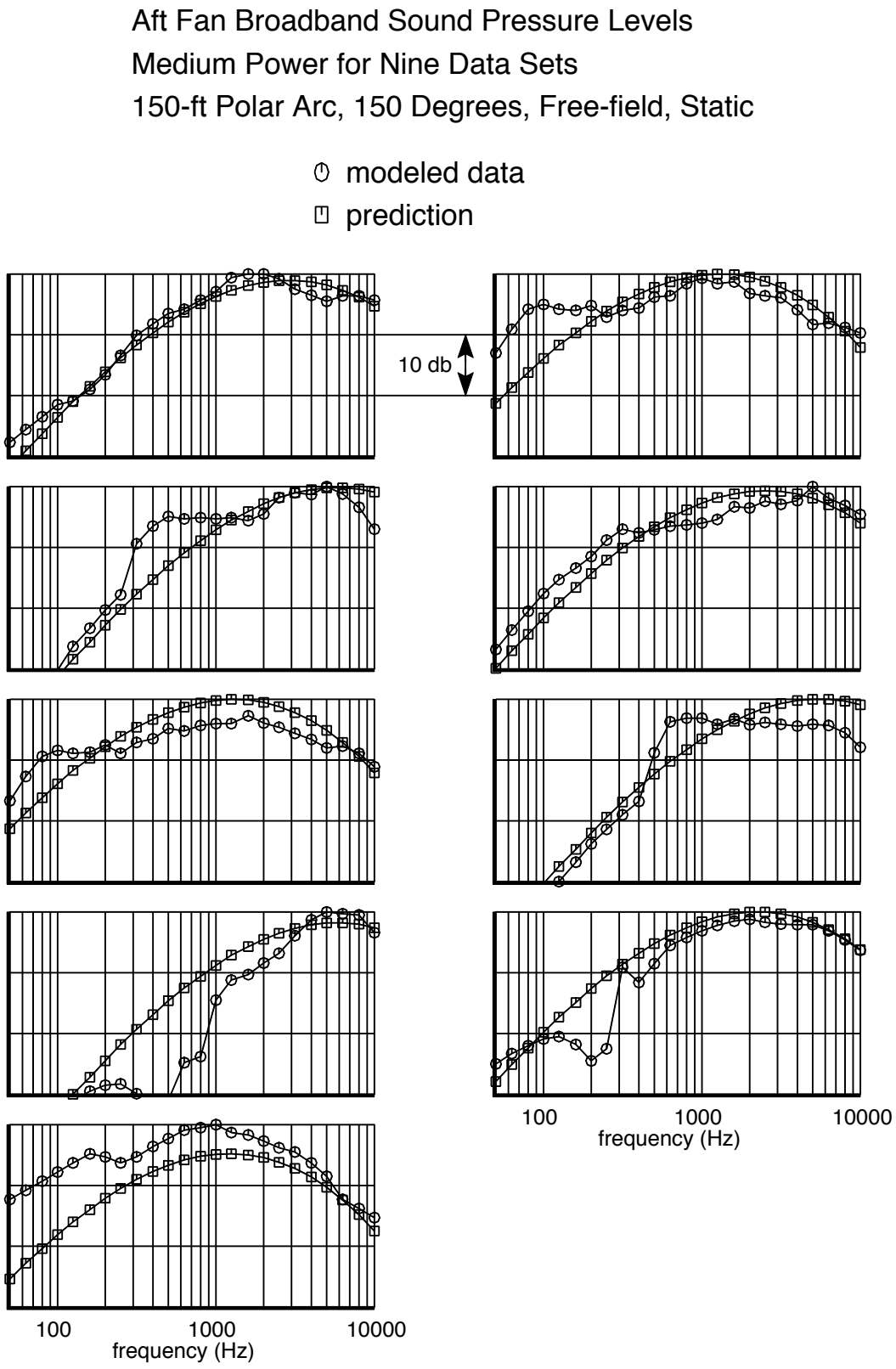

Figure 47 Aft Fan Broadband Comparison at Medium Power and 150 Degrees

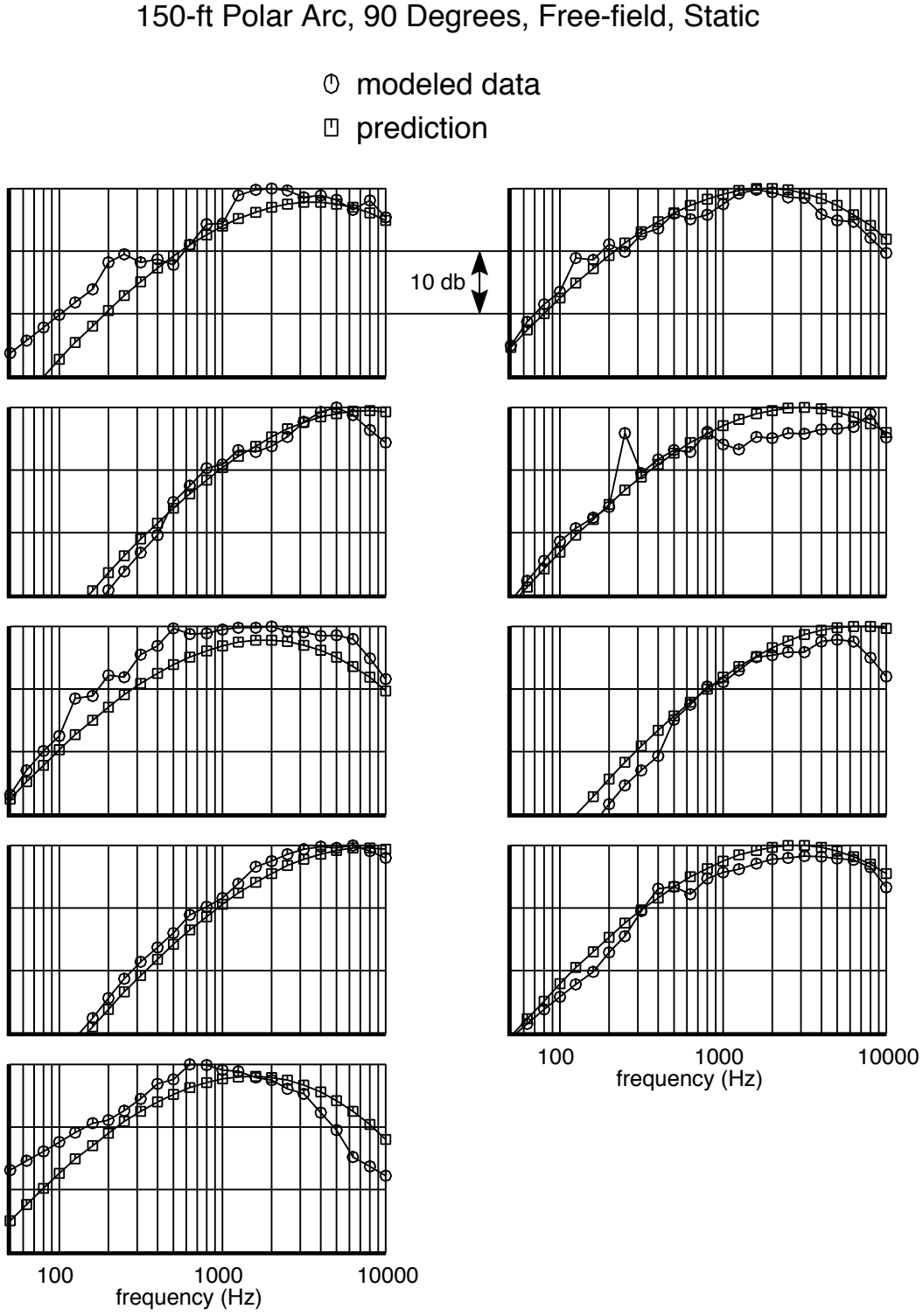

Figure 48 Aft Fan Broadband Comparison at High Power and 90 Degrees

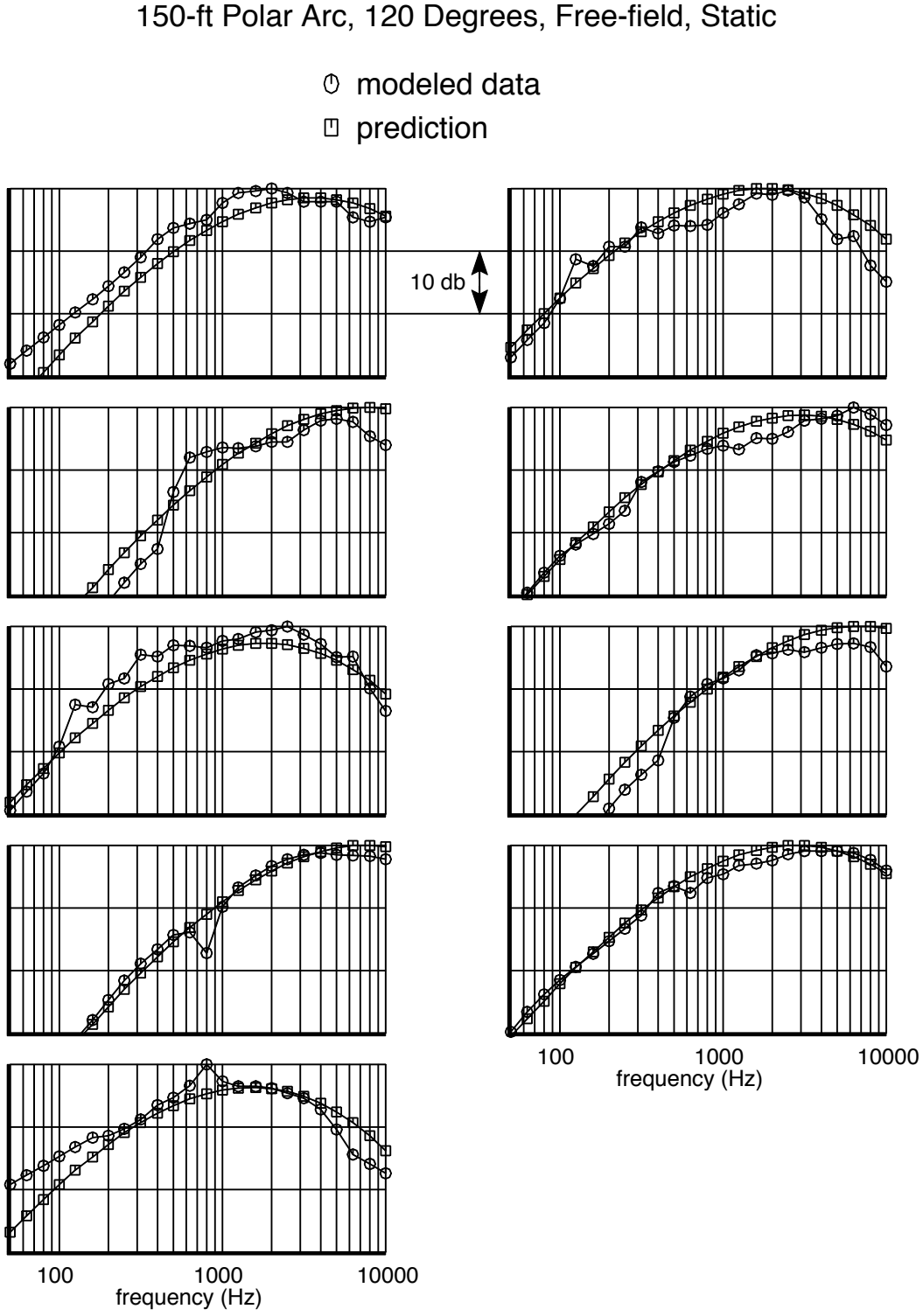

Figure 49 Aft Fan Broadband Comparison at High Power and 120 Degrees

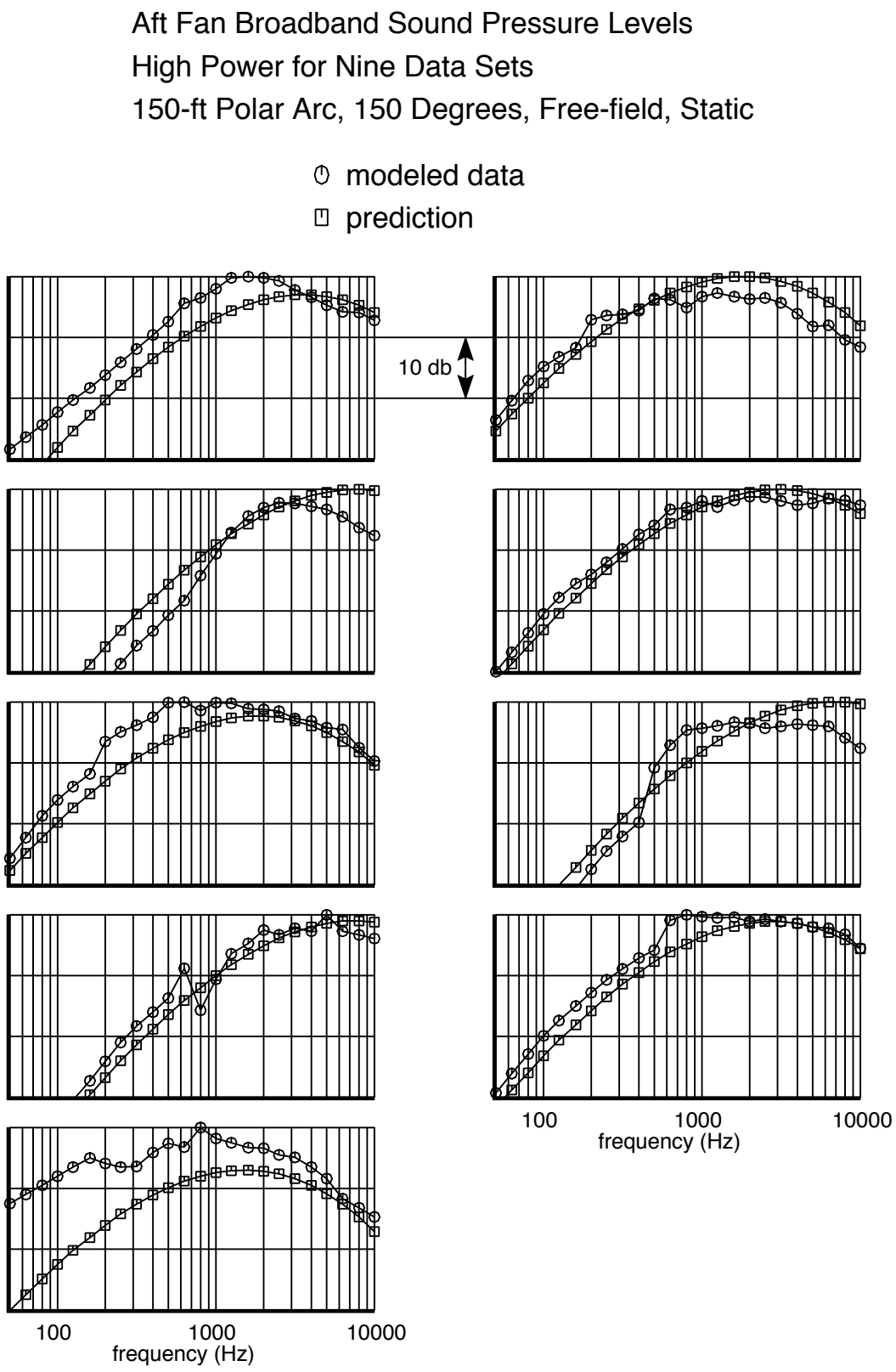

Figure 50 Aft Fan Broadband Comparison at High Power and 150 Degrees

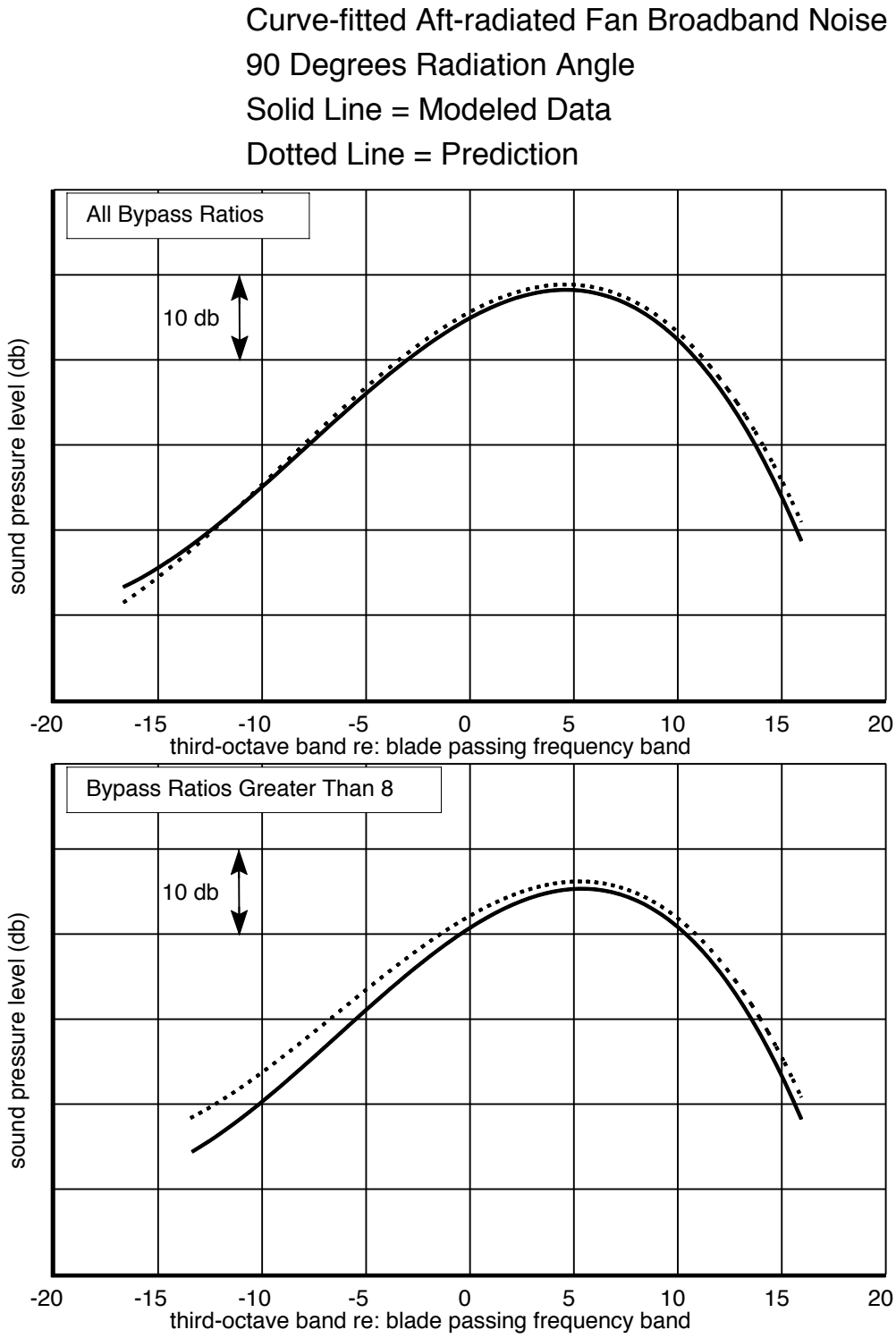

Figure 51 Averaged Aft-radiated Fan Broadband at 90 Degrees

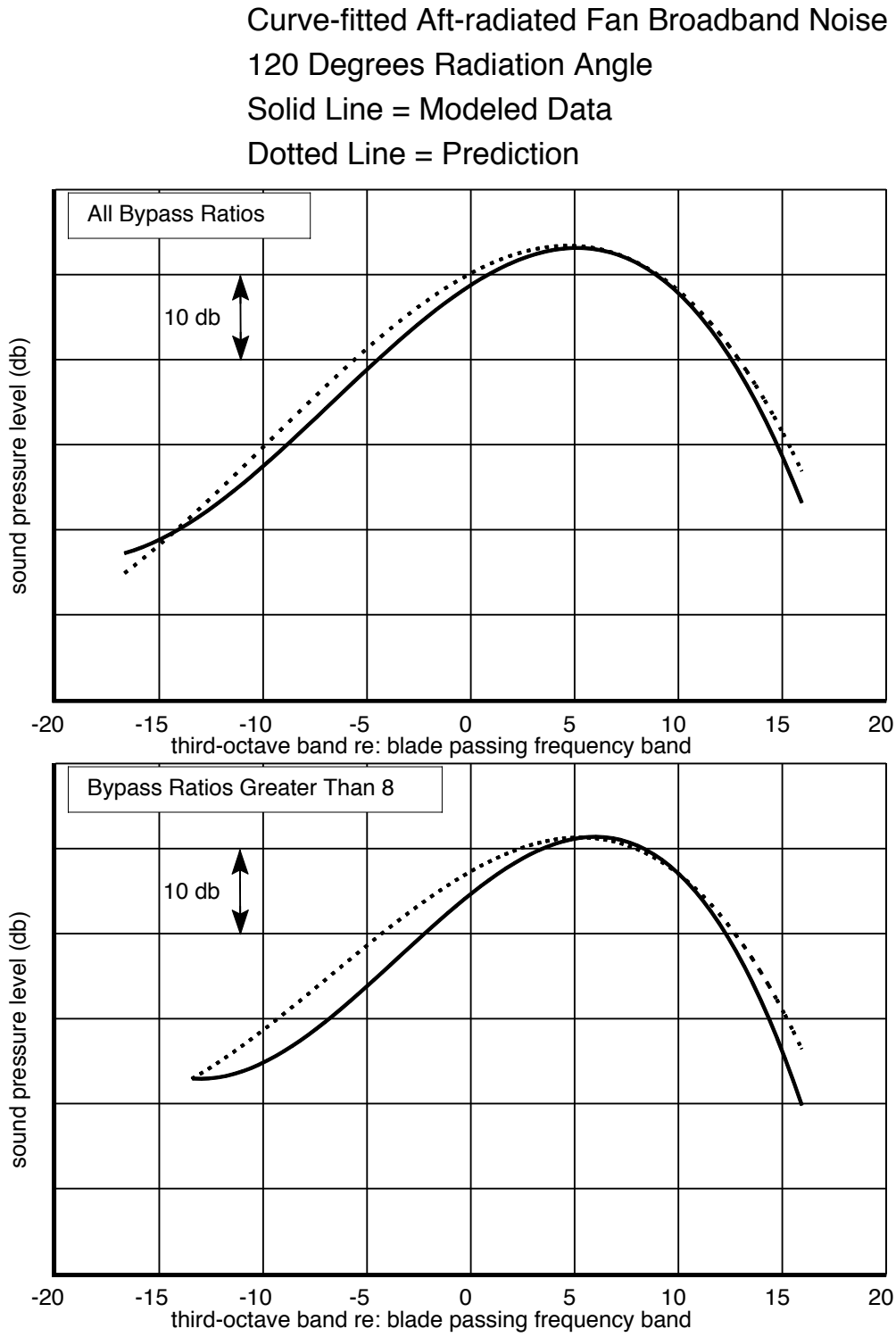

Figure 52 Averaged Aft-radiated Fan Broadband at 120 Degrees

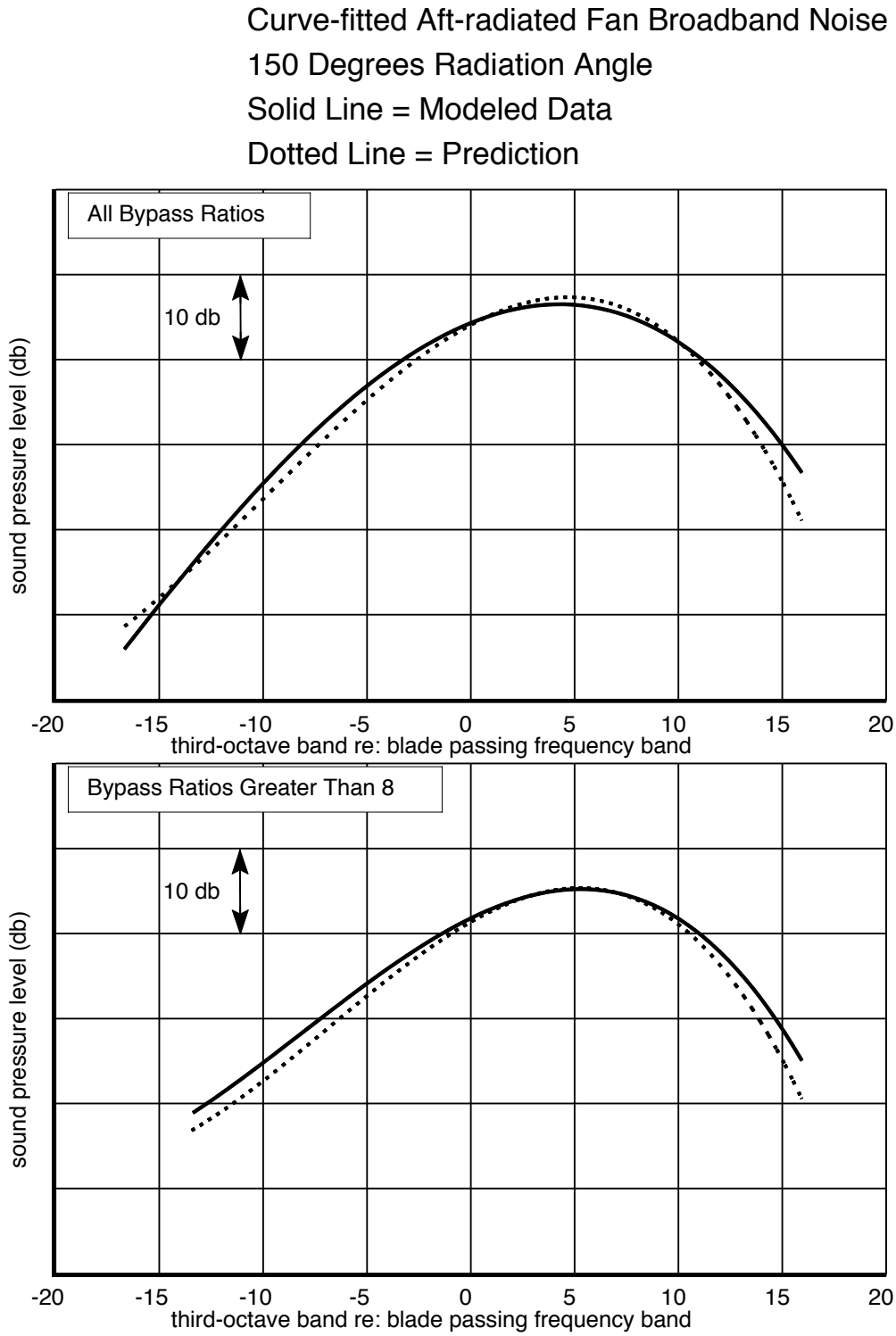

Figure 53 Averaged Aft-radiated Fan Broadband at 150 Degrees

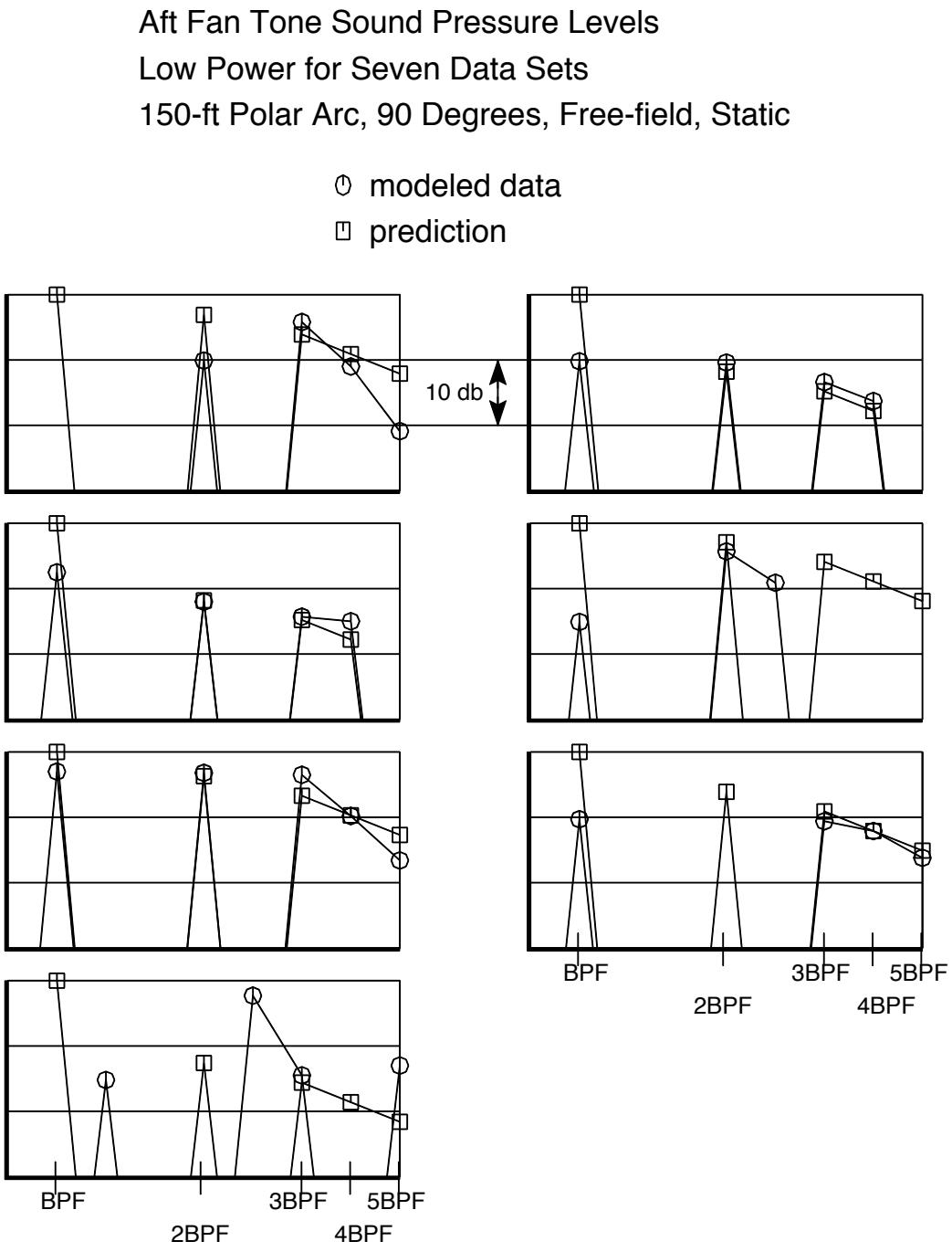

Figure 54 Aft Fan Tone Comparison at Low Power and 90 Degrees

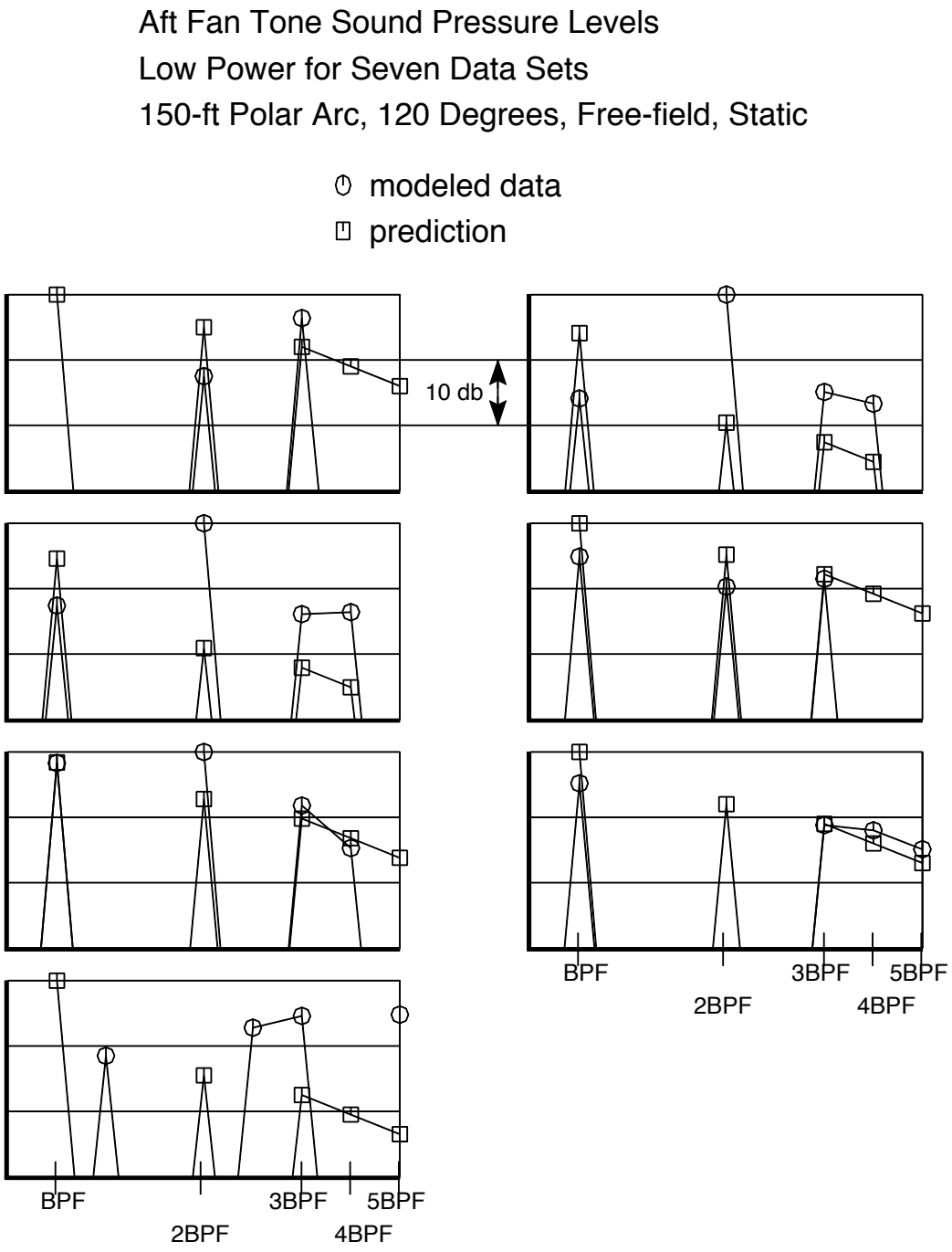

Figure 55 Aft Fan Tone Comparison at Low Power and 120 Degrees

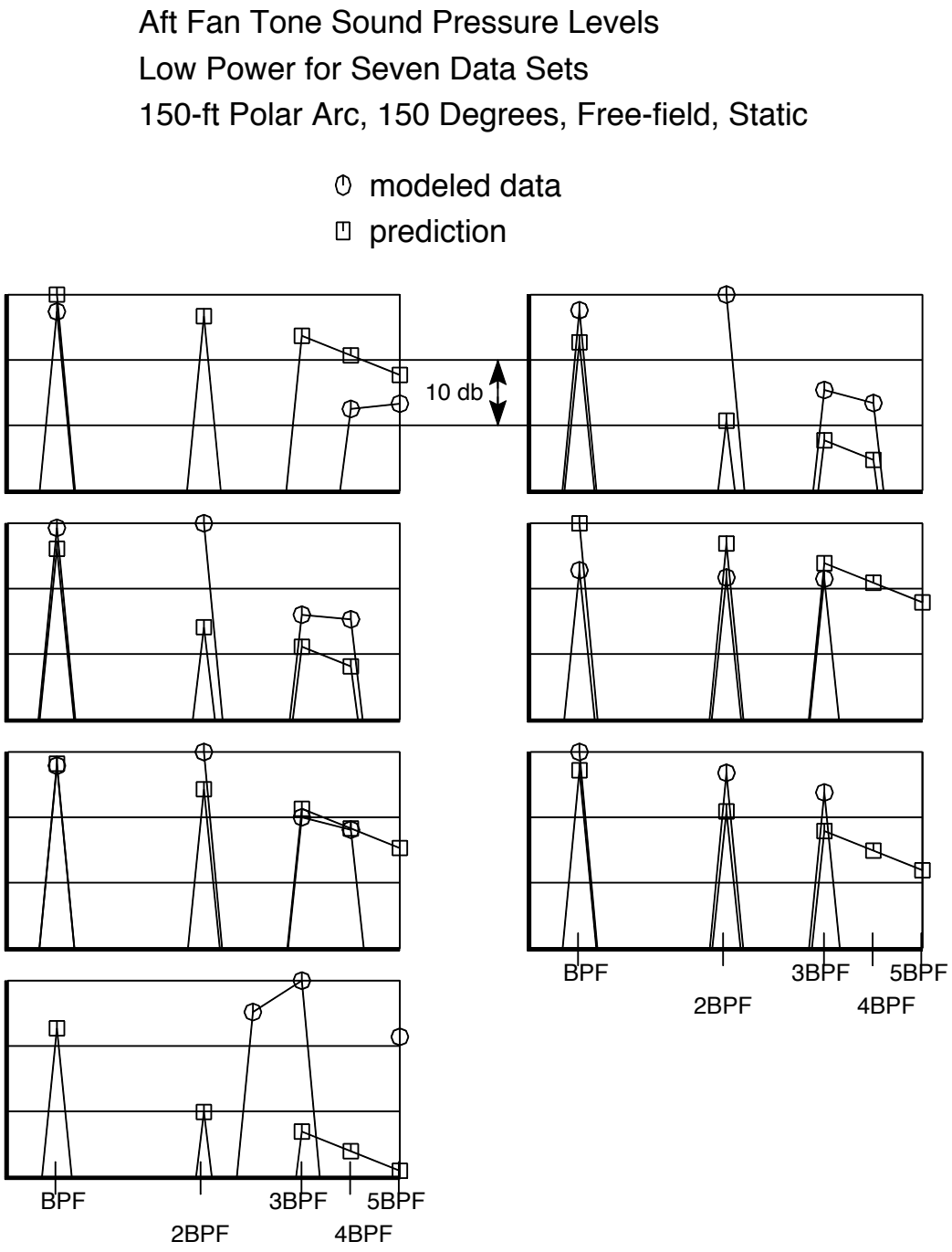

Figure 56 Aft Fan Tone Comparison at Low Power and 150 Degrees

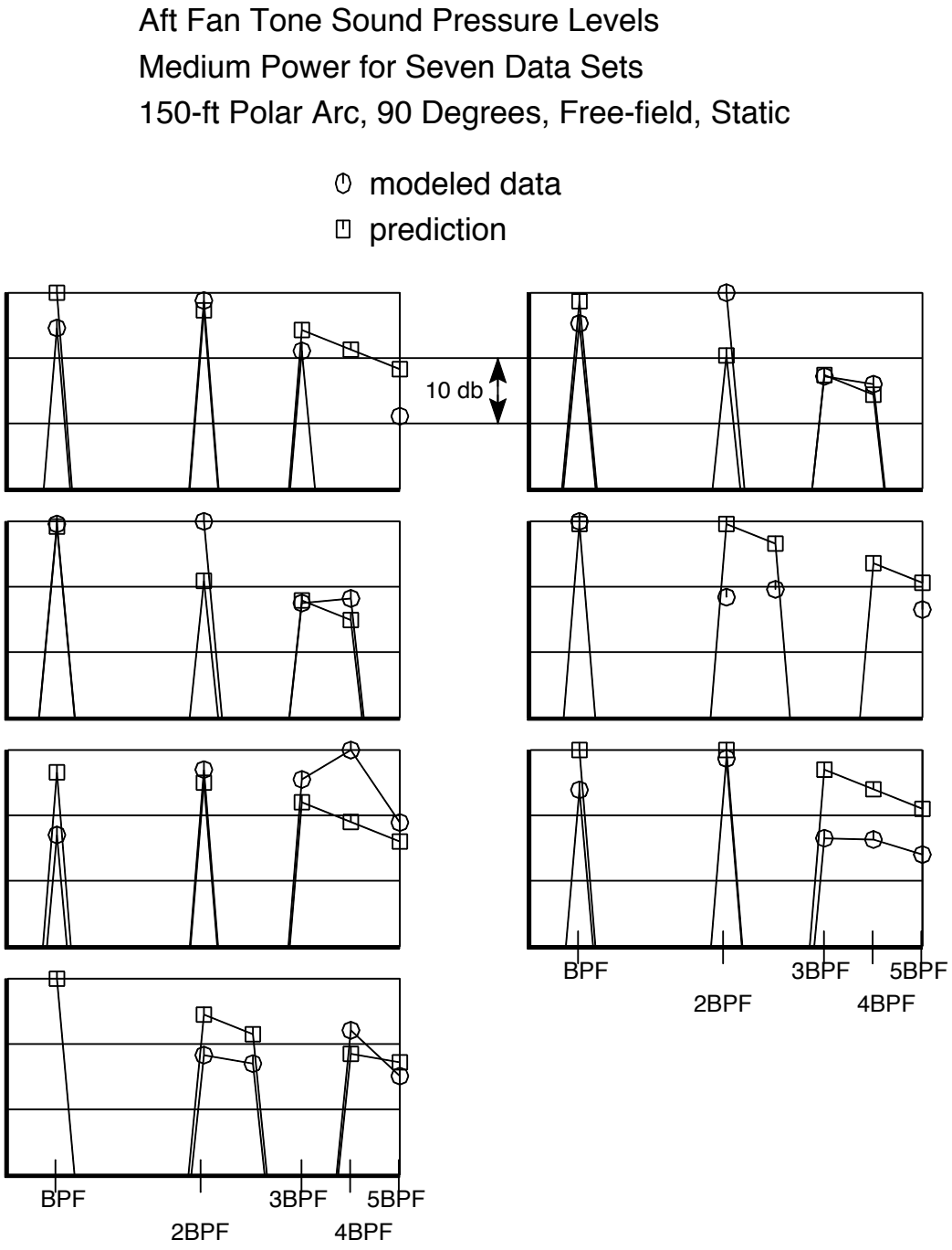

Figure 57 Aft Fan Tone Comparison at Medium Power and 90 Degrees

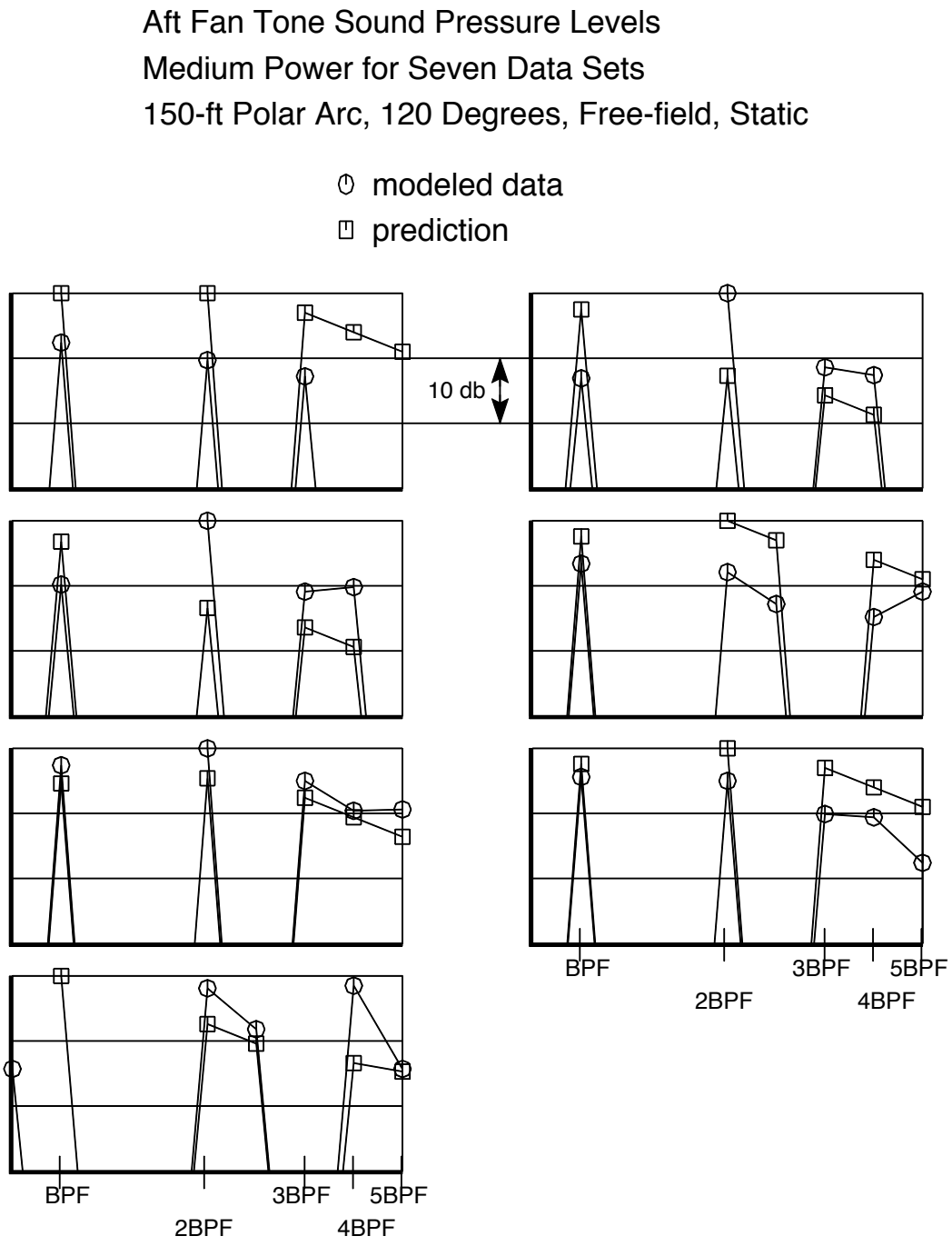

Figure 58 Aft Fan Tone Comparison at Medium Power and 120 Degrees

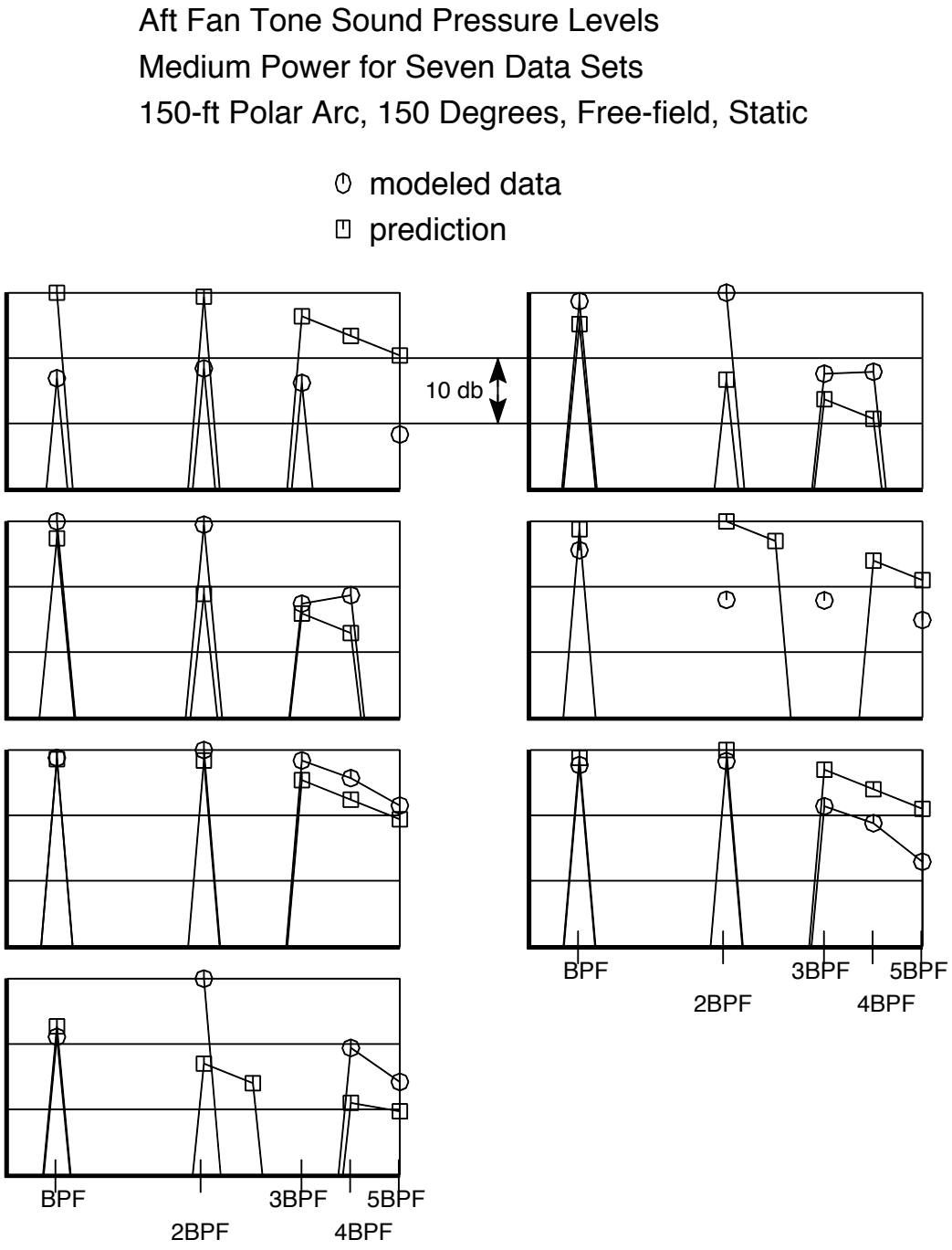

Figure 59 Aft Fan Tone Comparison at Medium Power and 150 Degrees

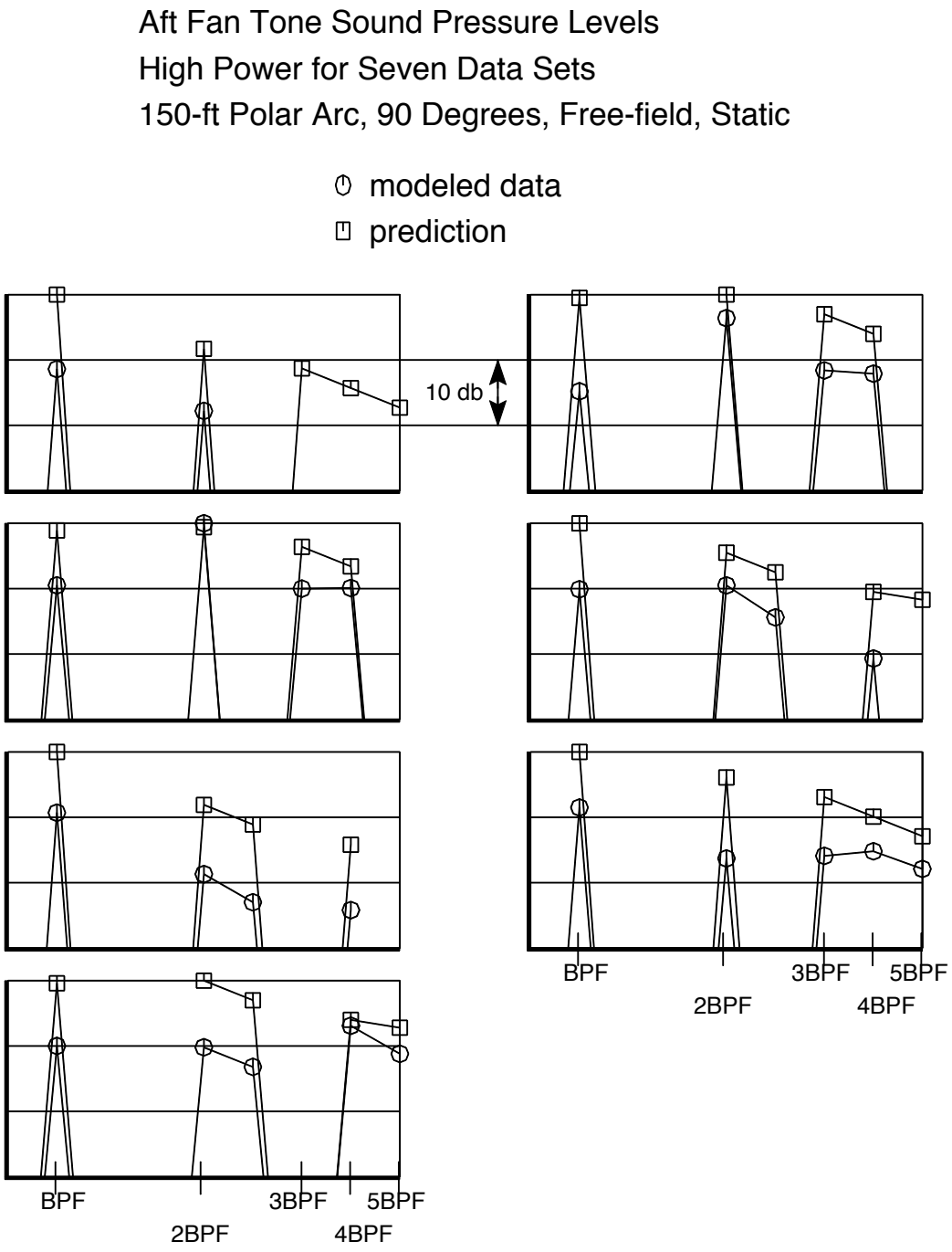

Figure 60 Aft Fan Tone Comparison at High Power and 90 Degrees

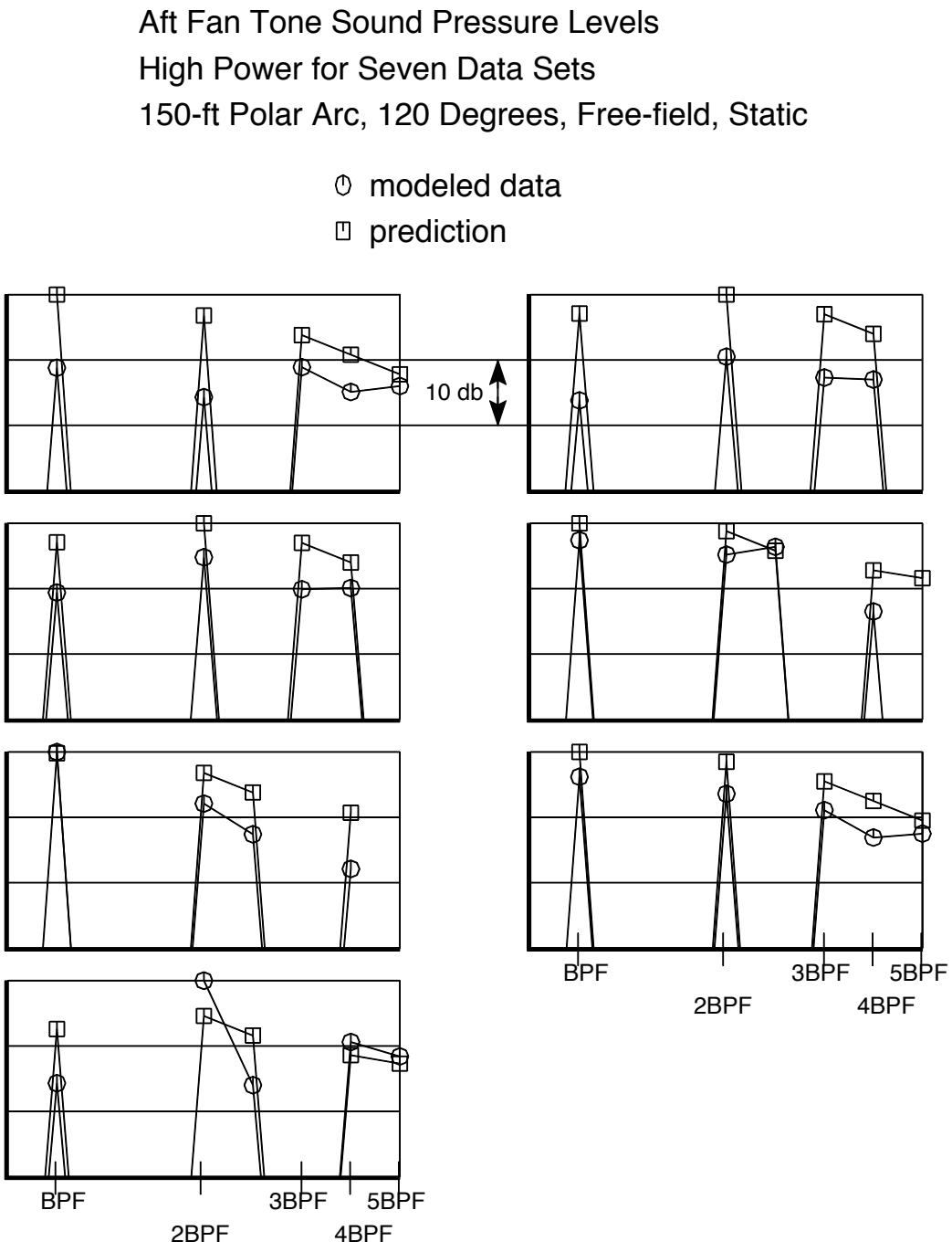

Figure 61 Aft Fan Tone Comparison at High Power and 120 Degrees

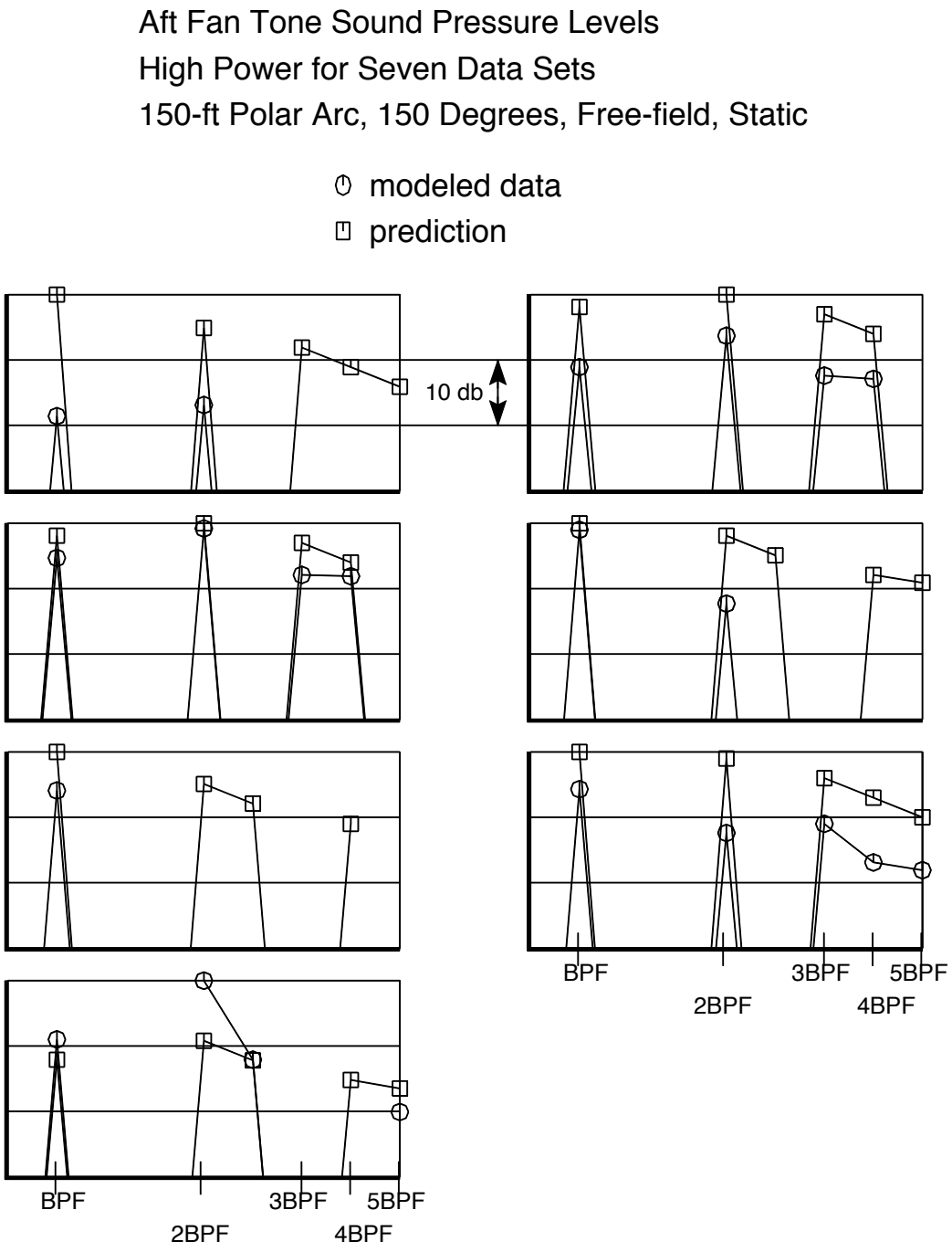

Figure 62 Aft Fan Tone Comparison at High Power and 150 Degrees

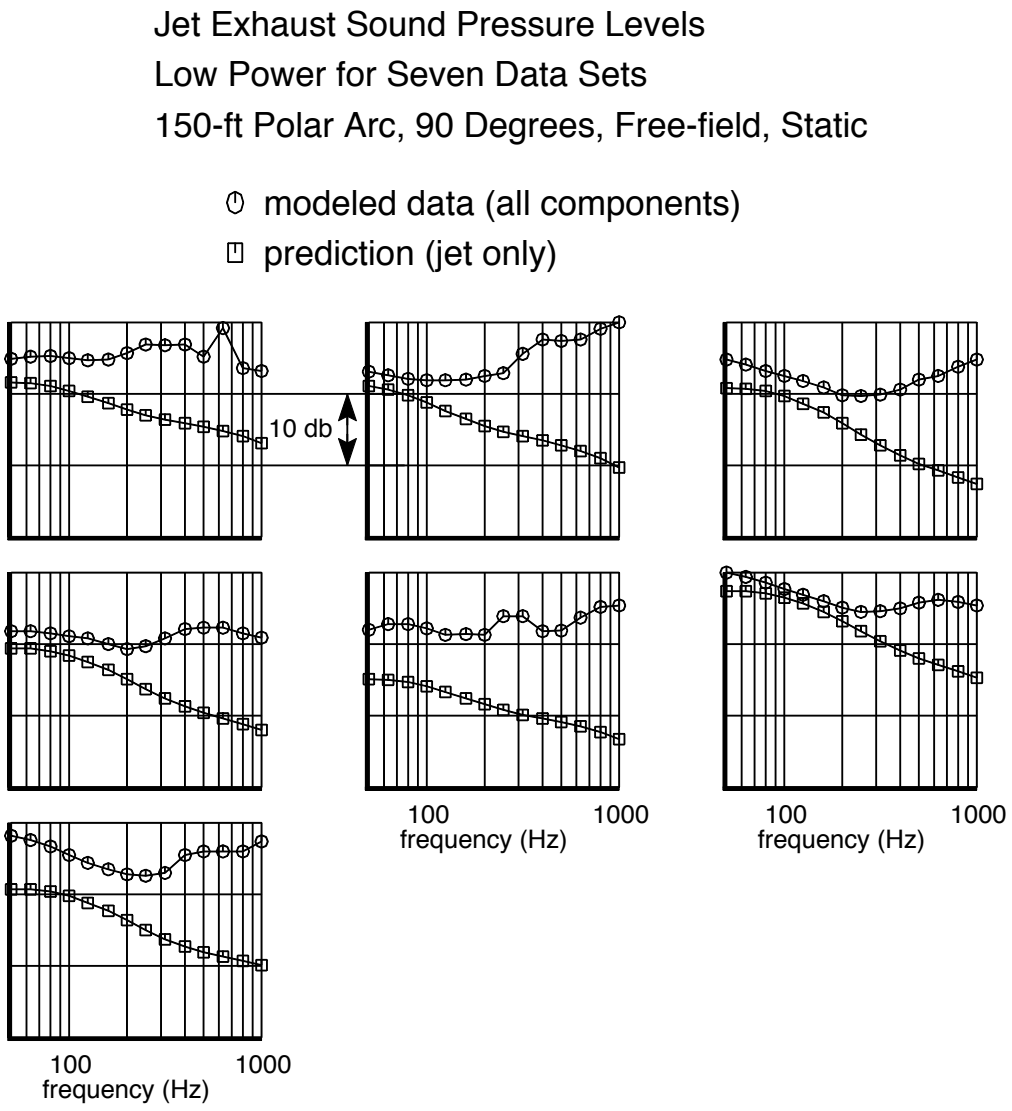

Figure 63 Jet Noise Comparison at Low Power and 90 Degrees

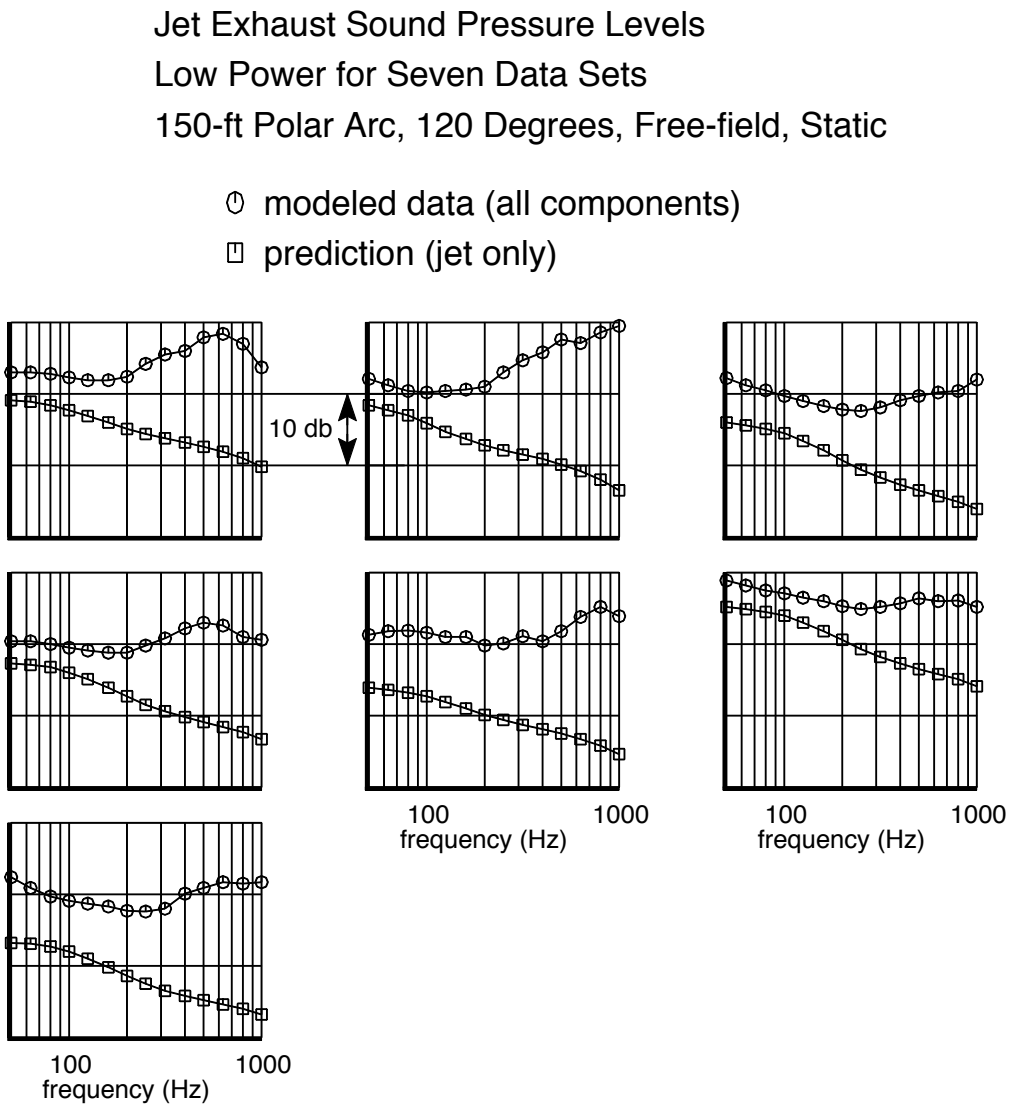

Figure 64 Jet Noise Comparison at Low Power and 120 Degrees

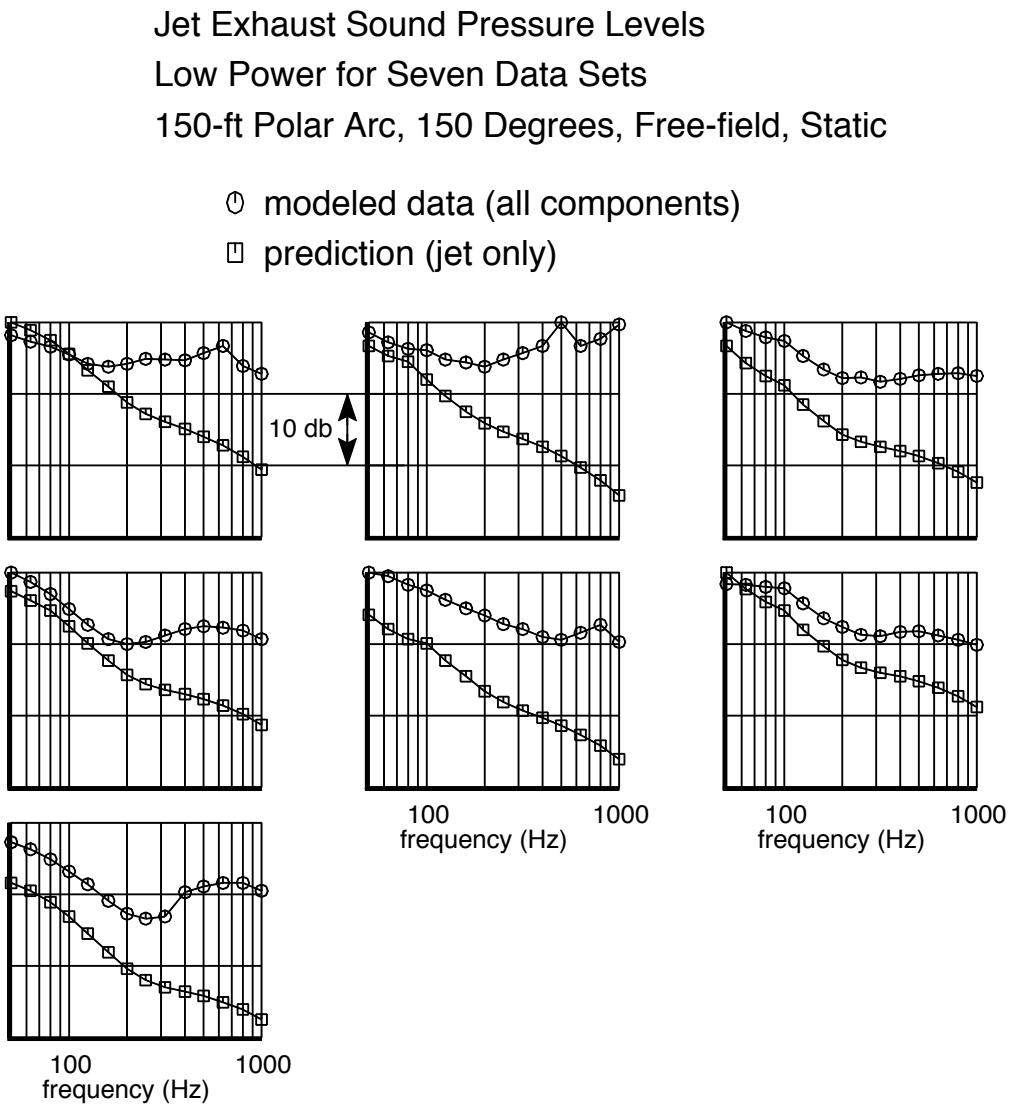

Figure 65 Jet Noise Comparison at Low Power and 150 Degrees

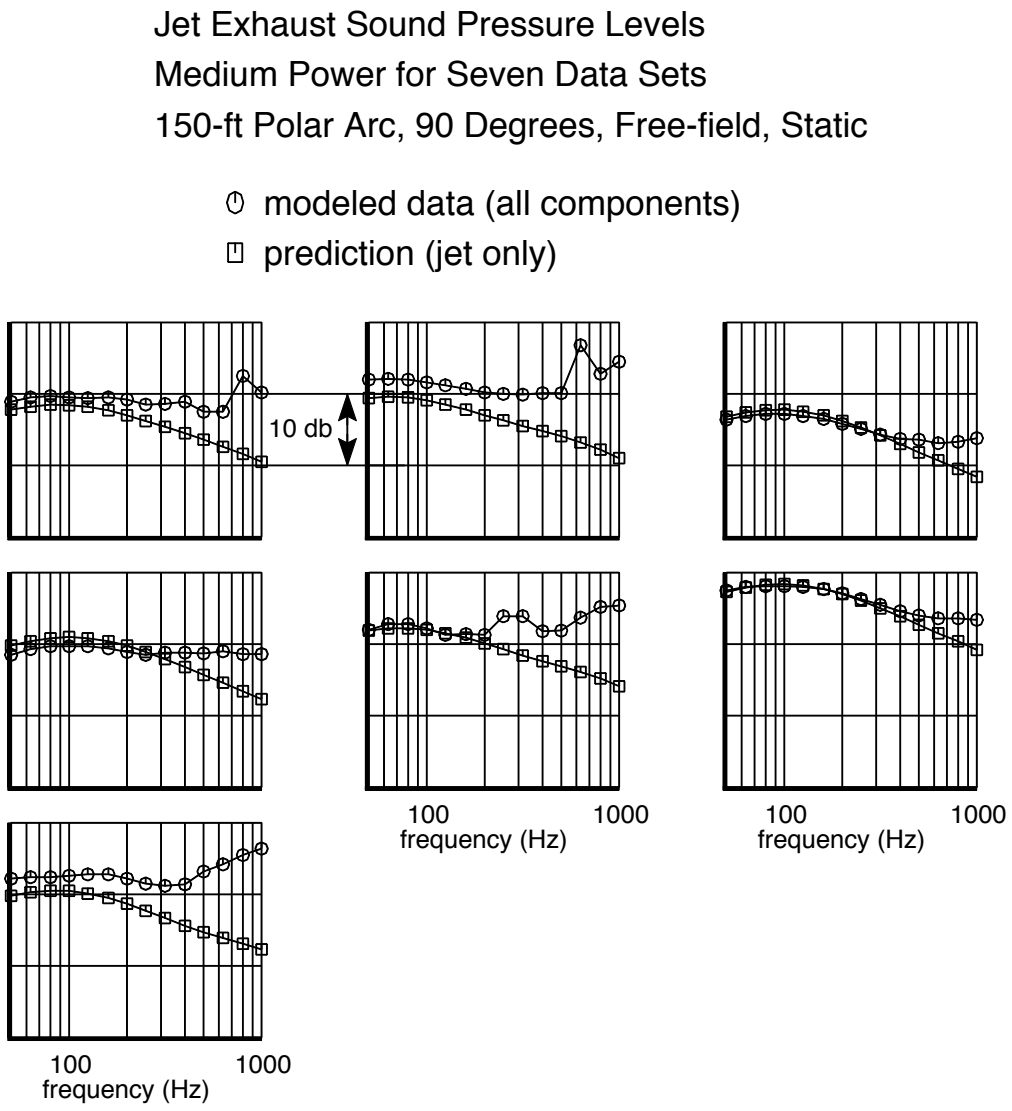

Figure 66 Jet Noise Comparison at Medium Power and 90 Degrees

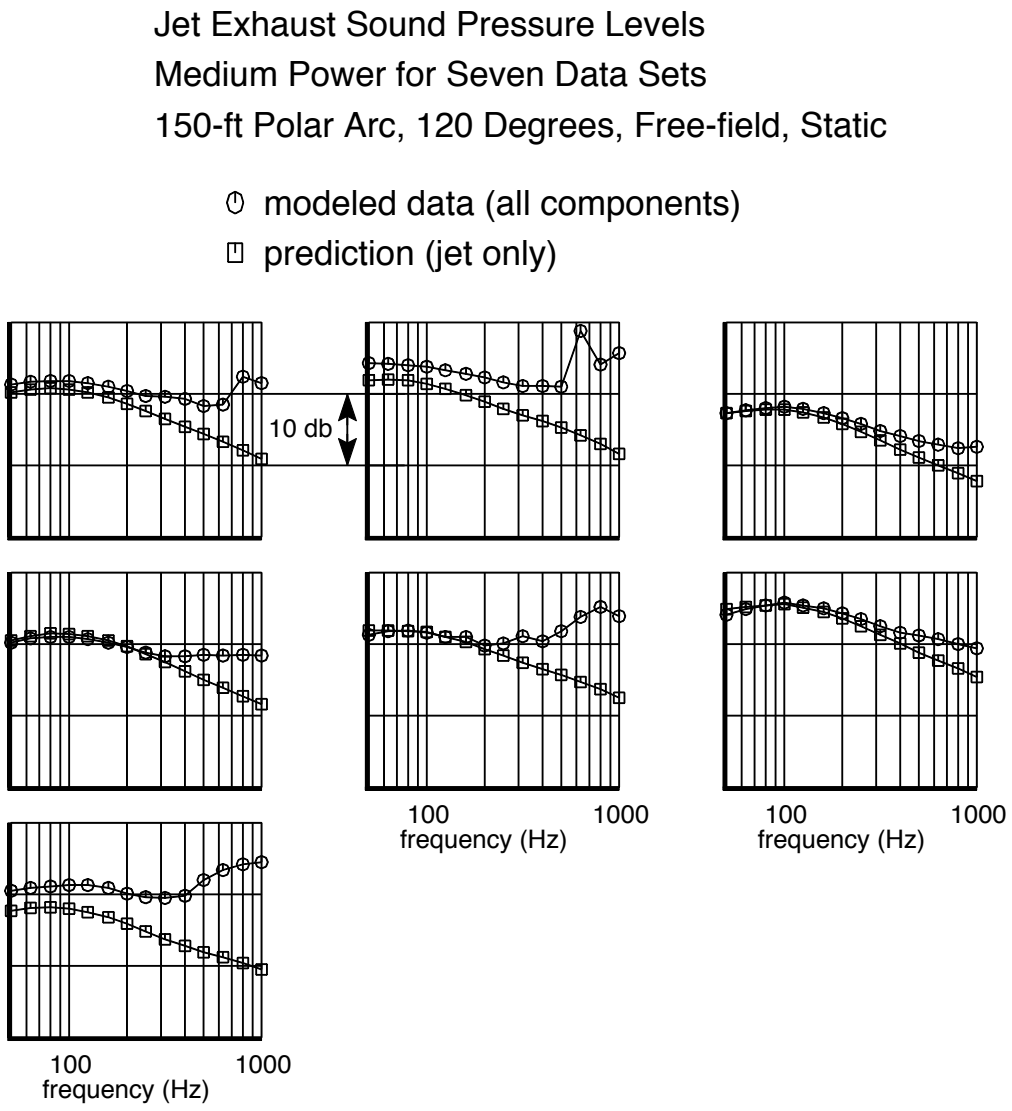

Figure 67 Jet Noise Comparison at Medium Power and 120 Degrees

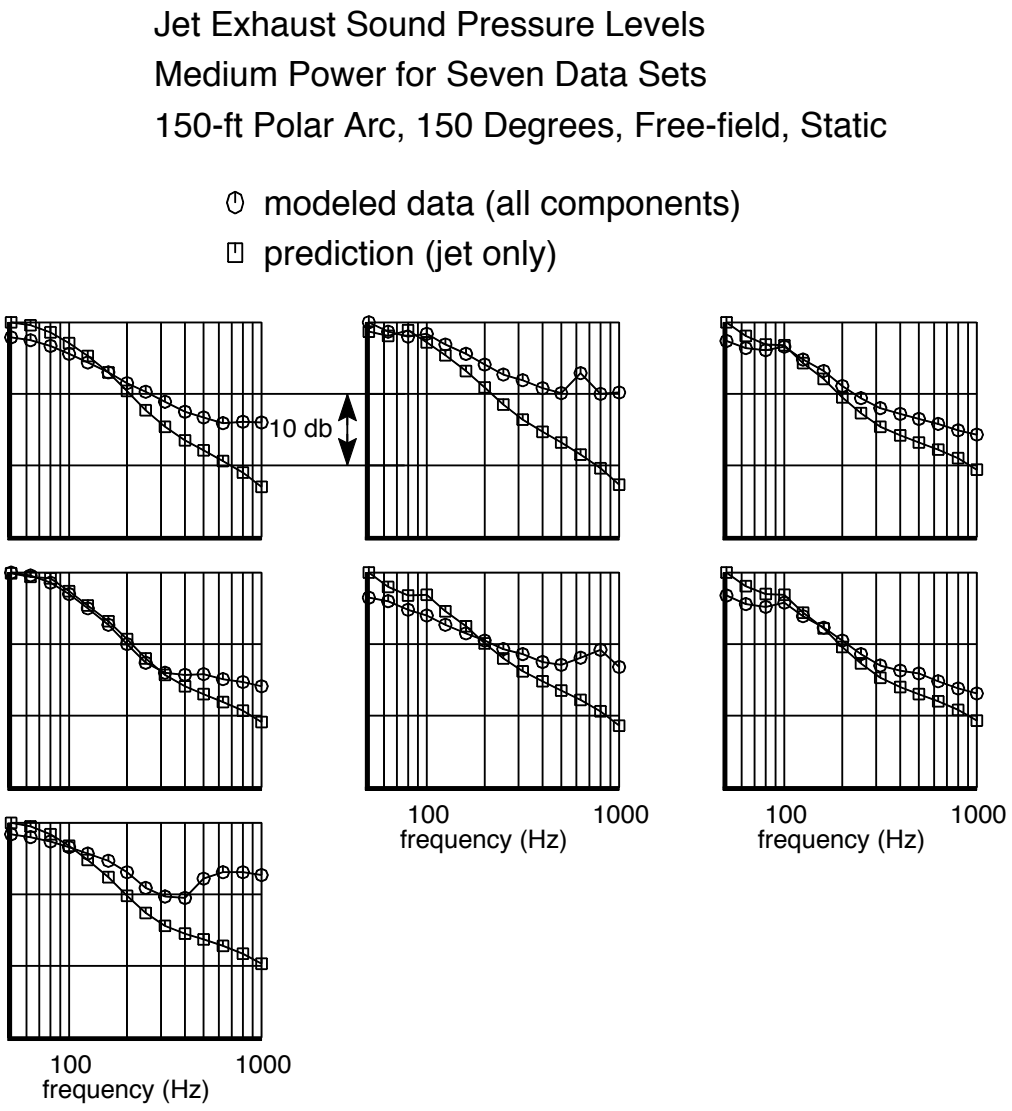

Figure 68 Jet Noise Comparison at Medium Power and 150 Degrees

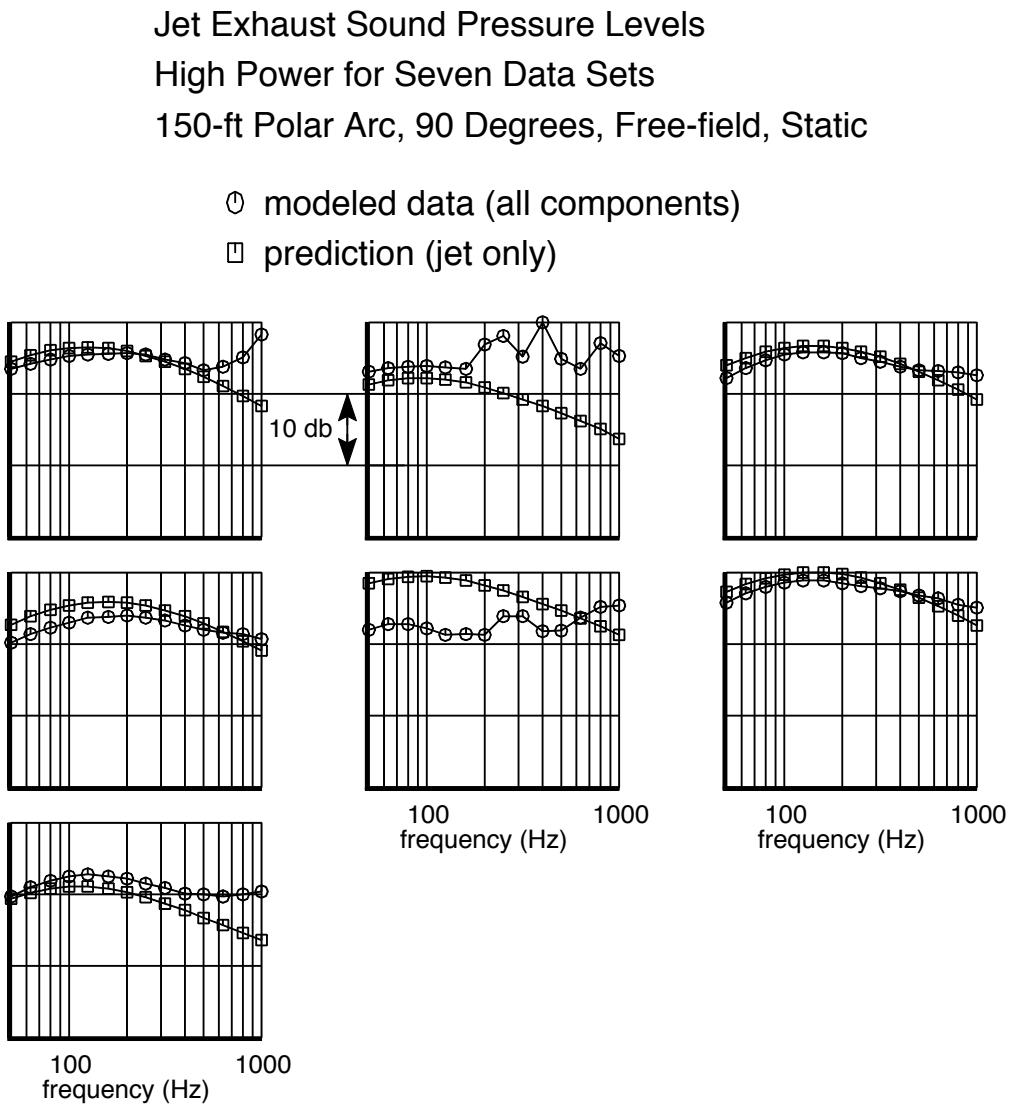

Figure 69 Jet Noise Comparison at High Power and 90 Degrees

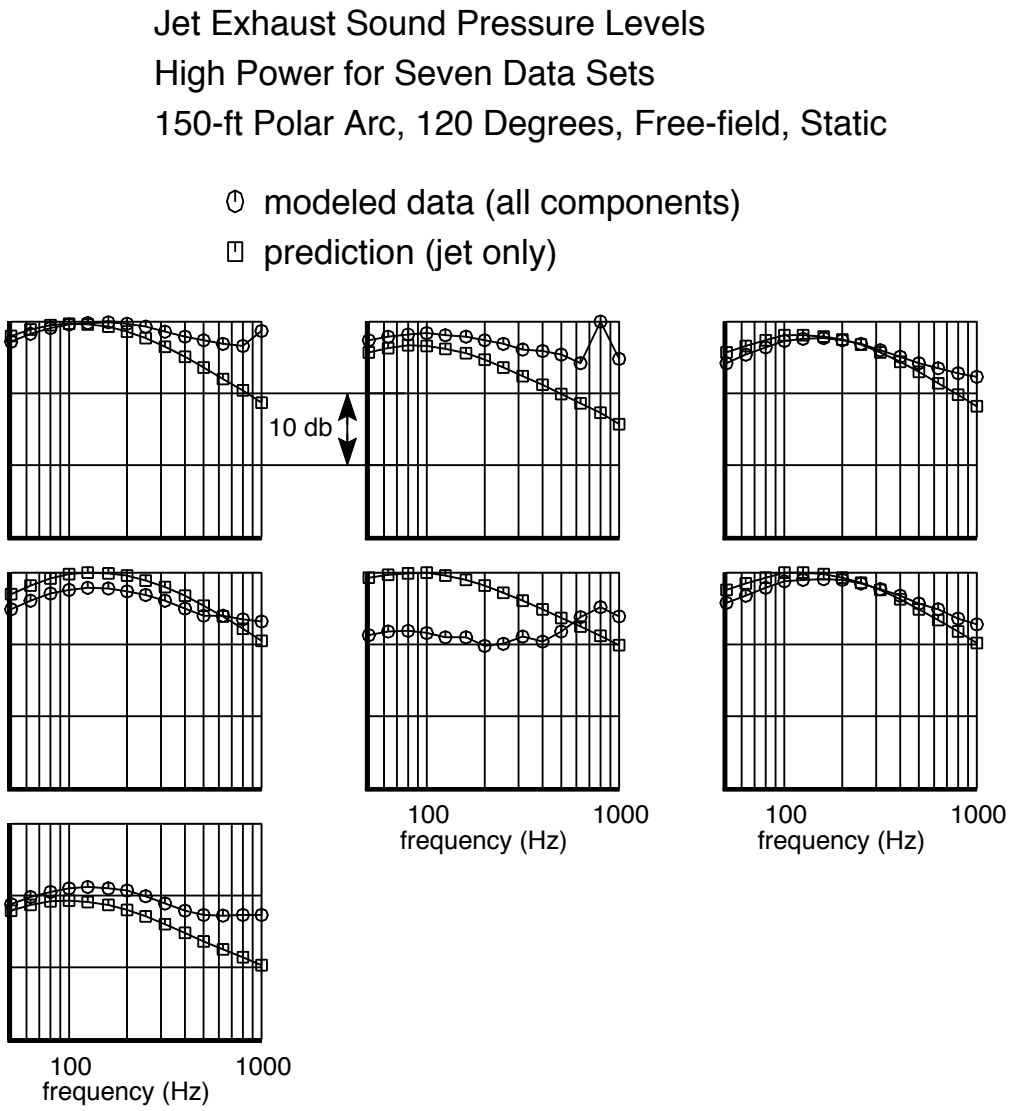

Figure 70 Jet Noise Comparison at High Power and 120 Degrees

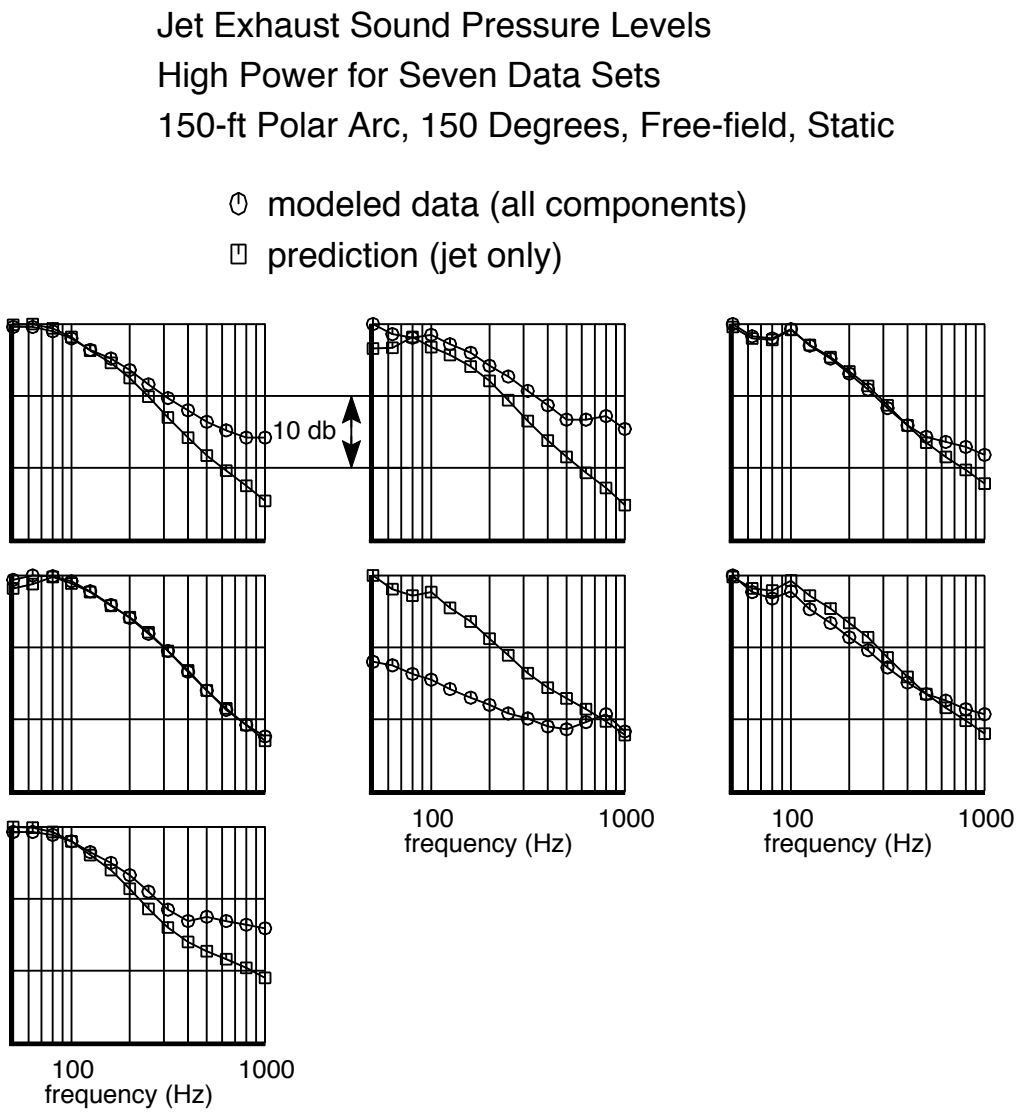

Figure 71 Jet Noise Comparison at High Power and 150 Degrees

REPORT DOCUMENTATION PAGE

Form Approved
OMB No. 0704-0188

1. REPORT DATE *(DD-MM-YYYY)*	2. REPORT TYPE	3. DATES COVERED *(From - To)*
01- 06 - 2005	Contractor Report	

4. TITLE AND SUBTITLE

Modular Engine Noise Component Prediction System (MCP) Technical Description and Assessment Document

5a. CONTRACT NUMBER

NAS1-97040

5b. GRANT NUMBER

5c. PROGRAM ELEMENT NUMBER

6. AUTHOR(S)

Herkes, William H.; and Reed, David H.

5d. PROJECT NUMBER

5e. TASK NUMBER

Task 10

5f. WORK UNIT NUMBER

23-781-20-12

7. PERFORMING ORGANIZATION NAME(S) AND ADDRESS(ES)

NASA Langley Research Center
Hampton, VA 23681-2199

Boeing Commercial Airplanes
Seattle, WA 98124

8. PERFORMING ORGANIZATION REPORT NUMBER

9. SPONSORING/MONITORING AGENCY NAME(S) AND ADDRESS(ES)

National Aeronautics and Space Administration
Washington, DC 20546-0001

10. SPONSOR/MONITOR'S ACRONYM(S)

NASA

11. SPONSOR/MONITOR'S REPORT NUMBER(S)

NASA/CR-2005-213526

12. DISTRIBUTION/AVAILABILITY STATEMENT

Unclassified - Unlimited
Subject Category 71
Availability: NASA CASI (301) 621-0390

13. SUPPLEMENTARY NOTES

Langley Technical Monitor: Robert A. Golub
An electronic version can be found at http://ntrs.nasa.gov

14. ABSTRACT

This report describes an empirical prediction procedure for turbofan engine noise. The procedure generates predicted noise levels for several noise components, including inlet- and aft-radiated fan noise, and jet-mixing noise. This report discusses the noise source mechanisms, the development of the prediction procedures, and the assessment of the accuracy of these predictions. Finally, some recommendations for future work are presented.

15. SUBJECT TERMS

Engine noise prediction; Fan noise prediction; Jet shock noise prediction; Jet noise prediction

16. SECURITY CLASSIFICATION OF:			17. LIMITATION OF ABSTRACT	18. NUMBER OF PAGES	19a. NAME OF RESPONSIBLE PERSON
a. REPORT	b. ABSTRACT	c. THIS PAGE			STI Help Desk (email: help@sti.nasa.gov)
					19b. TELEPHONE NUMBER *(Include area code)*
U	U	U	UU	91	(301) 621-0390